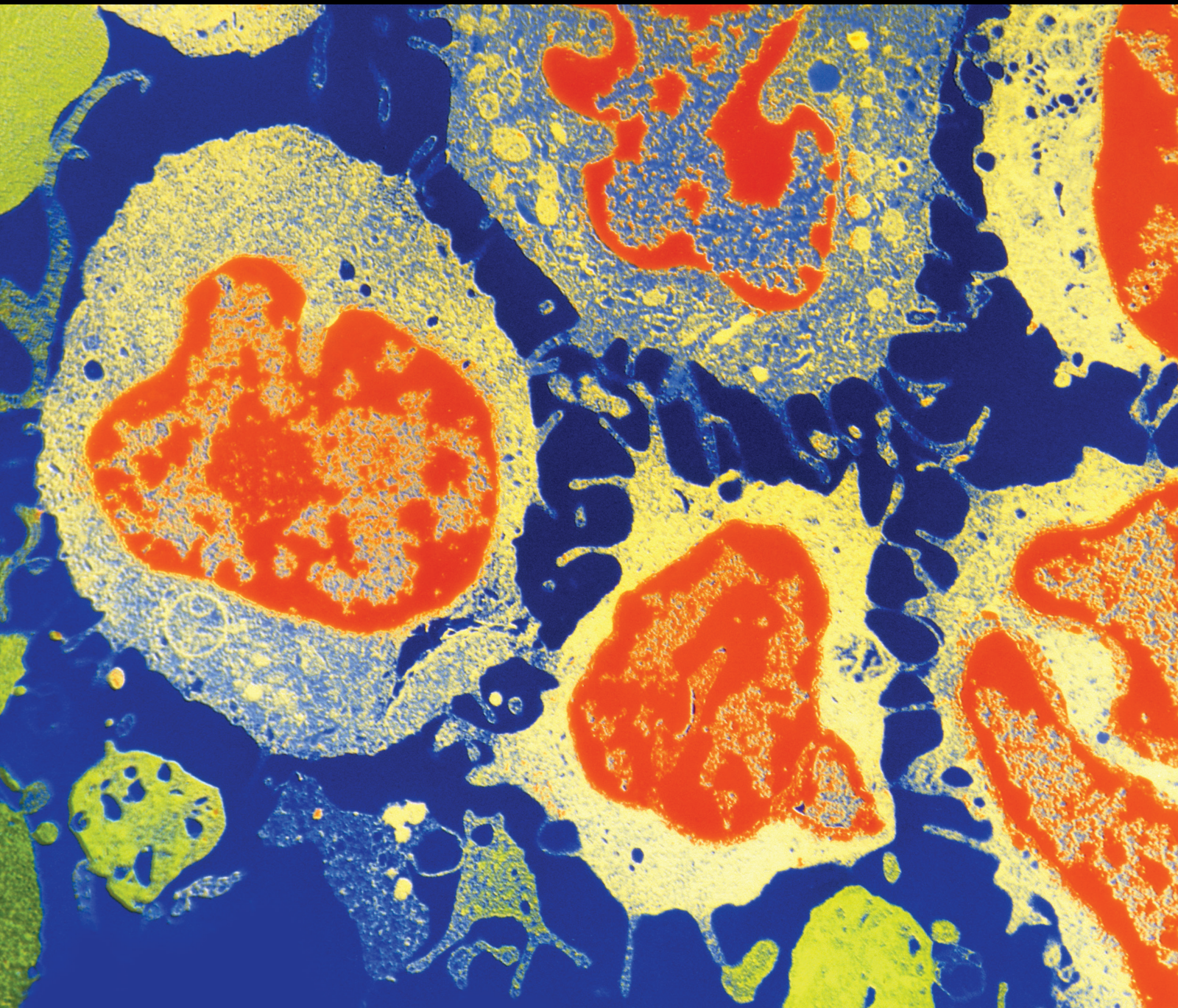


Mitochondrial Quality Control for Targeted Cancer Therapy

Lead Guest Editor: Yun-Dai Chen

Guest Editors: Rui Guo, Sam Toan, and Sang-Bing Ong





Mitochondrial Quality Control for Targeted Cancer Therapy

Journal of Oncology

Mitochondrial Quality Control for Targeted Cancer Therapy

Lead Guest Editor: Yun-Dai Chen

Guest Editors: Rui Guo, Sam Toan, and Sang-Bing Ong



Copyright © 2023 Hindawi Limited. All rights reserved.

This is a special issue published in "Journal of Oncology" All articles are open access articles distributed under the Creative Commons Attribution License, which permits unrestricted use, distribution, and reproduction in any medium, provided the original work is properly cited.

Chief Editor

Bruno Vincenzi, Italy

Academic Editors

Thomas E. Adrian, United Arab Emirates

Ruhai Bai , China

Jiaolin Bao, China

Rossana Berardi, Italy

Benedetta Bussolati, Italy

Sumanta Chatterjee, USA


Thomas R. Chauncey, USA

Gagan Chhabra, USA

Francesca De Felice , Italy

Giuseppe Di Lorenzo, Italy

Xiangya Ding , China

Peixin Dong , Japan

Xingrong Du, China

Elizabeth R. Dudnik , Israel

Pierfrancesco Franco , Italy

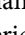
Ferdinand Frauscher , Austria

Rohit Gundamaraju, USA

Han Han , USA

Jitti Hanprasertpong , Thailand


Yongzhong Hou , China

Wan-Ming Hu , China


Jialiang Hui, China

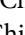
Akira Iyoda , Japan

Reza Izadpanah , USA

Kaiser Jamil , India

Shuang-zheng Jia , China

Ozkan Kanat , Turkey

Zhihua Kang , USA

Pashtoon M. Kasi , USA

Jorg Kleeff, United Kingdom

Jayaprakash Kolla, Czech Republic

Goo Lee , USA

Peter F. Lenehan, USA

Da Li , China

Rui Liao , China

Rengyun Liu , China

Alexander V. Louie, Canada

Weiren Luo , China


Cristina Magi-Galluzzi , USA

Kanjoormana A. Manu, Singapore


Riccardo Masetti , Italy

Ian E. McCutcheon , USA

Zubing Mei, China

Giuseppe Maria Milano , Italy

Nabiha Missaoui , Tunisia

Shinji Miwa , Japan

Sakthivel Muniyan , USA

Magesh Muthu , USA

Nandakumar Natarajan , USA


P. Neven, Belgium


Patrick Neven, Belgium

Marco Noventa, Italy

Liren Qian , China

Shuanglin Qin , China

Dongfeng Qu , USA

Amir Radfar , USA

Antonio Raffone , Italy


Achuthan Chathrattil Raghavamenon, India

Faisal Raza, China

Giandomenico Roviello , Italy


Subhadeep Roy , India

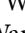
Prasannakumar Santhekadur , India

Chandra K. Singh , USA


Yingming Sun , China


Mohammad Tarique , USA

Federica Tomao , Italy

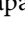
Vincenzo Tombolini , Italy

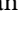
Maria S. Tretiakova, USA


Abhishek Tyagi , USA

Satoshi Wada , Japan


Chen Wang, China

Xiaosheng Wang , China

Guangzhen Wu , China

Haigang Wu , China


Yuan Seng Wu , Malaysia


Yingkun Xu , China

WU Xue-liang , China

ZENG JIE YE , China

Guan-Jun Yang , China

Junmin Zhang , China

Dan Zhao , USA

Dali Zheng , China

Contents

Retracted: Yap-Hippo Signaling Activates Mitochondrial Protection and Sustains Breast Cancer Viability under Hypoxic Stress

Journal of Oncology

Retraction (1 page), Article ID 9814758, Volume 2023 (2023)

Retracted: Development and Validation of a Novel Mitophagy-Related Gene Prognostic Signature for Hepatocellular Carcinoma Based on Immunoscore Classification of Tumor

Journal of Oncology

Retraction (1 page), Article ID 9803262, Volume 2023 (2023)

Retracted: Mst2 Overexpression Inhibits Thyroid Carcinoma Growth and Metastasis by Disrupting Mitochondrial Fitness and Endoplasmic Reticulum Homeostasis

Journal of Oncology

Retraction (1 page), Article ID 9894235, Volume 2023 (2023)

Retracted: Hyperfractionation versus Conventional Fractionation of Preoperative Intensity-Modulated Radiotherapy with Oral Capecitabine in Locally Advanced Mid-Low Rectal Cancer: A Propensity Score Matching Study

Journal of Oncology

Retraction (1 page), Article ID 9892163, Volume 2023 (2023)

Retracted: TMEM60 Promotes the Proliferation and Migration and Inhibits the Apoptosis of Glioma through Modulating AKT Signaling

Journal of Oncology

Retraction (1 page), Article ID 9767535, Volume 2023 (2023)

Retracted: Identification of the Novel Methylated Genes' Signature to Predict Prognosis in INRG High-Risk Neuroblastomas

Journal of Osteoporosis






Retraction (1 page), Article ID 9846323, Volume 2022 (2022)

Retracted: DNA Damage Response Genes in Osteosarcoma

Journal of Osteoporosis


Retraction (1 page), Article ID 9875928, Volume 2022 (2022)

[Retracted] Hyperfractionation versus Conventional Fractionation of Preoperative Intensity-Modulated Radiotherapy with Oral Capecitabine in Locally Advanced Mid-Low Rectal Cancer: A Propensity Score Matching Study

Chen Shi , Yangzi Zhang , Yongheng Li , Jianhao Geng, Xianggao Zhu, Hongzhi Wang, Yong Cai , and Weihu Wang 


Research Article (10 pages), Article ID 9119245, Volume 2022 (2022)

[Retracted] TMEM60 Promotes the Proliferation and Migration and Inhibits the Apoptosis of Glioma through Modulating AKT Signaling

Jingwen Wu, Xinghua Tang, Xuejuan Yu, Xiaoli Zhang, Wenjun Yang, Ashima Seth, and Qian Yang 











Research Article (11 pages), Article ID 9913700, Volume 2022 (2022)

[Retracted] DNA Damage Response Genes in Osteosarcoma

Ying Tang, Yan-xia Liu, Xiuning Huang, and Peng Li 


Research Article (9 pages), Article ID 9365953, Volume 2021 (2021)

[Retracted] Development and Validation of a Novel Mitophagy-Related Gene Prognostic Signature for Hepatocellular Carcinoma Based on Immunoscore Classification of Tumor

Hao Chen , Jinghua Wang , Ruijie Zeng , Yujun Luo , Kehang Guo , Huihuan Wu , Qi Yang , Rui Jiang , Weihong Sha , and Zewei Zhuo 


Research Article (16 pages), Article ID 5070099, Volume 2021 (2021)

[Retracted] Yap-Hippo Signaling Activates Mitochondrial Protection and Sustains Breast Cancer Viability under Hypoxic Stress

Chen Shi, Siyuan Zhang, Changkuo Guo, and Jian Tie 


Research Article (10 pages), Article ID 5212721, Volume 2021 (2021)

[Retracted] Mst2 Overexpression Inhibits Thyroid Carcinoma Growth and Metastasis by Disrupting Mitochondrial Fitness and Endoplasmic Reticulum Homeostasis

Haichao Zhang, Xin Qu, Lu Han, and Xu Di 

Research Article (10 pages), Article ID 1262291, Volume 2021 (2021)

[Retracted] Identification of the Novel Methylated Genes' Signature to Predict Prognosis in INRG High-Risk Neuroblastomas

Zhichao Liu and Changchun Li 

Research Article (10 pages), Article ID 1615201, Volume 2021 (2021)

Retraction

Retracted: Yap-Hippo Signaling Activates Mitochondrial Protection and Sustains Breast Cancer Viability under Hypoxic Stress

Journal of Oncology

Received 10 October 2023; Accepted 10 October 2023; Published 11 October 2023

Copyright © 2023 Journal of Oncology. This is an open access article distributed under the Creative Commons Attribution License, which permits unrestricted use, distribution, and reproduction in any medium, provided the original work is properly cited.

This article has been retracted by Hindawi following an investigation undertaken by the publisher [1]. This investigation has uncovered evidence of one or more of the following indicators of systematic manipulation of the publication process:

- (1) Discrepancies in scope
- (2) Discrepancies in the description of the research reported
- (3) Discrepancies between the availability of data and the research described
- (4) Inappropriate citations
- (5) Incoherent, meaningless and/or irrelevant content included in the article
- (6) Peer-review manipulation

The presence of these indicators undermines our confidence in the integrity of the article's content and we cannot, therefore, vouch for its reliability. Please note that this notice is intended solely to alert readers that the content of this article is unreliable. We have not investigated whether authors were aware of or involved in the systematic manipulation of the publication process.

In addition, our investigation has also shown that one or more of the following human-subject reporting requirements has not been met in this article: ethical approval by an Institutional Review Board (IRB) committee or equivalent, patient/participant consent to participate, and/or agreement to publish patient/participant details (where relevant).

Wiley and Hindawi regrets that the usual quality checks did not identify these issues before publication and have since put additional measures in place to safeguard research integrity.

We wish to credit our own Research Integrity and Research Publishing teams and anonymous and named external researchers and research integrity experts for contributing to this investigation.

The corresponding author, as the representative of all authors, has been given the opportunity to register their agreement or disagreement to this retraction. We have kept a record of any response received.

References

- [1] C. Shi, S. Zhang, C. Guo, and J. Tie, "Yap-Hippo Signaling Activates Mitochondrial Protection and Sustains Breast Cancer Viability under Hypoxic Stress," *Journal of Oncology*, vol. 2021, Article ID 5212721, 10 pages, 2021.

Retraction

Retracted: Development and Validation of a Novel Mitophagy-Related Gene Prognostic Signature for Hepatocellular Carcinoma Based on Immunoscore Classification of Tumor

Journal of Oncology

Received 10 October 2023; Accepted 10 October 2023; Published 11 October 2023

Copyright © 2023 Journal of Oncology. This is an open access article distributed under the Creative Commons Attribution License, which permits unrestricted use, distribution, and reproduction in any medium, provided the original work is properly cited.

This article has been retracted by Hindawi following an investigation undertaken by the publisher [1]. This investigation has uncovered evidence of one or more of the following indicators of systematic manipulation of the publication process:

- (1) Discrepancies in scope
- (2) Discrepancies in the description of the research reported
- (3) Discrepancies between the availability of data and the research described
- (4) Inappropriate citations
- (5) Incoherent, meaningless and/or irrelevant content included in the article
- (6) Peer-review manipulation

The presence of these indicators undermines our confidence in the integrity of the article's content and we cannot, therefore, vouch for its reliability. Please note that this notice is intended solely to alert readers that the content of this article is unreliable. We have not investigated whether authors were aware of or involved in the systematic manipulation of the publication process.

Wiley and Hindawi regrets that the usual quality checks did not identify these issues before publication and have since put additional measures in place to safeguard research integrity.

We wish to credit our own Research Integrity and Research Publishing teams and anonymous and named external researchers and research integrity experts for contributing to this investigation.

The corresponding author, as the representative of all authors, has been given the opportunity to register their agreement or disagreement to this retraction. We have kept a record of any response received.

References

- [1] H. Chen, J. Wang, R. Zeng et al., "Development and Validation of a Novel Mitophagy-Related Gene Prognostic Signature for Hepatocellular Carcinoma Based on Immunoscore Classification of Tumor," *Journal of Oncology*, vol. 2021, Article ID 5070099, 16 pages, 2021.

Retraction

Retracted: Mst2 Overexpression Inhibits Thyroid Carcinoma Growth and Metastasis by Disrupting Mitochondrial Fitness and Endoplasmic Reticulum Homeostasis

Journal of Oncology

Received 10 October 2023; Accepted 10 October 2023; Published 11 October 2023

Copyright © 2023 Journal of Oncology. This is an open access article distributed under the Creative Commons Attribution License, which permits unrestricted use, distribution, and reproduction in any medium, provided the original work is properly cited.

This article has been retracted by Hindawi following an investigation undertaken by the publisher [1]. This investigation has uncovered evidence of one or more of the following indicators of systematic manipulation of the publication process:

- (1) Discrepancies in scope
- (2) Discrepancies in the description of the research reported
- (3) Discrepancies between the availability of data and the research described
- (4) Inappropriate citations
- (5) Incoherent, meaningless and/or irrelevant content included in the article
- (6) Peer-review manipulation

The presence of these indicators undermines our confidence in the integrity of the article's content and we cannot, therefore, vouch for its reliability. Please note that this notice is intended solely to alert readers that the content of this article is unreliable. We have not investigated whether authors were aware of or involved in the systematic manipulation of the publication process.

Wiley and Hindawi regrets that the usual quality checks did not identify these issues before publication and have since put additional measures in place to safeguard research integrity.

We wish to credit our own Research Integrity and Research Publishing teams and anonymous and named external researchers and research integrity experts for contributing to this investigation.

The corresponding author, as the representative of all authors, has been given the opportunity to register their agreement or disagreement to this retraction. We have kept a record of any response received.

References

- [1] H. Zhang, X. Qu, L. Han, and X. Di, "Mst2 Overexpression Inhibits Thyroid Carcinoma Growth and Metastasis by Disrupting Mitochondrial Fitness and Endoplasmic Reticulum Homeostasis," *Journal of Oncology*, vol. 2021, Article ID 1262291, 10 pages, 2021.

Retraction

Retracted: Hyperfractionation versus Conventional Fractionation of Preoperative Intensity-Modulated Radiotherapy with Oral Capecitabine in Locally Advanced Mid-Low Rectal Cancer: A Propensity Score Matching Study

Journal of Oncology

Received 11 July 2023; Accepted 11 July 2023; Published 12 July 2023

Copyright © 2023 Journal of Oncology. This is an open access article distributed under the Creative Commons Attribution License, which permits unrestricted use, distribution, and reproduction in any medium, provided the original work is properly cited.

This article has been retracted by Hindawi following an investigation undertaken by the publisher [1]. This investigation has uncovered evidence of one or more of the following indicators of systematic manipulation of the publication process:

- (1) Discrepancies in scope
- (2) Discrepancies in the description of the research reported
- (3) Discrepancies between the availability of data and the research described
- (4) Inappropriate citations
- (5) Incoherent, meaningless and/or irrelevant content included in the article
- (6) Peer-review manipulation

The presence of these indicators undermines our confidence in the integrity of the article's content and we cannot, therefore, vouch for its reliability. Please note that this notice is intended solely to alert readers that the content of this article is unreliable. We have not investigated whether authors were aware of or involved in the systematic manipulation of the publication process.

Wiley and Hindawi regrets that the usual quality checks did not identify these issues before publication and have since put additional measures in place to safeguard research integrity.

We wish to credit our own Research Integrity and Research Publishing teams and anonymous and named external researchers and research integrity experts for contributing to this investigation.

The corresponding author, as the representative of all authors, has been given the opportunity to register their agreement or disagreement to this retraction. We have kept a record of any response received.

References

- [1] C. Shi, Y. Zhang, Y. Li et al., "Hyperfractionation versus Conventional Fractionation of Preoperative Intensity-Modulated Radiotherapy with Oral Capecitabine in Locally Advanced Mid-Low Rectal Cancer: A Propensity Score Matching Study," *Journal of Oncology*, vol. 2022, Article ID 9119245, 10 pages, 2022.

Retraction

Retracted: TMEM60 Promotes the Proliferation and Migration and Inhibits the Apoptosis of Glioma through Modulating AKT Signaling

Journal of Oncology

Received 12 January 2023; Accepted 12 January 2023; Published 23 January 2023

Copyright © 2023 Journal of Oncology. This is an open access article distributed under the Creative Commons Attribution License, which permits unrestricted use, distribution, and reproduction in any medium, provided the original work is properly cited.

Journal of Oncology has retracted the article titled “TMEM60 Promotes the Proliferation and Migration and Inhibits the Apoptosis of Glioma through Modulating AKT Signaling” [1] due to concerns that the peer review process has been compromised.

Following an investigation conducted by the Hindawi Research Integrity team [2], significant concerns were identified with the peer reviewers assigned to this article; the investigation has concluded that the peer review process was compromised. We therefore can no longer trust the peer review process, and the article is being retracted with the agreement of the Chief Editor.

The authors do not agree to the retraction.

References

- [1] J. Wu, X. Tang, X. Yu et al., “TMEM60 Promotes the Proliferation and Migration and Inhibits the Apoptosis of Glioma through Modulating AKT Signaling,” *Journal of Oncology*, vol. 2022, Article ID 9913700, 11 pages, 2022.
- [2] L. Ferguson, “Advancing Research Integrity Collaboratively and with Vigour,” 2022, <https://www.hindawi.com/post/advancing-research-integrity-collaboratively-and-vigour>.

Retraction

Retracted: Identification of the Novel Methylated Genes' Signature to Predict Prognosis in INRG High-Risk Neuroblastomas

Journal of Osteoporosis

Received 30 November 2022; Accepted 30 November 2022; Published 28 December 2022

Copyright © 2022 Journal of Oncology. This is an open access article distributed under the Creative Commons Attribution License, which permits unrestricted use, distribution, and reproduction in any medium, provided the original work is properly cited.

Journal of Oncology has retracted the article titled “Identification of the Novel Methylated Genes' Signature to Predict Prognosis in INRG High-Risk Neuroblastomas” [1] due to concerns that the peer review process has been compromised.

Following an investigation conducted by the Hindawi Research Integrity team [2], significant concerns were identified with the peer reviewers assigned to this article; the investigation has concluded that the peer review process was compromised. We therefore can no longer trust the peer review process, and the article is being retracted with the agreement of the Chief Editor.

The authors agree to the retraction.

References

- [1] Z. Liu and C. Li, “Identification of the Novel Methylated Genes' Signature to Predict Prognosis in INRG High-Risk Neuroblastomas,” *Journal of Oncology*, vol. 2021, Article ID 1615201, 10 pages, 2021.
- [2] L. Ferguson, “Advancing Research Integrity Collaboratively and with Vigour,” 2022, <https://www.hindawi.com/post/advancing-research-integrity-collaboratively-and-vigour/>.

Retraction

Retracted: DNA Damage Response Genes in Osteosarcoma

Journal of Osteoporosis

Received 12 November 2022; Accepted 12 November 2022; Published 15 December 2022

Copyright © 2022 Journal of Oncology. This is an open access article distributed under the Creative Commons Attribution License, which permits unrestricted use, distribution, and reproduction in any medium, provided the original work is properly cited.

Journal of Oncology has retracted the article titled “DNA Damage Response Genes in Osteosarcoma” [1] due to concerns that the peer review process has been compromised.

Following an investigation conducted by the Hindawi Research Integrity team [2], significant concerns were identified with the peer reviewers assigned to this article; the investigation has concluded that the peer review process was compromised. We therefore can no longer trust the peer review process, and the article is being retracted with the agreement of the Chief Editor.

References

- [1] Y. Tang, Y.-X. Liu, X. Huang, and P. Li, “DNA Damage Response Genes in Osteosarcoma,” *Journal of Oncology*, vol. 2021, Article ID 9365953, 9 pages, 2021.
- [2] L. Ferguson, “Advancing Research Integrity Collaboratively and with Vigour,” 2022, <https://www.hindawi.com/post/advancing-research-integrity-collaboratively-and-vigour/>.

Retraction

Retracted: Hyperfractionation versus Conventional Fractionation of Preoperative Intensity-Modulated Radiotherapy with Oral Capecitabine in Locally Advanced Mid-Low Rectal Cancer: A Propensity Score Matching Study

Journal of Oncology

Received 11 July 2023; Accepted 11 July 2023; Published 12 July 2023

Copyright © 2023 Journal of Oncology. This is an open access article distributed under the Creative Commons Attribution License, which permits unrestricted use, distribution, and reproduction in any medium, provided the original work is properly cited.

This article has been retracted by Hindawi following an investigation undertaken by the publisher [1]. This investigation has uncovered evidence of one or more of the following indicators of systematic manipulation of the publication process:

- (1) Discrepancies in scope
- (2) Discrepancies in the description of the research reported
- (3) Discrepancies between the availability of data and the research described
- (4) Inappropriate citations
- (5) Incoherent, meaningless and/or irrelevant content included in the article
- (6) Peer-review manipulation

The presence of these indicators undermines our confidence in the integrity of the article's content and we cannot, therefore, vouch for its reliability. Please note that this notice is intended solely to alert readers that the content of this article is unreliable. We have not investigated whether authors were aware of or involved in the systematic manipulation of the publication process.

Wiley and Hindawi regrets that the usual quality checks did not identify these issues before publication and have since put additional measures in place to safeguard research integrity.

We wish to credit our own Research Integrity and Research Publishing teams and anonymous and named external researchers and research integrity experts for contributing to this investigation.

The corresponding author, as the representative of all authors, has been given the opportunity to register their agreement or disagreement to this retraction. We have kept a record of any response received.

References

- [1] C. Shi, Y. Zhang, Y. Li et al., "Hyperfractionation versus Conventional Fractionation of Preoperative Intensity-Modulated Radiotherapy with Oral Capecitabine in Locally Advanced Mid-Low Rectal Cancer: A Propensity Score Matching Study," *Journal of Oncology*, vol. 2022, Article ID 9119245, 10 pages, 2022.

Research Article

Hyperfractionation versus Conventional Fractionation of Preoperative Intensity-Modulated Radiotherapy with Oral Capecitabine in Locally Advanced Mid-Low Rectal Cancer: A Propensity Score Matching Study

Chen Shi , Yangzi Zhang , Yongheng Li , Jianhao Geng, Xianggao Zhu, Hongzhi Wang, Yong Cai , and Weihu Wang 

Key Laboratory of Carcinogenesis and Translational Research (Ministry of Education/Beijing), Department of Radiation Oncology, Peking University Cancer Hospital and Institute, Beijing 100142, China

Correspondence should be addressed to Yong Cai; caiyongfl@163.com and Weihu Wang; wangweihu88@163.com

Received 25 September 2021; Revised 24 November 2021; Accepted 17 March 2022; Published 11 April 2022

Academic Editor: Alessandro Granito

Copyright © 2022 Chen Shi et al. This is an open access article distributed under the Creative Commons Attribution License, which permits unrestricted use, distribution, and reproduction in any medium, provided the original work is properly cited.

Purpose. In theory, the hyperfractionated radiotherapy can enhance biological effect dose against tumor and alleviate normal tissue toxicity. This study is to assess the efficacy and safety of preoperative hyperfractionated intensity-modulated radiotherapy (IMRT) with oral capecitabine in patients with locally advanced rectal cancer (LARC). **Methods.** We retrospectively screened patients with LARC from January 2015 to June 2016. Patients that received hyperfractionated IMRT or conventional fractionated IMRT were eligible in the hyperfractionation (HF) group or conventional fractionation (CF) group, respectively. The primary outcome was the complete response rate. Secondary outcomes included toxicity, postoperative complications, anus-reservation operation rate, local recurrence and distant metastases rate, overall survival (OS), cancer-specific survival (CSS), and disease-free survival (DFS). **Results.** 335 patients were included in the analysis. The complete response rate for the hyperfractionated and conventional fractionated IMRT was 20.41% vs. 23.47% ($P=0.583$). The anus-reservation operation rate was 68.37% vs. 65.31% ($P=0.649$). There were no cases of grade 4 toxicity during radiotherapy; the rate of grade 3 toxicity and postoperative complications was both comparable between groups. However, in the CF group, more patients had a second operation due to complications (0.0% vs. 5.68%, $P=0.011$). The cumulative local regional recurrence and distant metastases rates of the HF group and CF group were 5.10% vs. 9.18% ($P=0.267$) and 22.45% vs. 24.49% ($P=0.736$), respectively. The 5-year OS, CSS, and DFS in the HF group and CF group were 86.45% vs. 73.30% ($P=0.503$), 87.34% vs. 75.23% ($P=0.634$), and 70.80% vs. 68.11% ($P=0.891$), respectively. **Conclusions.** The preoperative hyperfractionated IMRT with oral capecitabine, with an acceptable toxicity and favorable response and survival, could reduce the rate of secondary surgery.

1. Introduction

Rectal cancer, one of the most common malignant tumors, is usually occult in onset. Most rectal cancer patients have locally advanced or advanced-stage disease at the time of diagnosis. As the living standards improved in the recent years in China, so has the incidence of rectal cancer, while the age of onset has decreased [1]. As a result, exploring best

modes of rectal cancer treatment has been considered a priority.

Preoperative concurrent radiochemotherapy followed by total mesorectal excision (TME) surgery has become the standard treatment for patients with locally advanced rectal cancer (LARC) [2–5]. As for the choice of synchronized chemotherapy regimen, studies have demonstrated that oral fluoropyrimidine, capecitabine, may be as effective as

intravenous 5-FU in neoadjuvant treatment of LARC, with the added advantage of oral administration [6, 7].

Over the years, intensity-modulated radiotherapy (IMRT) is increasingly used to treat gross tumor with greater accuracy and lower risk of damage to normal tissue, compared to three-dimensional conformal radiotherapy (3DCRT) [8]. Since 2007, our center has adopted conventional fractionated concomitant boost IMRT (2.3 Gy/f for primary tumor and 1.9 Gy/f for pelvic lymphatic drainage areas, 50.6 Gy and 41.8 Gy in 22 fractions, a single fraction per day) combined with capecitabine for preoperative chemoradiotherapy in locally advanced, resectable mid-low primary rectal cancer patients [9]. To date, over 800 patients have been treated with this strategy, which is associated with favorable efficacy and tolerable toxicity.

From a radiobiological perspective, the hyperfractionated radiotherapy has such characteristics as shortened time of total dose to be given and higher relative biological effectiveness. What is more, it does not increase normal tissue damage due to the lower dose of a single radiotherapy and the ability to give adequate repair time to normal tissue. Rectal cancer is a moderately sensitive tissue for radiotherapy, in which the hyperfractionated radiotherapy may provide comparable or improved local control with favorable tolerance.

Therefore, the combination of hyperfractionated radiotherapy and concomitant boost IMRT technology may further improve the pathological complete response (ypCR) rate and local control, while it does not increase the damage of normal tissue. Little research on the preoperative hyperfractionated IMRT in LARC patients has been published to date. This study was aimed at assessing the efficacy and safety of hyperfractionated IMRT, compared to conventional fractionated, with concomitant boost technique with capecitabine in LARC.

2. Materials and Methods

2.1. Patients. This is a historical cohort study, which retrospectively recruited patients with locally advanced, resectable mid-low primary adenocarcinoma of the rectum who had undergone preoperative IMRT from January 2015 to June 2016 in our center. This trial was approved by a relevant ethics committee, according to the Helsinki Declaration. All patients had given informed consent for chemoradiotherapy or for surgery before treatment.

Pretreatment evaluation included medical history, physical examination, complete laboratory tests, and preoperative staging. Complete laboratory tests included complete blood counts, urine and stool analysis, liver and kidney function tests, and gastrointestinal tumor markers. Preoperative staging included total colonoscopy, pelvic magnetic resonance imaging (MRI) scans or endoscopic ultrasound (EUS) combined with pelvic computed tomography (CT) scans, and chest and abdominal CT scans. In cases of staging discrepancy between the two modalities, the higher stage was recorded, following the guidelines from the seventh edition of the TNM staging standard of American Joint Committee on Cancer (AJCC).

2.2. Inclusion Criteria. All patients had histologically confirmed primary rectal adenocarcinoma, within 10 cm from the anal verge, with no evidence of distant metastases. The T/N classification was stage T3 or resectable T4 (R0 or R1 resection deemed possible) with any N, or any T with N1 or N2 disease. Patients presenting with T2N0 tumors located within 5 cm from the anal verge were also included. The age at diagnosis was between 18 and 80 years. Patients were required to have an Eastern Collaborative Oncology Group (ECOG) performance status of 0, 1, or 2, with adequate liver, kidney, and bone marrow function.

2.3. Exclusion Criteria. Patients with history of chemotherapy, surgery, pelvic radiation, or any other antitumor therapy were excluded. Patients with history of another malignancy within 5 years were also excluded. Other exclusion criteria included acute obstructive symptoms, unresectable disease with radical radiotherapy dose, or any serious comorbidities precluding chemoradiotherapy and surgery.

2.4. Treatment. All patients received preoperative concomitant boost IMRT combined with capecitabine. Patients underwent CT-based simulation with 5 mm slices in the supine position with a full bladder [10, 11]. An MRI scan was simultaneously performed to accurately define the extent of the tumor if without taboo. These scans extended from the upper edge of L4 vertebrae to below the perineum. Intravenous contrast was used. And a custom immobilization device was used to minimize setup variability. Daily patient positioning was performed using skin marks and weekly cone-beam CT (CBCT). The gross target volumes (GTV) and clinical target volumes (CTV) were contoured on the axial CT/MRI fusion scan slices. GTV was defined as primary rectal tumor and involved lymph nodes. The CTV was defined as primary tumor, mesorectal region, presacral region, mesorectal lymph nodes, lateral lymph nodes, internal iliac lymph node chain, and pelvic wall area [12]. The external iliac lymph nodes and inguinal lymph nodes were considered part of the CTV when these lymph nodes were involved. The superior border of pelvic fields was the L5–S1 interspace, and the inferior border was the bottom of the obturator foramen, or the anal verge for low-lying tumors [9]. The radiation dose was prescribed for planning gross target volumes (PGTV) and planning target volumes (PTV) by adding a 5 mm margin to the GTV and CTV, respectively. The boost to the primary tumor (GTV) was administered synchronously with the whole pelvis (CTV) radiotherapy. The 95% isodose line was planned to encompass the 95% PGTV and PTV as a planning objective. Five-field dynamic IMRT technique was used to shape the fields.

Patients eligible for hyperfractionation (HF) group received hyperfractionated IMRT with 2 dose levels simultaneously: 95% PGTV 51 Gy and 95% PTV 40.8 Gy in 34 fractions, 1.5 Gy and 1.2 Gy per fraction, 2 fractions with at least 8 hours interval per day. Treatment was delivered 5 times per week, over 23 days. In conventional fractionation (CF) group (control group), the patients received conventional fractionated IMRT with 2 dose levels simultaneously: 95%

PGTV 50.6 Gy and 95% PTV 41.8 Gy in 22 fractions, 2.3 Gy and 1.9 Gy per fraction, a single fraction per day. Treatment was delivered 5 times per week, over 30 days.

The small bowel, bladder, and femoral heads were contoured and designated as organs at risk. Bladder constraints were $V50 \leq 35$ Gy and $V5 \leq 50$ Gy. Small bowel constraints were such that no more than 120 cm³ of the volume should receive more than 15 Gy, no more than 80 cm³ should receive more than 45 Gy, and no more than 20 cm³ should receive more than 50 Gy [13]. The constraints of femoral head were $V50 \leq 30$ Gy and $V5 \leq 50$ Gy⁹.

Capecitabine was administered at 825 mg/m² orally twice daily, 5 days per week, during radiotherapy [7].

All patients underwent reassessment of clinical staging and resectability 6–8 weeks after completion of chemoradiotherapy. Patients with resectable tumors received TME surgery. As per the Habr-Gama and Memorial Sloan-Kettering Cancer Center (MSKCC) criteria, patients with clinical complete response (cCR) or near cCR could choose radical surgery, transanal local resection, or the “wait and see” strategy [14, 15]. The last category of patients was subject to regular follow-up, and remedial surgery was performed if local tumor regeneration occurred.

The choice between abdominoperineal resection and anterior resection was left to the discretion of the attending surgeon. Patients with low rectal cancer (defined as ≤ 5 cm from the anal verge) undergoing sphincter-preserving surgery also received prophylactic ileostomy.

Administration of adjuvant chemotherapy was individualized. The regimen of capecitabine or CapeOX for 4–6 months was both for recommendations [16–18].

2.5. Follow-Up. All patients were evaluated weekly for adverse events during chemoradiotherapy. Toxicities were analyzed according to the criteria for acute radiation injury of the Radiation Therapy Oncology Group (RTOG) and Common Terminology Criteria for Adverse Events (CTCAE), version 4.0.

Following antitumor treatments, patients were evaluated every 3 months for the first year, every 6 months for the second and third year, and annually for the fourth and fifth years. Posttreatment follow-up included measurement of complete blood counts, liver and kidney function tests, and gastrointestinal tumor markers, as well as total colonoscopy, chest X-ray or CT scans, abdominal ultrasound or CT scans, and pelvic CT or MRI scans.

2.6. Study Endpoints. The primary endpoint was tumor complete response rate, including ypCR and cCR rate. The secondary endpoints included toxicity, postoperative complications, R0 resection rate, sphincter-preserving surgery rate, downstaging rate, tumor response grading (TRG), local recurrence rate, distant metastasis rate, overall survival (OS), cancer-specific survival (CSS), and disease-free survival (DFS).

The TRG system was recommended by the National Comprehensive Cancer Network (NCCN) Guideline version 2.2019 Rectal Cancer modified from Ryan et al. [19–21]. The OS was defined as the time from the diagnosis of rectal can-

cer to the date of death from any cause or to last follow-up appointment. The CSS was defined as the time from diagnosis to rectal cancer-related death. The DFS time was defined as the time from diagnosis to the occurrence of local recurrence or any form of distant metastasis. Local regeneration after nonsurgical strategy or partial resection, which could undergo salvage radical resection, was not considered a regional recurrence and not counted as a positive event.

2.7. Statistical Analysis. Statistical analysis was performed with STATA version 13.0. Quantitative data were compared using independent sample *t*-tests or Wilcoxon rank-sum tests, based on the distribution of the variables. The chi-square test was used to compare the differences between the classification groups. We used the Kaplan–Meier method to estimate the OS, CSS, and DFS. The log-rank test was used to test for statistical significance. All statistical tests were two-tailed, and the *P* value < 0.05 was considered statistically significant.

2.8. Propensity Score Matching. The clinically important factors and variables associated with complete response rate as indicated in univariate Cox models (*P* < 0.10) were used for calculating propensity score matching (PSM). The covariates included were age, gender, BMI, comorbidities, history of smoking and drinking, ECOG scores, tumor gross and histopathologic types, the distance from the anal verge, clinical T and N stage, the status of mesorectal fascia (MRF), and extramural venous invasion (EMVI) (yes/no).

3. Results

In total, 335 patients were included. There were significantly more patients with ECOG 2 (0.76% vs. 1.96%, *P* = 0.001) and MRF involvement (12.31% vs. 25.98%, *P* = 0.003) in the control group. In the 196 matched pairs of patients generated by the PSM, all variables were well balanced between groups (Table 1, all *P* values > 0.05).

3.1. Toxicity during Chemoradiation. All patients received concurrent radiochemotherapy. The rate of radiotherapy and chemotherapy completion in the HF group and CF group was 98.47% vs. 98.52% (*P* > 0.999) and 96.95% vs. 97.06% (*P* > 0.999), respectively. All patients underwent toxicity evaluation. There were no cases of grade 4 toxicity in either group. Grade 3 toxicities included leukopenia [2 (1.53%) vs. 3 (1.47%), *P* = 0.988], neutropenia [2 (1.53%) vs. 2 (0.98%), *P* = 0.650], diarrhea [2 (1.53%) vs. 2 (0.98%), *P* = 0.650], and radiation proctitis [3 (2.29%) vs. 2 (0.98%), *P* = 0.383]. The rates of grade 1–2 toxicities were also comparable between the two groups (Table S1, all *P* values > 0.05).

3.2. Surgical Procedure and Complications. In the HF group, 113 patients underwent radical surgery and 4 patients with cCR selected “wait and see” strategy. In the CF group, 179 patients underwent surgery and 3 patients with cCR selected observation. Surgery was performed after a median interval of 67 days (41–127 days) and 64 days (37–148 days) in the HF group and CF group, respectively (*P* = 0.872). Among the patients who underwent surgery, 113 and 178 patients

TABLE 1: Baseline characteristics by preoperative IMRT cohort.

Variable	Overall population		P	Matched cohorts		P
	HF n = 131 (%)	CF n = 204 (%)		HF n = 98 (%)	CF n = 98 (%)	
<i>Age (years)</i>			0.219			0.702
≤40	9 (6.87)	6 (2.94)		7 (7.14)	5 (5.10)	
41-65	93 (70.99)	147 (72.06)		66 (67.35)	71 (72.45)	
≥65	29 (22.14)	51 (25.00)		25 (25.51)	22 (22.45)	
<i>Gender</i>			0.388			0.881
Male	87 (66.41)	126 (61.76)		63 (64.29)	64 (65.31)	
Female	44 (33.59)	78 (28.24)		35 (35.71)	34 (24.69)	
<i>BMI</i>			0.352*			0.975*
<18.5	4 (3.05)	5 (2.45)		3 (3.06)	4 (4.08)	
18.5-23.9	70 (53.44)	86 (42.16)		51 (52.04)	47 (47.96)	
24-26.9	33 (25.19)	63 (30.88)		27 (27.55)	28 (28.57)	
27-29.9	14 (10.69)	30 (14.71)		11 (11.22)	14 (14.29)	
≥30	3 (2.29)	10 (4.90)		3 (3.06)	3 (3.06)	
NA	7 (5.34)	10 (4.90)		3 (3.06)	2 (2.04)	
<i>Comorbidities</i>						
Hypertension	36 (27.48)	64 (31.37)	0.448	29 (29.59)	30 (30.61)	0.876
Diabetes	16 (12.21)	35 (17.16)	0.219	12 (12.24)	12 (12.24)	>0.999
CHD	8 (6.11)	9 (4.41)	0.490	3 (3.06)	6 (6.12)	0.497*
Atrial fibrillation	5 (3.82)	4 (1.96)	0.321*	1 (1.02)	2 (2.04)	>0.999*
Cerebrovascular- disease	4 (3.05)	8 (3.92)	0.677	4 (4.08)	3 (3.06)	>0.999*
Abdominal and pelvic surgery history	24 (18.32)	45 (22.06)	0.409	20 (20.41)	20 (20.41)	>0.999
Smoking history	62 (47.33)	92 (46.94)	0.945	44 (44.90)	48 (48.98)	0.567
Drinking history	42 (32.06)	63 (32.14)	0.988	29 (29.59)	40 (40.82)	0.100
<i>ECOG scores</i>			0.001			0.820*
0-1	130 (99.24)	200 (98.04)		97 (98.98)	96 (97.96)	
2	1 (0.76)	4 (1.96)		1 (1.02)	2 (2.04)	
<i>Gross types</i>			0.140*			0.828*
Borrmann I	77 (58.78)	119 (58.33)		59 (60.20)	60 (61.22)	
Borrmann II	29 (22.14)	32 (15.69)		20 (20.41)	17 (17.35)	
Borrmann III	3 (2.29)	2 (0.98)		2 (2.04)	1 (1.02)	
Complex	22 (16.79)	51 (25.00)		17 (17.35)	20 (20.41)	
<i>Histopathologic types</i>			0.262*			0.277*
Well-differentiated	10 (7.63)	9 (4.41)		6 (6.12)	2 (2.04)	
Moderately differentiated	102 (77.86)	161 (78.92)		76 (77.55)	83 (84.69)	
Poorly differentiated	13 (9.92)	16 (7.84)		10 (10.20)	9 (9.18)	
Signet-ring cell	2 (1.53)	4 (1.96)		2 (2.04)	1 (1.02)	
Mucinous adenocarcinoma	3 (2.29)	4 (1.96)		3 (3.06)	0 (0.00)	
Adenocarcinoma	1 (0.76)	10 (4.90)		1 (1.02)	3 (3.06)	
<i>Distance from anal verge</i>			0.553			0.165
≤5 cm	87 (66.41)	129 (63.24)		63 (64.29)	72 (74.37)	
5.1-10 cm	44 (33.59)	75 (36.76)		35 (35.71)	26 (26.63)	
<i>cT stage</i>			0.988*			0.248*
T2	4 (3.05)	6 (2.94)		2 (2.04)	2 (2.04)	
T3	99 (75.57)	151 (74.02)		72 (73.47)	83 (84.69)	
T4a	22 (16.79)	37 (18.14)		19 (19.39)	11 (11.22)	
T4b	6 (4.58)	10 (4.90)		5 (5.10)	2 (2.04)	

TABLE 1: Continued.

Variable	Overall population		P	Matched cohorts		P
	HF n = 131 (%)	CF n = 204 (%)		HF n = 98 (%)	CF n = 98 (%)	
<i>cN stage</i>			0.198*			>0.999*
N0	6 (4.58)	4 (1.96)		4 (4.08)	3 (3.06)	
N1-2	125 (95.42)	200 (98.04)		94 (95.92)	95 (96.94)	
<i>MRF+</i>	16 (12.31)	53 (25.98)	0.003	15 (15.31)	12 (12.24)	0.534
<i>EMVI+</i>	10 (7.69)	8 (3.92)	0.137	8 (8.16)	5 (5.10)	0.389

Abbreviations: IMRT = intensity-modulated radiotherapy; HF = hyperfractionation; CF = conventional fractionation; BMI = body mass index; CHD = coronary heart disease; ECOG = Eastern Collaborative Oncology Group; c = clinical; MRF = mesorectal fascia; EMVI = extramural venous invasion. * Fisher's exact.

of the HF group and CF group had R0 resection (113/113 [100.00%] vs. 178/179 [99.44%], $P = 0.788$), respectively. The rates of sphincter preservation operation in the HF group and CF group were 64.60% and 60.89%, respectively ($P = 0.524$). Among the 181 patients with low rectal cancer (≤ 5 cm from anal verge) who underwent surgery, 90 patients received sphincter-preserving surgery with prophylactic ileostomy. The sphincter preservation operation rate for the low rectal in the HF group and CF group was 50.70% (36 out of 71) and 49.09% (54 out of 110), respectively ($P = 0.832$). In matched cohorts, there were also no statistical differences in the rate of radical surgery, R0 resection, and anus-reservation operation between the two groups (Table 2 (all P values > 0.05)).

Among patients who received surgery, 28 (24.78%) and 44 (24.58%) patients of the HF group and CF group, respectively, developed postoperative complications ($P = 0.970$). However, the CF group had a higher rate of secondary surgery due to postoperative complications (0/113 [0.0%] vs. 8/179 [4.47%], $P = 0.019$). In matched cohorts, the control group still had a higher rate of secondary surgery (0/87 [0.0%] vs. 5/88 [5.68%], $P = 0.011$) (Table 2).

3.3. Tumor Response. Twenty-four and thirty-seven patients in the hyperfractionation and control group, respectively, acquired tumor complete remission (18.32% vs. 18.14%, odds ratio [OR] = 1.012, 95% confidence interval [CI] 0.574-1.787). In 196 patients selected through the PSM, the rates of tumor complete remission in the HF group and CF group were 20.41% vs. 23.47%, respectively (OR = 0.736, 95% CI 0.313-1.295).

According to the NCCN-TRG system, there were 20, 38, 52, 3 and 34, 60, 80, 5 patients with a score of 0, 1, 2, and 3, respectively, in the HF group and CF group, without significant difference. The primary tumor and lymph nodes downstaging rate of the HF group and CF group were 68.70% vs. 66.18% and 78.63% vs. 79.90%, respectively (P values > 0.05). In matched cohorts, there were also no differences in the T or N downstaging rates between the groups (Table 3).

3.4. Relapse and Survival. Up to November 2020, the median follow-up was 42.0 months in the hyperfractionation group

(range 3.9–72.1 months) and 45.8 months in the control group (range 3.8–70.2 months) ($P = 0.322$).

To date, cumulatively, there were 6 locoregional relapses and 28 systemic relapses in the hyperfractionation group and 22 locoregional relapses and 49 systemic relapses in the control group. Hyperfractionated RT showed a lower local recurrence rate (4.58% vs. 10.78%, $P = 0.045$). However, in matched cohort, hyperfractionated RT did not show this advantage of local control. Besides, there were no differences between the matched cohorts on distant metastasis rate. The 5-year DFS of the HF group and CF group was 70.27% vs. 68.99% (hazard ratio [HR] = 0.889, 95% CI 0.570-1.386) (Table 4).

During the follow-up, 14 and 29 patients, respectively, in the HF group and CF group, have died. The 5-year OS of the HF group and CF group was 78.40% vs. 81.32% (HR = 0.875, 95% CI 0.461-1.662). The 5-year CSS of the HF group and CF group was 79.93% vs. 82.94% (HR = 0.843, 95% CI 0.424-1.676) (Table 4).

In matched cohorts, the 5-year OS, CSS, and DFS between the two groups were 86.45% vs. 73.30% (HR = 0.763, 95% CI 0.594-2.885), 87.34% vs. 75.23% (HR = 0.815, 95% CI 0.529-2.845), and 70.80% vs. 68.11% (HR = 0.962, 95% CI 0.602-1.791), respectively (Table 4 and Figure 1). There were no statistically significant differences in the survival rates between groups.

4. Discussion

Preoperative concurrent radiochemotherapy based on capecitabine followed with TME surgery has become the standard treatment for patients with LARC [2–5]. However, the specific implementation of the radiotherapy process, covering the choice of radiotherapy technology and the segmentation mode of radiotherapy dose, is varied between different centers. With the update of radiotherapy technology, more and more centers use IMRT, which is characterized by increasing accuracy of higher-dose delivery in the tumor area while synchronously reducing the risk of damage to normal tissue, compared to 3DCRT with first pelvic field irradiation and then boosts to the tumor area.

Hyperfractionated radiotherapy, compared to the conventional fractionated radiotherapy, can give similar doses in a shorter period of treatment time and increase the

TABLE 2: Surgical procedure and complications in preoperative IMRT cohort.

Variable	Overall population		P	Matched cohorts		P
	HF n = 131 (%)	CF n = 204 (%)		HF n = 98 (%)	CF n = 98 (%)	
<i>Surgery</i>			0.692			0.817
Yes	113 (86.26)	179 (87.75)		87 (88.78)	88 (89.80)	
No	18 (13.74)	25 (12.25)		11 (11.22)	10 (10.20)	
<i>R0 resection</i>	113/113 (100.00)	178/179 (99.44)	0.788*	87/87 (100.00)	87/88 (98.86)	0.635*
<i>Anus-reservation operation</i>	73/113 (64.60)	109/179 (60.89)	0.524	67/87 (68.37)	64/88 (65.31)	0.649
<i>Complications</i>	28/113 (24.78)	44/179 (24.58)	0.970	21/87 (24.14)	23/88 (26.14)	0.761
Anastomotic fistula/hemorrhage	6/113 (5.31)	11/179 (6.15)	0.766	6/87 (6.90)	6/88 (6.82)	0.984
Rectovesical/rectovaginal fistula	0/113 (0.00)	4/179 (2.23)	0.161*	0/87 (0.00)	3/88 (3.41)	0.246*
Pelvic infection/abscess	5/113 (4.42)	11/179 (6.15)	0.529	5/87 (5.75)	7/88 (7.95)	0.563
Ileus	5/113 (4.42)	12/179 (6.70)	0.418	1/87 (1.15)	5/88 (5.68)	0.211*
Perineal wound infection	8/113 (7.08)	14/179 (7.82)	0.815	8/87 (9.20)	7/88 (7.95)	0.769
Abdominal wound infection	1/113 (0.88)	6/179 (3.35)	0.255*	1/87 (1.15)	4/88 (4.55)	0.368*
Other infections**	5/113 (4.42)	4/179 (2.23)	0.315*	3/87 (3.45)	0/88 (0.00)	0.121*
Other complications***	4/113 (3.54)	4/179 (2.23)	0.715*	1/87 (1.15)	0/88 (0.00)	0.497*
<i>Complication treatments</i>			0.019*			0.011*
Conservative	28/28 (100.00)	36/44 (81.82)		21/21 (100.00)	18/23 (78.26)	
Operative	0/28 (0.00)	8/44 (18.18)		0/21 (0.00)	5/23 (21.74)	

Abbreviations: IMRT = Intensity-modulated radiotherapy; HF = hyperfractionation; CF = conventional fractionation. *Fisher's exact. **Other infections included urinary system infection and pulmonary infection. ***Other complications included lower limb venous thrombosis, pulmonary thromboembolism, and acute myocardium infarction.

TABLE 3: Tumor responses in preoperative IMRT cohort.

Variable	Overall population		P	Matched cohorts		P
	HF n = 131 (%)	CF n = 204 (%)		HF n = 98 (%)	CF n = 98 (%)	
<i>cCR+ypCR</i>	24 (18.32)	37 (18.14)	0.966	20 (20.41)	23 (23.47)	0.583
<i>NCCN-TRG</i>						
TRG 0	20/113 (17.70)	34/179 (18.99)	0.795*	18/87 (20.69)	21/88 (23.86)	0.417*
TRG 1	38/113 (33.63)	60/179 (33.52)		26/87 (29.89)	25/88 (28.41)	
TRG 2	52/113 (46.02)	80/179 (44.69)		40/87 (45.98)	40/88 (45.45)	
TRG 3	3/113 (2.65)	5/179 (2.79)		3/87 (3.45)	2/88 (2.27)	
<i>Downstaging</i>						
Downstaging of primary tumor	90 (68.70)	135 (66.18)	0.631	64 (65.31)	63 (64.29)	0.881
Downstaging of lymph nodes	103 (78.63)	163 (79.90)	0.778	78 (79.59)	81 (82.65)	0.769

Abbreviations: IMRT = intensity-modulated radiotherapy; HF = hyperfractionation; CF = conventional fractionation; cCR = clinical complete response; pCR = pathological complete response; NCCN = National Comprehensive Cancer Network; TRG = tumor regression grading. *Fisher's exact.

relative biologically effective dose (BED) to gross tumor but may not increase normal tissue damage. There are few reports on preoperative hyperfractionated radiotherapy used for LARC. Movsas et al. illustrated the applicability of hyperfractionated radiotherapy in their single-arm studies [22–25]. In LARC, neoadjuvant hyperfractionated radiotherapy showed the favorable local control and OS. However, these studies were in the era of two-dimensional radiotherapy. In Marsh Rde et al.'s single-arm study, patients received preoperative 3DCRT with hyperfractionation and gained favorable

short-term effects with tolerable acute toxicity [26, 27], whereas the sample size of the above two studies were relatively small (17 and 53 cases, respectively).

Another two studies compared preoperative hyperfractionated and conventional fractionated 3DCRT for LARC. In Ceelen et al.'s nonrandomized controlled study, hyperfractionated radiotherapy group showed lower pCR rate and sphincter preservation rate, which may be related to the absence of simultaneous chemotherapy and radiotherapy-surgical interval [28]. But the incidence of

TABLE 4: Tumor relapses and survivals in preoperative IMRT cohort.

Variable	Overall population		OR/HR	95% CI	P	Matched cohorts		OR/HR	95% CI	P
	HF n = 131	CF n = 204				HF n = 98	CF n = 98			
Local recurrence	6 (4.58)	22 (10.78)	0.397	0.157-0.997	0.045	5 (5.10)	9 (9.18)	0.532	0.172-1.648	0.267
Distant metastasis	28 (21.37)	49 (24.02)	0.860	0.508-1.456	0.574	22 (22.45)	24 (24.49)	0.893	0.578-2.170	0.736
Cumulative relapses	30 (22.90)	56 (27.45)	0.785	0.471-1.308	0.352	25 (25.51)	27 (27.55)	0.900	0.477-1.699	0.746
Cumulative death	14 (10.69)	29 (14.22)	0.722	0.366-1.424	0.346	12 (12.24)	13 (13.27)	0.912	0.473-1.845	0.830
Survival										
5-year DFS	70.27%	68.99%	0.889	0.570-1.386	0.604	70.80%	68.11%	0.962	0.602-1.791	0.891
5-year OS	78.40%	81.32%	0.875	0.461-1.662	0.684	86.45%	73.30%	0.763	0.594-2.885	0.503
5-year CSS	79.93%	82.94%	0.843	0.424-1.676	0.626	87.34%	75.23%	0.815	0.529-2.845	0.634

Abbreviations: IMRT = intensity-modulated radiotherapy; HF = hyperfractionation; CF = conventional fractionation; OR = odds ratio; HR = hazard ratio; DFS = disease-free survival; OS = overall survival; CSS = cancer-specific survival.

anastomotic leakage, pelvic recurrence rate, and 5-year OS was not statistically different between the hyper- and conventional fractionation groups. In another study, the only randomized controlled trial, RTOG-0012 study, showed that concurrent hyperfractionated (45.6 Gy in 38 fractions, 1.2 Gy per fraction, 2 fractions per day) and 5-FU chemoradiotherapy had a higher pCR rate than conventional fractionated (45.0 Gy in 25 fractions, 1.8 Gy per fraction, 1 fraction per day) chemoradiotherapy (30% vs. 26%) while lower 5-year OS and DFS (61% vs. 75% and 78% vs. 85%). But for T4 disease, the hyperfractionated group showed a higher 5-year DFS (87.5% vs. 71.4%). In addition to favorable short-term effect and survival, 3-4 grade nonhematologic radiochemotherapy acute toxicity in hyperfractionated group was relatively slight (38% vs. 45%) [29, 30].

In a word, hyperfractionation is feasible in neoadjuvant radiotherapy of LARC. However, little research on the hyperfractionated IMRT has been published to date. To the best of the authors' knowledge, the present study is the biggest comparison of hyperfractionated and conventional fractionated concomitant boost IMRT in LARC. In this study, except RT fractionation, other treatment regimens, including concurrent chemotherapy, radiotherapy-surgical interval, and operation principle, were concordant.

According to the computational formula of the BED ($BED = n * d * [1 + d/\alpha/\beta \text{ value}] - \gamma/\alpha * [T - Tk]$, where n is as number of fractions, d is as dose of per fraction, α/β value of tumor is considered 10 and of normal tissues is considered 3, γ/α represents repair rate always considered 0.6 Gy per day, T represents total days of radiotherapy regimen, and Tk represents days of delayed proliferation always considered 7 days), the hyperfractionation RT slightly increased the BED value of primary tumor (49.1 Gy vs. 48.4 Gy) and significantly reduced the BED value of normal tissues in the target area (43.3 Gy vs. 50.1 Gy). As a result, the hyperfractionated IMRT described in this study may reduce normal tissue damage while ensuring treatment efficacy.

The results of this study, including rate of complete remission and 5-year DFS, were consistent with the results of RTOG-0012 study. What is more, our findings show bet-

ter 5-year OS and fewer side effects of radiotherapy. In a word, in this study, the hyperfractionated and conventional fractionated preoperative concomitant boost IMRT both showed favorable safety and effectiveness in LARC. But there were no statistically significant differences between groups in this study of the tumor response rate, likelihood of complete remission, downstaging, R0 resection, or sphincter preservation. Among the 335 eligible patients, patients who received hyperfractionation IMRT showed lower cumulative local recurrence rate. Nevertheless, in the matched cohort, this result was not withstanding. These results about recurrence may be related to the more patients with MRF involvement in the control group before match. Anyhow, both RT fractionation regimens showed favorable tumor outcomes in this study, as evidenced by comparable survival rates.

Moreover, this study showed that in terms of acute radiotherapy toxicity, these two RT regimens were comparable. However, in patients who had postoperative complications, the conventional fractionation group had a higher rate of secondary surgery. The postoperative complications that need surgical treatment, such as anastomotic fistula or hemorrhage, rectovesical or rectovaginal fistula, or ileus, of which the events number in their CF group were always higher than that in the HF group (Table 2), tend to correlate with radiation target volume delivered to adjacent normal tissues. The lower risk of secondary surgery was consistent with the reduced BED of organs at risk in hyperfractionated group. Overall, hyperfractionation IMRT might be less likely to cause serious surgical complications in LARC than the conventional fractionation IMRT.

In addition, the hyperfractionated radiotherapy, which shortens the total number of treatment days (23 vs. 30 days), may have additional advantages in terms of public health economics. Among the daily admissions to our hospital, about 70% of patients are from other provinces, who always pay a lot for extra living expenses including room and board, hotel fees, and transportation costs. For these patients, shortened treatment days always means reduced living expenses. On the other hand, referring to the national charging standard, the cost of hyperfractionated radiotherapy (IMRT)

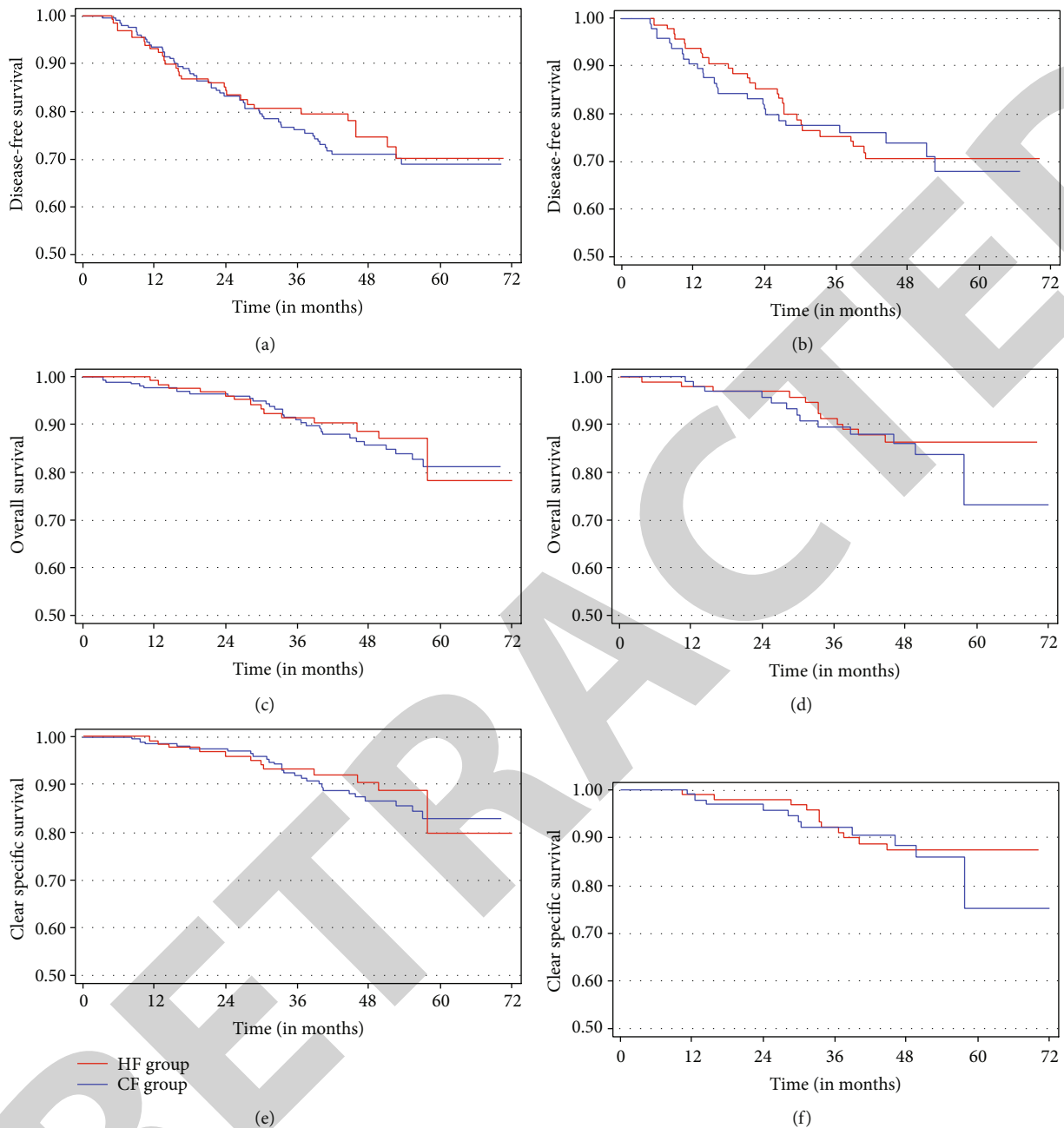


FIGURE 1: DFS, OS, and CSS curves in preoperative IMRT cohort. (a) DFS in overall population ($n = 335$); (b) DFS in matched cohorts ($n = 196$); (c) OS in overall population ($n = 335$); (d) OS in matched cohorts ($n = 196$); (e) CSS in overall population ($n = 335$); and (f) CSS in matched cohorts ($n = 196$). Abbreviations: DFS = disease-free survival; OS = overall survival; CSS = cancer-specific survival; IMRT = intensity-modulated radiotherapy; HF = hyperfractionation; CF = conventional fractionation.

does not increase too much because of the capped fee for 24-fractionated radiotherapy, even if the actual fractionations of radiotherapy are more than 24.

All in all, the evidence this paper presented may provide an appropriate option for the clinical practice of LARC in the field of radiation oncology. We believe that our study makes a significant contribution to the literature because little research on the combination of hyperfractionated radiotherapy and concomitant boost IMRT technology in LARC patients has been published to date.

Of course, this study has several limitations. Firstly, it was a retrospective study in which the information bias was inevitable. Secondly, we did not assess the long-term complications of radiotherapy or the differences in the quality of life of patient subject to different treatments. Next, the effect of adjuvant chemotherapy on recurrence, metastasis, and survival was also not assessed. Besides, according to literature data, extranodal extension (ENE) of nodal metastasis has emerged as an important prognostic factor in rectal cancer. However, whether the presence of ENE in patients with

rectal cancer who receive preoperative chemoradiotherapy has impact on survival outcome is controversial [31, 32]. In this study, due to the lack of pathological findings of ENE in the lymph node metastasis after neoadjuvant chemoradiotherapy, we could not further determine whether ENE was an additional prognostic factor between the HF and CF group.

5. Conclusion

The hyperfractionated preoperative concomitant boost IMRT may be associated with favorable response and survival and reduced rate of secondary surgery due to postoperative complications compared to conventional therapy in LARC. It may be an appropriate option for these out-of-town patients who require cost savings.

Data Availability

The datasets used and/or analyzed during the current study are available from the corresponding author on reasonable request.

Conflicts of Interest

The authors declare that they have no competing interests.

Authors' Contributions

Yong Cai and Weihua Wang were responsible for the conception, study design, and manuscript revision. Chen Shi was responsible for statistical analyses and manuscript writing. Yangzi Zhang, Jianhao Geng, and Hongzhi Wang were responsible for the follow-up and acquisition of data. Yongheng Li and Xianggao Zhu supervised the study. Chen Shi and Yangzi Zhang contributed equally to this work as the first authors. All authors read and approved the final manuscript.

Acknowledgments

This work was supported by the Beijing Municipal Science & Technology Commission (No. Z181100001718192); Science Foundation of Peking University Cancer Hospital (No. 18-03); and National Natural Science Foundation (No. 82073333).

Supplementary Materials

Table S1: toxicity during chemoradiation in preoperative IMRT cohort. Abbreviations: IMRT = intensity-modulated radiotherapy; HF = hyperfractionation; CF = conventional fractionation. (*Supplementary Materials*)

References

- [1] W. Chen, R. Zheng, P. D. Baade et al., "Cancer statistics in China, 2015," *CA: a Cancer Journal for Clinicians*, vol. 66, no. 2, pp. 115–132, 2016.
- [2] R. Sauer, H. Becker, W. Hohenberger et al., "Preoperative versus postoperative chemoradiotherapy for rectal cancer," *The New England Journal of Medicine*, vol. 351, no. 17, pp. 1731–1740, 2004.
- [3] R. Sauer, T. Liersch, S. Merkel et al., "Preoperative versus postoperative chemoradiotherapy for locally advanced rectal cancer: results of the German CAO/ARO/AIO-94 randomized phase III trial after a median follow-up of 11 years," *Journal of Clinical Oncology*, vol. 30, no. 16, pp. 1926–1933, 2012.
- [4] D. Sebag-Montefiore, R. J. Stephens, R. Steele et al., "Preoperative radiotherapy versus selective postoperative chemoradiotherapy in patients with rectal cancer (MRC CR07 and NCIC-CTG C016): a multicentre, randomised trial," *Lancet*, vol. 373, no. 9666, pp. 811–820, 2009.
- [5] M. S. Roh, L. H. Colangelo, M. J. O'Connell et al., "Preoperative multimodality therapy improves disease-free survival in patients with carcinoma of the rectum: NSABP R-03," *Journal of Clinical Oncology*, vol. 27, no. 31, pp. 5124–5130, 2009.
- [6] R. D. Hofheinz, F. Wenz, S. Post et al., "Chemoradiotherapy with capecitabine versus fluorouracil for locally advanced rectal cancer: a randomised, multicentre, non-inferiority, phase 3 trial," *The Lancet Oncology*, vol. 13, no. 6, pp. 579–588, 2012.
- [7] M. J. O'Connell, L. H. Colangelo, R. W. Beart et al., "Capecitabine and oxaliplatin in the preoperative multimodality treatment of rectal cancer: surgical end points from National Surgical Adjuvant Breast and Bowel Project trial R-04," *Journal of Clinical Oncology*, vol. 32, no. 18, pp. 1927–1934, 2014.
- [8] A. Ballonoff, B. Kavanagh, M. McCarter et al., "Preoperative capecitabine and accelerated intensity-modulated radiotherapy in locally advanced rectal cancer: a phase II trial," *American Journal of Clinical Oncology*, vol. 31, no. 3, pp. 264–270, 2008.
- [9] J. L. Li, J. F. Ji, Y. Cai et al., "Preoperative concomitant boost intensity-modulated radiotherapy with oral capecitabine in locally advanced mid-low rectal cancer: a phase II trial," *Radiotherapy and Oncology*, vol. 102, no. 1, pp. 4–9, 2012.
- [10] A. S. Allal, S. Bischof, and P. Nouet, "Impact of the "bello board" device on treatment reproducibility in preoperative radiotherapy for rectal cancer," *Strahlentherapie und Onkologie*, vol. 178, no. 5, pp. 259–262, 2002.
- [11] J. C. Lin, J. T. Tsai, L. J. Chen, M. H. Li, and W. H. Liu, "Compared planning dosimetry of TOMO, VMAT and IMRT in rectal cancer with different simulated positions," *Oncotarget*, vol. 8, no. 26, pp. 42020–42029, 2017.
- [12] S. Roels, W. Duthoy, K. Haustermans et al., "Definition and delineation of the clinical target volume for rectal cancer," *International Journal of Radiation Oncology • Biology • Physics*, vol. 65, no. 4, pp. 1129–1142, 2006.
- [13] K. L. Baglan, R. C. Frazier, D. Yan, R. R. Huang, A. A. Martinez, and J. M. Robertson, "The dose-volume relationship of acute small bowel toxicity from concurrent 5-FU-based chemotherapy and radiation therapy for rectal cancer," *International Journal of Radiation Oncology • Biology • Physics*, vol. 52, no. 1, pp. 176–183, 2002.
- [14] A. Habr-Gama, R. O. Perez, G. Wynn, J. Marks, H. Kessler, and J. Gama-Rodrigues, "Complete clinical response after neoadjuvant chemoradiation therapy for distal rectal cancer: characterization of clinical and endoscopic findings for standardization," *Diseases of the Colon and Rectum*, vol. 53, no. 12, pp. 1692–1698, 2010.
- [15] J. J. Smith, O. S. Chow, M. J. Gollub et al., "Organ preservation in rectal adenocarcinoma: a phase II randomized controlled

Retraction

Retracted: TMEM60 Promotes the Proliferation and Migration and Inhibits the Apoptosis of Glioma through Modulating AKT Signaling

Journal of Oncology

Received 12 January 2023; Accepted 12 January 2023; Published 23 January 2023

Copyright © 2023 Journal of Oncology. This is an open access article distributed under the Creative Commons Attribution License, which permits unrestricted use, distribution, and reproduction in any medium, provided the original work is properly cited.

Journal of Oncology has retracted the article titled “TMEM60 Promotes the Proliferation and Migration and Inhibits the Apoptosis of Glioma through Modulating AKT Signaling” [1] due to concerns that the peer review process has been compromised.

Following an investigation conducted by the Hindawi Research Integrity team [2], significant concerns were identified with the peer reviewers assigned to this article; the investigation has concluded that the peer review process was compromised. We therefore can no longer trust the peer review process, and the article is being retracted with the agreement of the Chief Editor.


The authors do not agree to the retraction.

References

- [1] J. Wu, X. Tang, X. Yu et al., “TMEM60 Promotes the Proliferation and Migration and Inhibits the Apoptosis of Glioma through Modulating AKT Signaling,” *Journal of Oncology*, vol. 2022, Article ID 9913700, 11 pages, 2022.
- [2] L. Ferguson, “Advancing Research Integrity Collaboratively and with Vigour,” 2022, <https://www.hindawi.com/post/advancing-research-integrity-collaboratively-and-vigour>.

Research Article

TMEM60 Promotes the Proliferation and Migration and Inhibits the Apoptosis of Glioma through Modulating AKT Signaling

Jingwen Wu,¹ Xinghua Tang,¹ Xuejuan Yu,¹ Xiaoli Zhang,¹ Wenjun Yang,² Ashima Seth,² and Qiuhan Yang¹ 

¹Department of Radiation Oncology, Qilu Hospital, Cheeloo College of Medicine, Shandong University, Jinan, China

²Master of Healthcare Administration at Price School of Public Policy, University of Southern California, Los Angeles, CA, USA

Correspondence should be addressed to Qiuhan Yang; qayang9966@126.com

Received 29 September 2021; Revised 16 October 2021; Accepted 26 October 2021; Published 3 January 2022

Academic Editor: Yun-dai Chen

Copyright © 2022 Jingwen Wu et al. This is an open access article distributed under the Creative Commons Attribution License, which permits unrestricted use, distribution, and reproduction in any medium, provided the original work is properly cited.

Glioma is a highly fatal malignancy with aggressive proliferation, migration, and invasion metastasis due to aberrant genetic regulation. This work aimed to determine the function of transmembrane protein 60 (TMEM60) during glioma development. The level of TMEM60 in glioma tissues and normal tissues and its correlation with glioma prognosis were checked in The Cancer Genome Atlas (TCGA) database. The levels of TMEM60 in glioma cell lines and normal astrocytes were determined by quantitative real-time PCR and western blotting assay. TMEM60 knockdown and overexpression were conducted, followed by detection of cell viability, migration, invasion, and apoptosis. CCK-8 and colony formation assay were adopted to detect cell viability proliferation. Transwell assay was performed to measure cell migration and invasion. Cell apoptosis was evaluated by flow cytometry. The alternation of key proteins in the PI3K/Akt signaling pathway was measured by western blotting. TMEM60 expression was significantly higher in glioma tissues than that in the healthy control and was correlated with poor overall survival of patients. The protein and mRNA levels of TMEM60 were both elevated in glioma cell lines in comparison with the normal cell lines. Elevated level of TMEM60 led to enhanced proliferation, migration, and invasion and suppressed cell apoptosis. TMEM60 promoted the activation of PI3K/Akt signaling. Our data suggested that TMEM60 plays an oncogenic role in glioma progression via activating the PI3K/Akt signaling pathway.

1. Introduction

Glioma is the most commonly occurring brain malignancy in adults, exhibiting highly aggressive feature and grave prognosis [1–3]. Numerous studies have disclosed that the progression of glioma is closely correlated with abnormal metabolism, vascular endothelial proliferation, and suppressed immune response [4–7]. Large-scale genome analysis and accumulating studies on molecular mechanisms have presented multiple oncogenes that contribute to glioma onset, such as Notch, platelet-derived growth factor receptor alpha (PDGFRA), and epithelial growth factor receptor (EGFR) [8–12]. For example, Notch signaling participates in the regulation of glioma cell stemness and promotes self-renewal of glioma cells [13–15]. Genomic sequencing unraveled the alteration of the EGFR gene in over 50% of glioma [8, 16].

Over the past decades, the developed therapeutic manners including surgical operation and chemo- and radiotherapy have successfully achieved partial remission in glioma patients, yet there still exist some patients who show slight response, and the 5-year relative survival is only 5% [9, 10, 17]. Therefore, it is urgent to decipher the mechanisms underlying the pathogenesis of glioma and develop safe and efficient therapeutic strategies. The phosphatidylinositol 3-kinases (PI3Ks)/Akt signaling pathway is a central regulator of signaling transduction during biological processes of cancer cells, such as viability, metastasis, metabolism, and angiogenesis [18–20]. The PI3K/Akt pathway could be activated by receptor tyrosine kinases (RTKs) or G protein-coupled receptors (GPCRs), during which the PI3K activates PIP3 to anchor Akt to cell membranes. The Akt is then phosphorylated activated by mTOR at Thr308 and

Ser473 residues [21–23]. Previous studies have reported the important function of PI3K/Akt signaling in glioma and its potential as therapeutic targets [24–26].

In this present work, we, for the first time, confirmed the elevated expression of transmembrane protein 60 (TMEM60) in glioma tissue samples and cell lines. We evaluated cell viability, migration, invasion, and apoptosis after knockdown or ectopic expression of TMEM60 and determined the changes on the PI3K/Akt pathway. Our basic experimental findings provided novel evidences to uncover the TMEM60/PI3K/Akt signaling in glioma and supplied a notable perception concerning the regulatory axis in glioma advancement and novel therapeutic approaches for glioma.

2. Methods

2.1. Clinical Samples. We performed gene profiling of glioma patients from the Cancer Genome Atlas (TCGA) and healthy donors from the GTEx database by using the online website GEPIA (<https://gepia2.cancer-pku.cn/#help>). The expression of TMEM60 in tumor and nontumor tissues and the correlation between TMEM60 and GBM (glioblastoma multiforme) or LGG (brain lower grade glioma) prognosis were analyzed.

2.2. Cell Culture. Normal human brain astroglia cell line SVGP12, normal human astrocyte (HA), glioma cell line TJ905, GOS-3, U87MG, and SHG-44 were obtained from ATCC (Manassas, VA, USA). SVGP12 and U87 were cultured in EMEM (Hyclone, USA). HA was cultured in Astrocyte Medium (ScienCell, USA). GOS-3 and TJ905 were cultured in DMEM (Hyclone, USA). SHG-44 was cultured in RPMI 1640 (Hyclone, USA) [27]. All cells were cultured in a medium supplemented with 10% FBS (Gibco, USA) at 37°C incubation with 5% CO₂.

2.3. Lentivirus Packaging and Infection. To generate the lentiviral shRNA constructs against human TMEM60, the TMEM60 shRNA sequences were cloned into the pLKO-puro vector. The sequences of shTMEM60 are as follows: shTMEM60-1, 5'-GAGTAACCCATGTAAATTACT-3'; shTMEM60-2, 5'-CGAGCTGGACTATCTGTGACT-3'. pLKO.1, pVSVG, pREV, and pGAG were cotransfected into HEK293T cells for 24 h, and cell culture media were collected. The full-length TMEM60 sequences were cloned into the pCDH-puro vector. pCDH, pSPAX.2, and pMD.2G were cotransfected into HEK293T cells for 24 h, and cell culture media were collected. The viruses were used to infect cells in the presence of polybrene. Forty-eight hours later, SHG-44 and U87MG cells were cultured in a medium containing puromycin for the selection of stable clones. The clones stably knocking down or overexpressing TMEM60 were identified and verified by western blotting [28].

2.4. Cell Viability and Apoptosis. Cell viability was determined by Cell Counting Kit-8 (CCK-8) assay and colony formation. For CCK-8 assay, cells were transfected with

indicated oligonucleotides and seeded in 96-well plates at a density of 5,000 cells per well. After incubation for 24, 48, and 72 hours, 20 μ l CCK-8 (5 mg/ml) was added to each well, and the cells were incubated for another 4 hours. After that, the absorbance values at 450 nm were measured by using a microplate reader (Thermo, USA). For colony formation assay, the cells were suspended as single cells and seeded in 6-well plates (1,000 cells per well) and incubated for 10 days to form colonies [29]. The colonies were washed with PBS and dyed with 1% crystal violet for 20 minutes, captured, and counted. Cell apoptosis was evaluated by using the Annexin V/FITC Apoptosis Detection kit (Beyotime, China) as per the manufacturer's protocol. The cells were collected and detected on a flow cytometer (BD Biosciences, USA).

2.5. Western Blotting. The total proteins were extracted from cells after homogenization with RIPA lysis buffer (Beyotime), quantified by using a BCA assay kit (Beyotime). An equal amount of proteins was separated by SDS-PAGE, shifted to polyvinylidene fluoride (PVDF) membranes, and blocked with 5% skim milk in PBST for 2 hours, followed by incubation with primary antibodies against TMEM60, PARP, cleaved PARP, caspase-3, cleaved caspase-3, p-AKT, AKT, GSK3 β , p-GSK3 β , mTOR, p-mTOR, p70S6K, p-p70S6K, 4E-BP1, p-4E-BP1, and β -actin, at 4°C overnight. The next day, the protein bands were incubated with the corresponding horseradish peroxidase- (HRP-) coupled secondary antibodies, and enhanced chemiluminescence (ECL) visualization was performed on a gel image system (Bio-Rad) [30, 31].

2.6. Colony Formation. U87MG and SHG-44 cells were trypsinized, counted, and seeded in 6-well plates for 24 hours. Cells were cultured for 10 days to form visible clones. The clones were then washed, fixed, and stained with crystal violet, captured, and counted [32, 33].

2.7. Transwell Assay. The migration and invasion of glioma cells were determined by Transwell assay (Corning, USA). In brief, cells were placed into top chambers of 24-well plates with a serum-free medium, and the lower chambers were filled with complete medium [34]. After 48 hours incubation, the migrated cells were fixed with 4% paraformaldehyde (PFA) and then dyed with 1% crystal violet. For cell invasion, the upper chambers were coated with Matrigel (BD Biosciences, USA). The stained cells were observed and captured under a microscope [35].

2.8. Flow Cytometry. Flow cytometry was used to evaluate apoptosis of glioma cancer cells after TMEM60 knockdown. Glioma cancer cells were plated in 6-well plates with TMEM60 overexpression or vector as control. After double staining with fluorescein isothiocyanate- (FITC-) Annexin V and propidium iodide was performed using an FITC Annexin V Apoptosis Detection Kit (BD Biosciences) according to the manufacturer's recommendations [36], the cells were analyzed with a flow cytometer (FACScan; BD

Biosciences) equipped with Cell Quest software (BD Biosciences). Cells were sorted into viable cells, dead cells, early apoptotic cells, and apoptotic cells, and the relative ratio of early apoptotic cells was compared with that of control cells in each experiment [37].

2.9. Statistics. Data in this study were presented as mean \pm standard deviation (SD) of at least three independent experiments and processed by using the GraphPad software (USA). The student's *t* test or one-way analysis of variance (ANOVA) were conducted to compare differences between two or multiple groups. The *P* value <0.05 was considered statistically significant.

3. Results

3.1. The Expression of TMEM60 in Glioma Tissues and Cell Lines. We first identified the correlation between TMEM60 and glioma. The analysis on glioma patient samples and healthy donors from TCGA and the GTEx database showed that the levels of TMEM60 in glioma were remarkably elevated in GBM and LGC tumor tissues, compared with those in healthy tissues, and this elevated level of TMEM60 was correlated with poor overall survival of patients (Figures 1(a) and 1(b)). Moreover, the expression of TMEM60 was notably higher in glioma cell lines, including the TJ905, GOS-3, U87, and SHG-44, than that in normal human astrocyte cell lines (HA and SVG P12), as was manifested by mRNA and protein quantification (Figures 1(c) and 1(d)). These data suggested the abnormal upregulation of TMEM60 in glioma and its potential oncogenic role.

3.2. TMEM60 Facilitates Glioma Cell Proliferation. The abnormal overexpression of TMEM60 indicated that it may facilitate glioma progression [38]. To verify this speculation, we conducted stable knockdown or overexpression of TMEM60 in U87 and SHG-44 cells by infecting shRNAs (shTMEM60-1 and shTMEM60-2) or overexpressing vectors. The efficacy of infecting was determined by western blotting (Figures 2(a) and 2(b)). Results from CCK-8 indicated that TMEM60 knockdown alleviated cell viability in a time-dependent manner (Figure 2(c)), whereas the overexpression of TMEM60 facilitated cell viability (Figure 2(d)). Similarly, the decreased colony number in TMEM60-depleted GBM cells supported the proliferative role of TMEM60 in GBM (Figures 2(e) and 2(f)).

3.3. TMEM60 Promotes Glioma Cell Migration and Invasion. The high aggressiveness of glioma cells was also exhibited by cell migration and invasion [39]. Here, we performed Transwell assay to detect the metastatic ability of U87 and SHG-44 cells. As shown in Figures 3(a) and 3(b), knockdown of TMEM60 significantly suppressed the migrated and invaded glioma cells, and the histogram confirmed the statistical significance of the alteration (Figure 3(c)). By contrast, the overexpression of TMEM60 facilitated cell migration and invasion (Figures 3(d)–3(f)). These findings

indicated that TMEM60 aggravated the aggressive phenotypes of glioma cells.

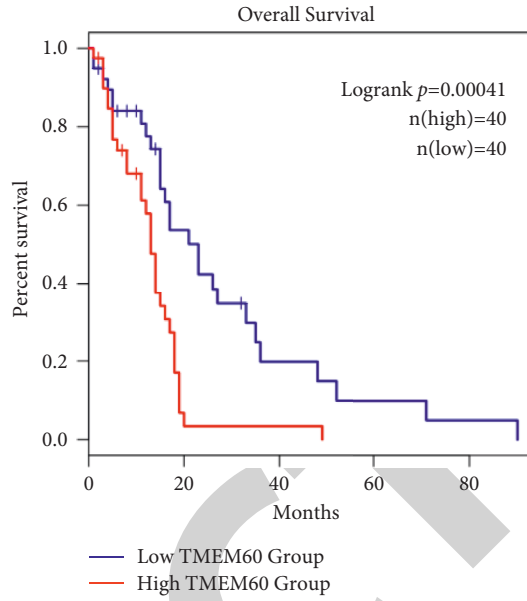
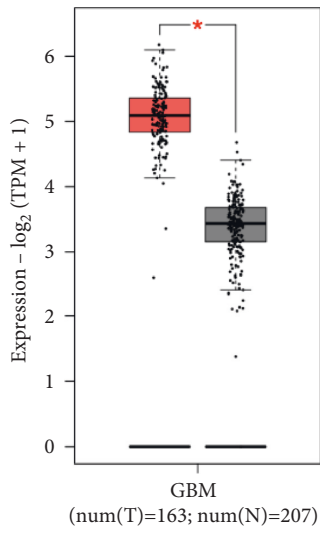
3.4. TMEM60 Suppresses Glioma Cell Apoptosis. After determination of cell proliferation and metastasis, we detected the apoptosis of U87 and SHG-44 cells [40]. As shown in Figures 4(a) and 4(b), the depletion of TMEM60 led to elevated apoptosis of glioma cells, as was manifested by the increased portion of early- and late-phase apoptotic cells. The detection of apoptosis-related signaling presented the emergence of cleaved PARP and caspase-3, along with the notable decrease of PARP and caspase-3 (Figures 4(c) and 4(d)). These results indicated that TMEM60 protects glioma cells from apoptosis.

3.5. TMEM60 Promotes the Glioma Cell Phenotype through PI3K/AKT Signaling. Studies have proved that the PI3K/AKT signaling contributed to aggressiveness of cancers, including glioma. Here in this work, we investigated whether TMEM60 modulates glioma cell behaviors through regulating the PI3K/AKT signaling pathway. Knockdown of TMEM60 suppressed the activation of PI3K/AKT signaling, as was manifested by decreased phosphorylation of Akt, GSK-3 β , mTOR, p70-S6K, and 4E-BP1 (Figures 5(a) and 5(b)). Moreover, the overexpression of TMEM60 promoted the activation of PI3K/AKT signaling, as was manifested by increased phosphorylation of Akt, GSK-3 β , mTOR, p70-S6K, and 4E-BP1 (Figures 5(c) and 5(d)). Therefore, TMEM60 promotes the hyperactivation of the PI3K/AKT signaling pathway in glioma cells.

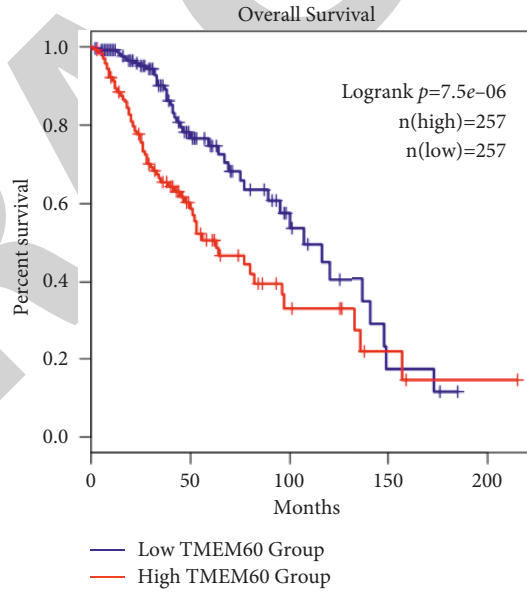
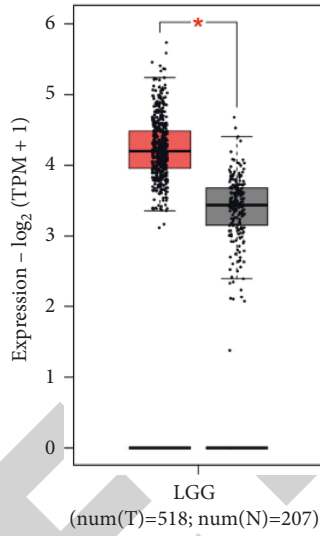
4. Discussion

In the present work, we evaluated the role of a rarely reported gene TMEM60 in glioma carcinogenesis. We analyzed the expression of TMEM60 in patients with glioma and healthy donors and spotted its upregulation in glioma tissues compared with the nontumor tissues. The overall survival analysis also unraveled the correlation between high TMEM60 level with poor prognosis. It is well known that glioma is a highly aggressive malignancy with rapid proliferation [5]. Moreover, the glioma cells are capable of infiltrating to the neighboring brain tissues, causing pseudopalisading necrosis and angiogenesis, which consequently contribute to the poor prognosis of patients [17, 41, 42]. Other than the elevated level of TMEM60 in tumor tissues, we also found an elevation of TMEM60 in glioma cells compared with the normal human astrocyte cell lines.

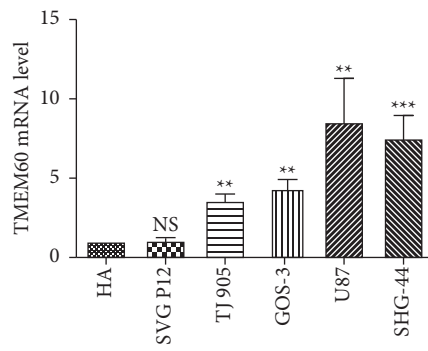
To determine the specific role of TMEM60 in glioma carcinogenesis, we conducted knockdown and overexpression of TMEM60 in glioma cell lines and confirmed that TMEM60 overexpression led to enhanced cell viability, proliferation, migration, and invasion, as well as decreased cell apoptosis, which is consistent with the abnormal low level of TMEM60 in glioma tumor sections. Also, the knockdown of TMEM60 exerted opposite effects on GBM cell phenotypes. All these findings suggested that TMEM60 plays a potential oncogenic role in glioma [43, 44]. We next



(a)



(b)



(c)

FIGURE 1: Continued.

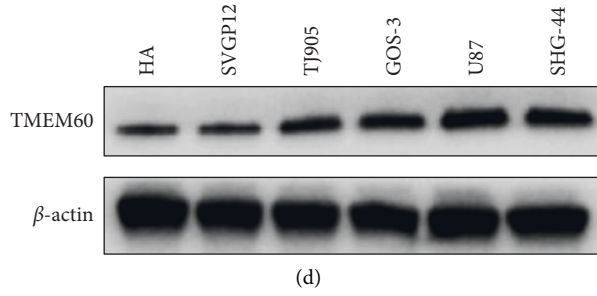


FIGURE 1: TMEM60 expression in glioma. (a, b) Expression profile of TMEM60 in GBM and LGG from TCGA database was analyzed by the GEPIA website. T, tumor; N, nontumor adjacent tissue. (c, d) The transcription and protein expression of TMEM60 in human astrocyte cell lines, HA and SVG P12, and glioma cell lines, TJ905, GOS-3, U87, and SHG-44 by western blotting.

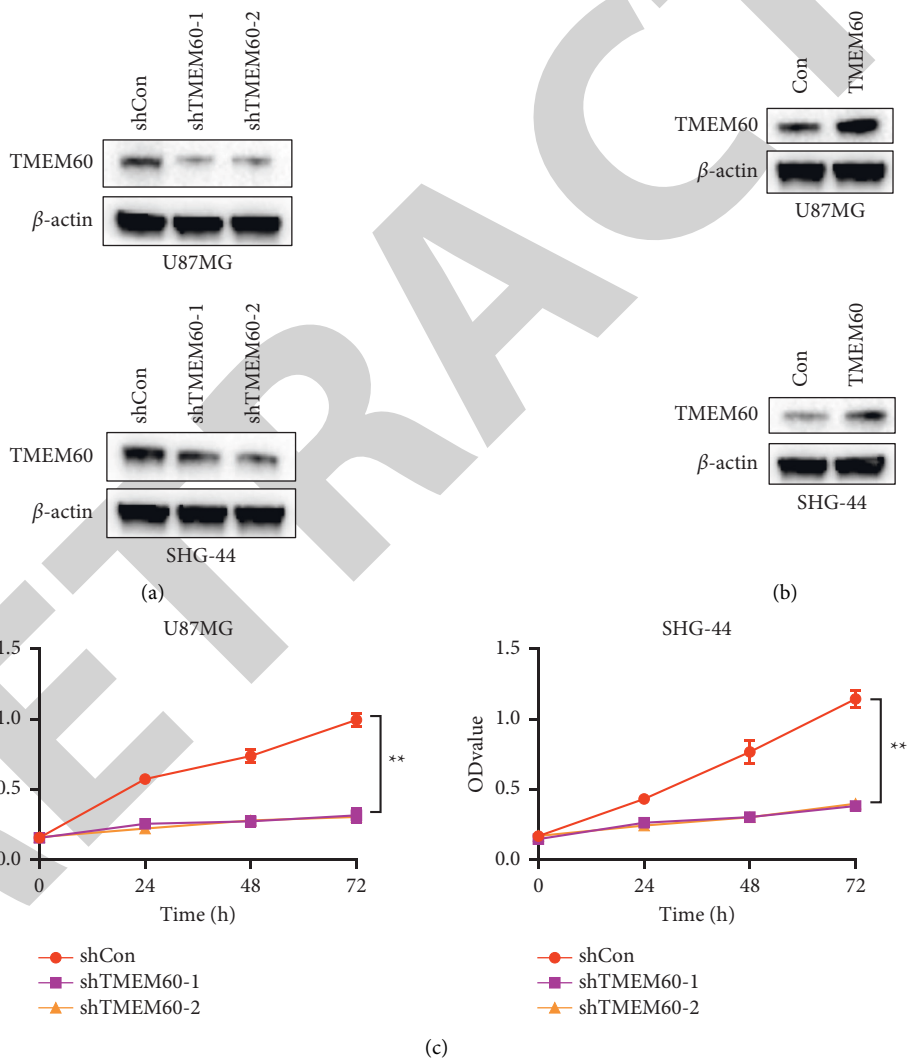


FIGURE 2: Continued.

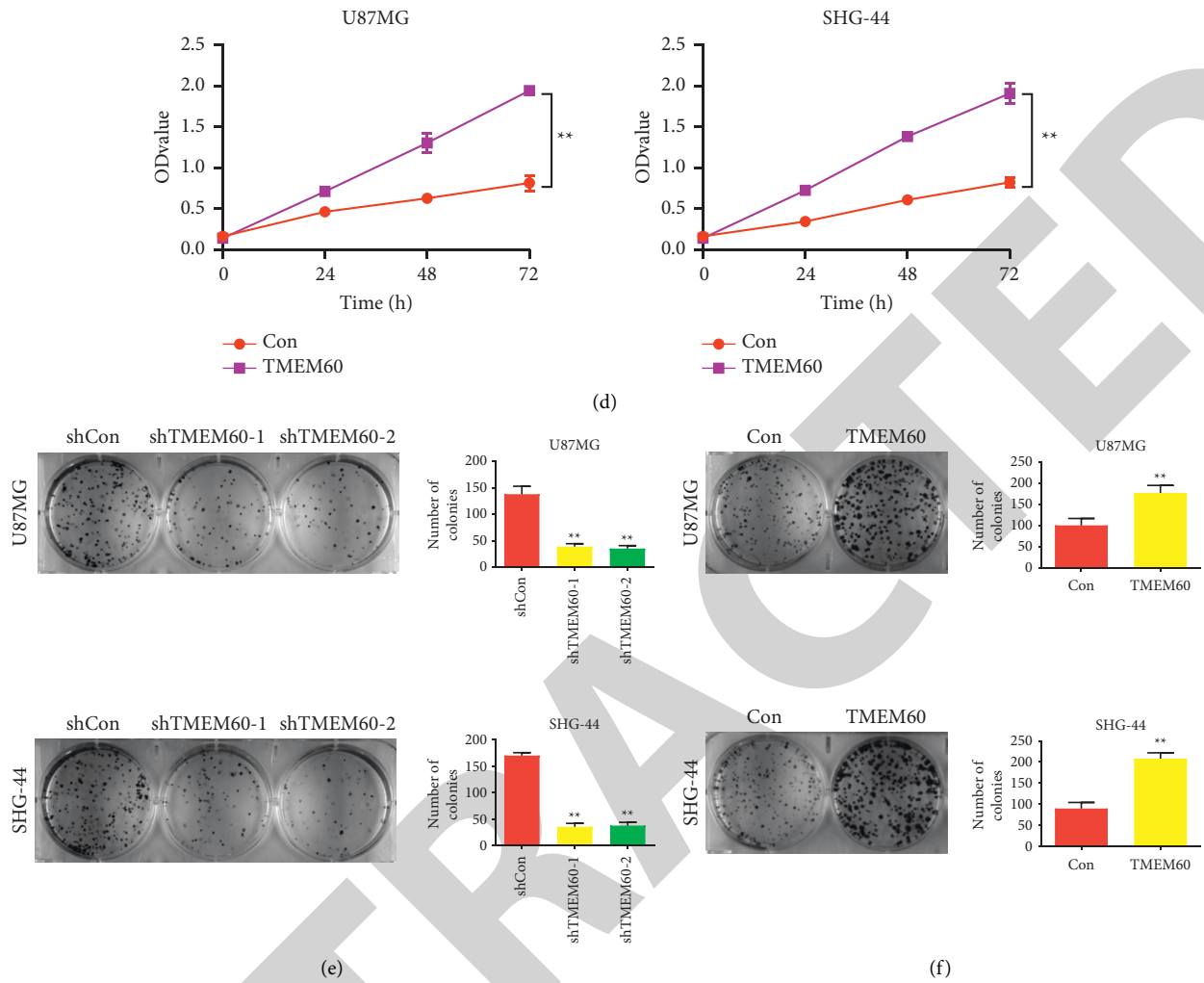


FIGURE 2: TMEM60 promotes glioma cell proliferation. U87 and SHG-44 cells were infected with shTMEM60 or negative control (shcon). (a) Western blotting experiment to detect the efficacy of shTMEM60 infection. (b) Western blotting to detect TMEM60 overexpression efficacy. (c, d) CCK8 assay was used to the proliferation of U87 and SHG-44 cells after infection of shTMEM60 or TMEM60 overexpression. (e, f) Colony formation assay was used for the proliferation of U87 and SHG-44 cells after infection of shTMEM60 or TMEM60 overexpression. The ratio of colony formation was quantified and calculated as histograms. All experiments were repeated independently for three times, and the representative one was shown. ** $P < 0.01$ vs. shcon.

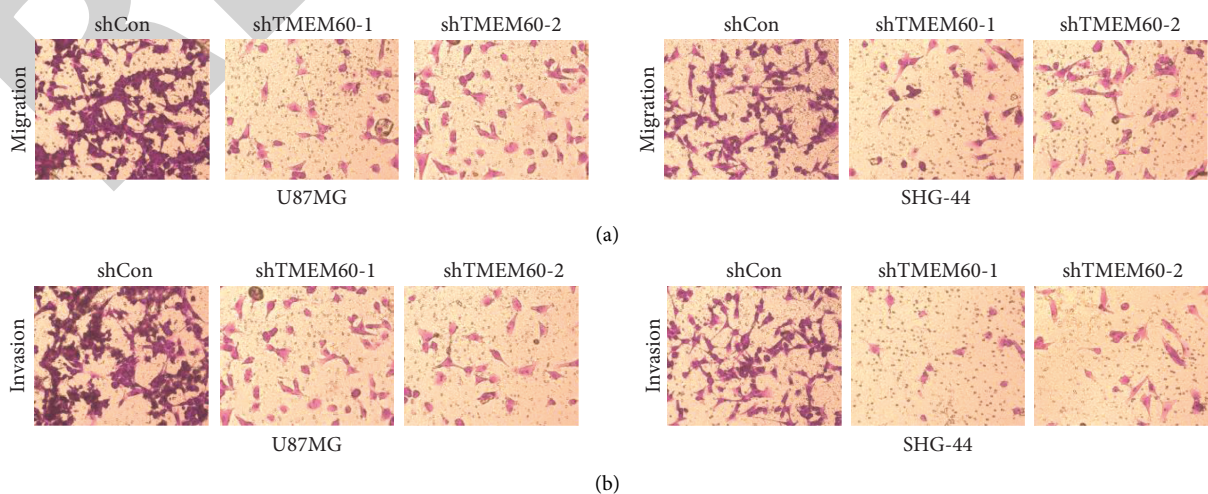


FIGURE 3: Continued.

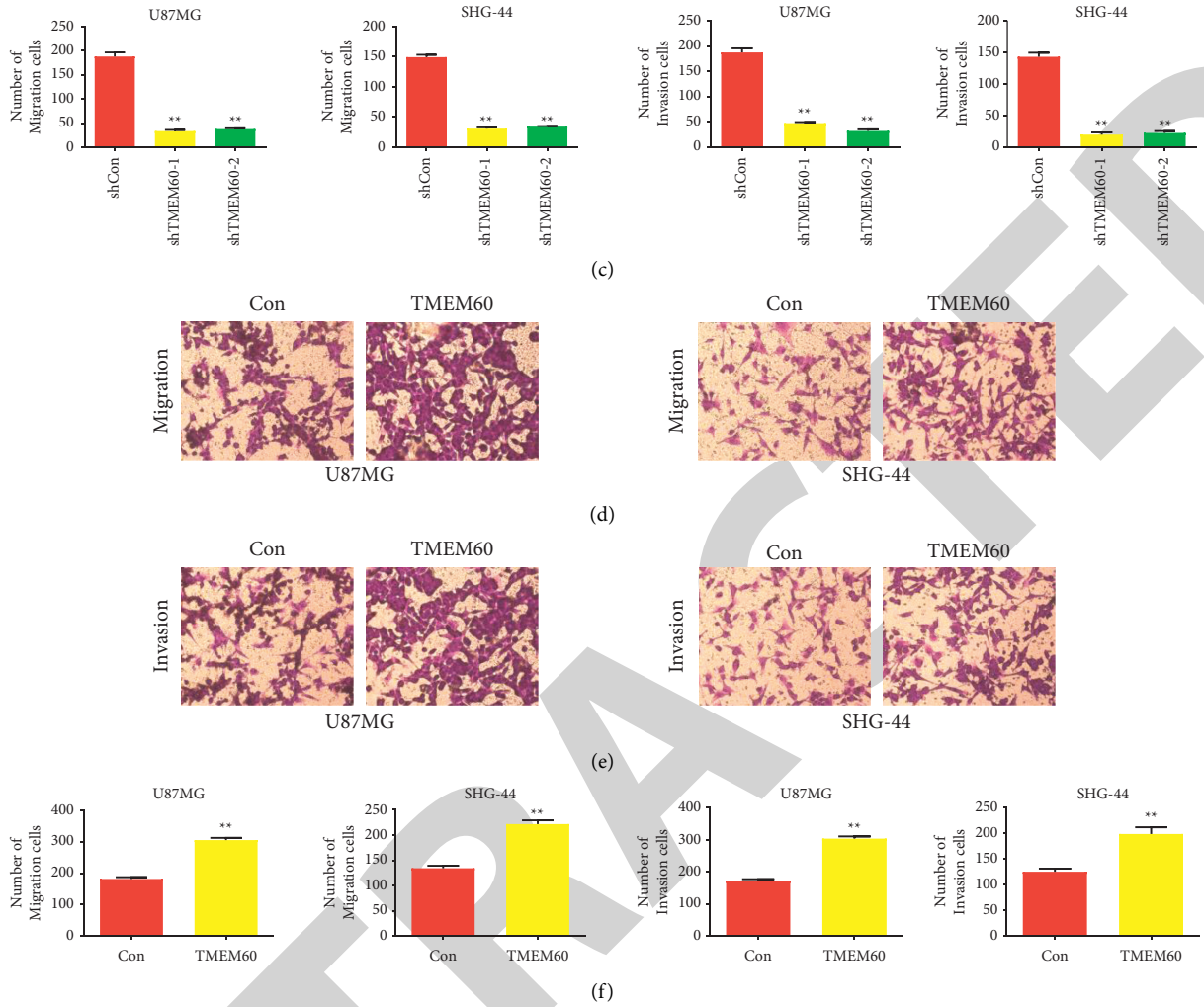
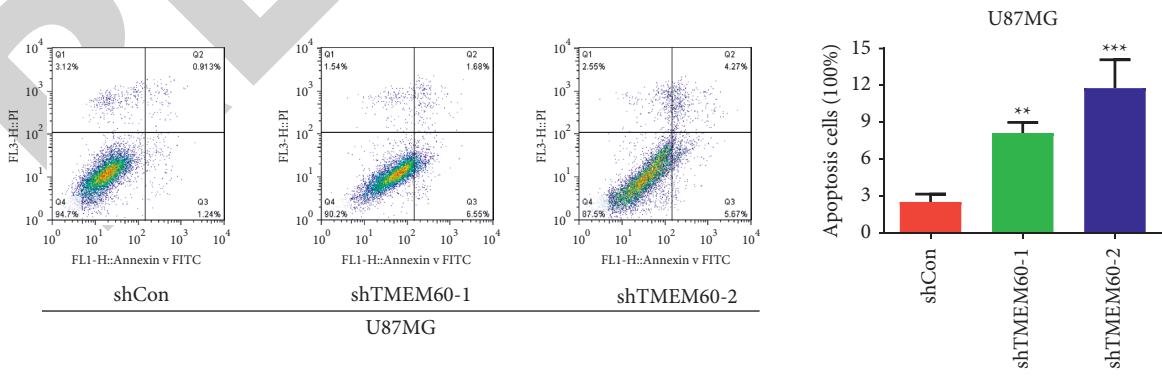


FIGURE 3: Effects of TMEM60 overexpression and knockdown on glioma migration and invasion. (a, b, c) U87 and SHG-44 cells of TMEM60 knockdown were examined for cell migration and invasion by Transwell assay. (d, e, f) U87 and SHG-44 cells of TMEM60 overexpression were examined for cell migration and invasion by Transwell assay. $N = 3$, * $P < 0.05$, ** $P < 0.01$ compared to the shcon or con group.



(a)
FIGURE 4: Continued.

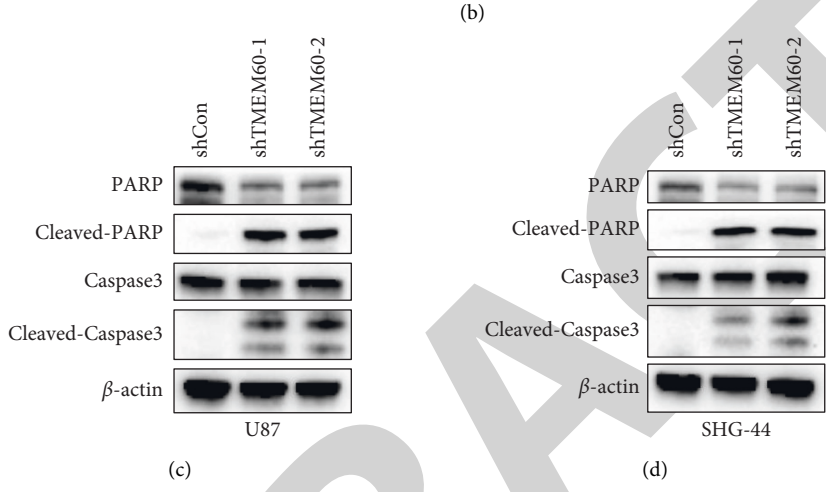
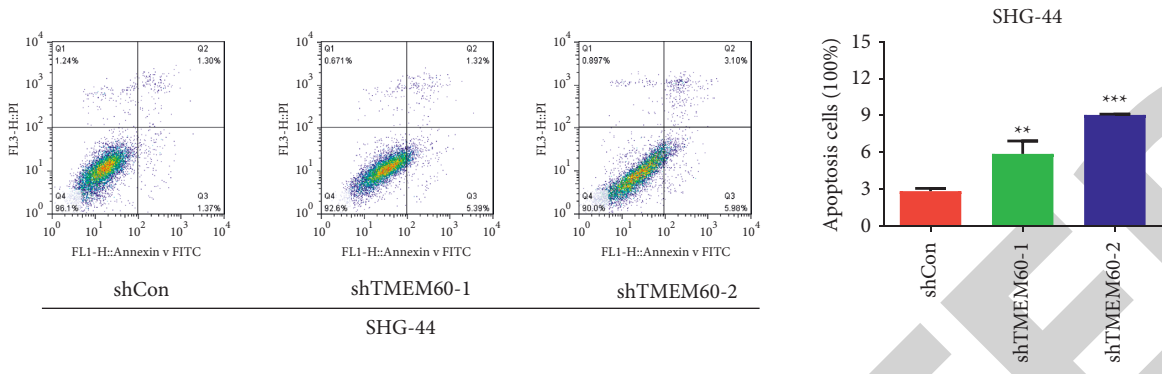


FIGURE 4: TMEM60 affects apoptosis of glioma cells. (a, b) Flow cytometry to detect U87 and SHG-44 cells' apoptosis alteration under the knockdown of TMEM60. The ratio of apoptotic cells was calculated and shown. (c, d) Western blotting assay to detect the expression of caspase-3, cleaved caspase-3, PARP, and cleaved PARP. All experiments were repeated independently three times, and the representative one was shown. ** $P < 0.01$ vs. shcon. *** $P < 0.001$ vs. shcon.

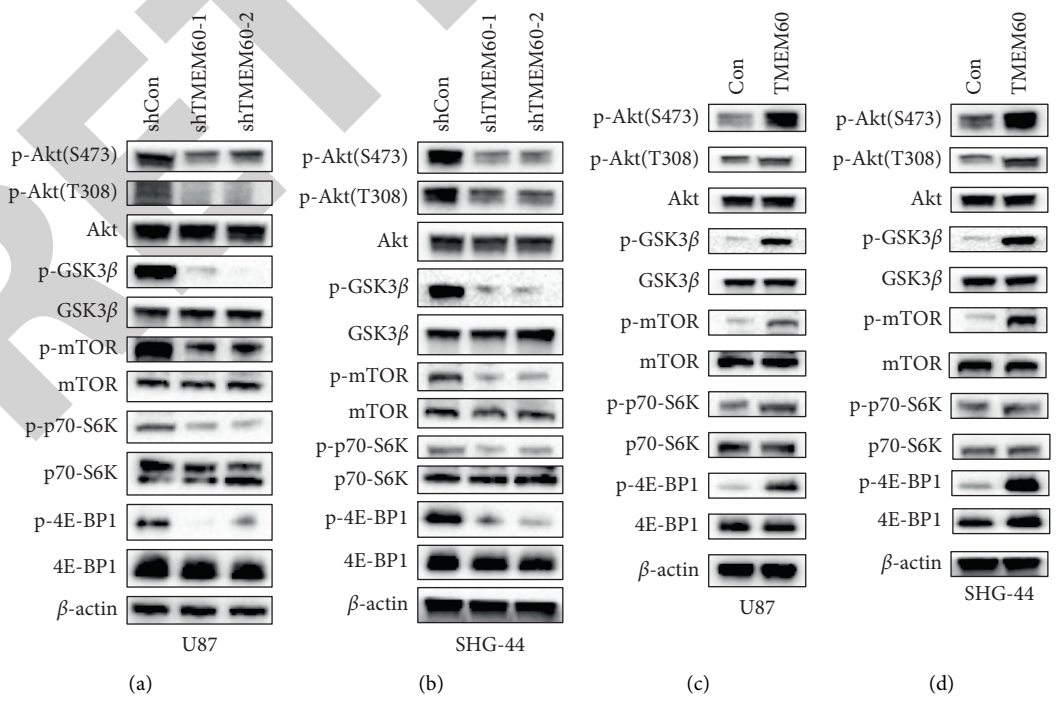


FIGURE 5: The PI3K/AKT signaling pathway is involved in the effects of TMEM60. (a, b) The cell lysates were subjected to analysis of the phosphorylation levels of Akt and its downstream targets under the knockdown of TMEM60. (c, d) The cell lysates were subjected to the analysis of the phosphorylation levels of Akt and its downstream targets under the overexpression of TMEM60.

tried to decipher the mechanisms underlying the functions of TMEM60 during glioma carcinogenesis. Numerous studies have disclosed the high frequency of genetic aberrations in glioma, including the tumor protein p53 (TP53) [45, 46], cyclin-dependent kinase inhibitor 2A/B (CDKN2A/B) [47–49], tensin homolog (PTEN) [50, 51], EGFR [52, 53], PDGFRA [54], and PIK3CA, which leads to dysregulation of downstream signaling pathways such as the RB transcriptional corepressor 1 (RB1), PI3K/Akt/mTOR, and p53 [55–57]. The exploration of these genetic aberrations led to the discovery of targeted therapies against glioma [58–60]. PI3K/Akt/mTOR is a widely recognized signaling pathway that modulates the proliferation, motility, apoptosis, and angiogenesis in glioma [61–63].

Due to the abnormal cellular functions, elevated levels of PI3K and Akt are poor prognostic indicators for patients with malignancies [31, 64, 65]. Our study disclosed the alterations in the PI3K/Akt signaling under the overexpression or knockdown of TMEM60. Consistent with the prospected oncogenic role of TMEM60, TMEM60 overexpression upregulated the phosphorylation of PI3K/Akt signaling.

Taken together, we determined the aberrant expression of TMEM60 in glioma tissue samples and cell lines compared with the normal control. TMEM60 play an oncogenic role in glioma by promoting glioma cell proliferation, migration, and invasion and impairing cell apoptosis via activating the PI3K/Akt signaling pathway.

Abbreviations

TCGA: The Cancer Genome Atlas
 TMEM60: Transmembrane protein 60
 PI3K: Phosphatidylinositol 3-kinase.

Data Availability

The datasets used and/or analyzed during the current study are available from the corresponding author on reasonable request.

Consent

Consent for publication was obtained from the participants.

Conflicts of Interest

The authors declare no conflicts of interest.

Authors' Contributions

Jingwen Wu and Qian Yang contributed to the study conception and design. Xinghua Tang, Xuejuan Yu, Xiaoli Zhang, Wenjun Yang, and Ashima Seth analyzed and interpreted the data. All authors provided final approval of the work.

Acknowledgments

The authors would like to thank Licun Wu, Latner Thoracic Surgery Laboratories, Division of Thoracic Surgery and

Princess Margaret Cancer Centre, University Health Network (UHN), Toronto, ON, Canada, for his editing on the written expression and grammar of this manuscript.

References

- [1] R. L. Siegel, K. D. Miller, and A. Jemal, "Cancer statistics, 2020," *CA: a Cancer Journal for Clinicians*, vol. 70, no. 1, pp. 7–30, 2020.
- [2] C. Alifieris and D. T. Trafalis, "Glioblastoma multiforme: pathogenesis and treatment," *Pharmacology & Therapeutics*, vol. 152, pp. 63–82, 2015.
- [3] A. L. Bayliss, A. Sundararaman, C. Granet, and H. Mellor, "Raftlin is recruited by neuropilin-1 to the activated VEGFR2 complex to control proangiogenic signaling," *Angiogenesis*, vol. 23, no. 3, pp. 371–383, 2020.
- [4] A. Poff, A. P. Koutnik, K. M. Egan, S. Sahebjam, D. D'Agostino, and N. B. Kumar, "Targeting the warburg effect for cancer treatment: ketogenic diets for management of glioma," *Seminars in Cancer Biology*, vol. 56, pp. 135–148, 2019.
- [5] R. Chen, M. Smith-Cohn, A. L. Cohen, and H. Colman, "Glioma subclassifications and their clinical significance," *Neurotherapeutics*, vol. 14, no. 2, pp. 284–297, 2017.
- [6] E. Bridges, H. Sheldon, E. Kleibeuker et al., "RHOQ is induced by DLL4 and regulates angiogenesis by determining the intracellular route of the notch intracellular domain," *Angiogenesis*, vol. 23, no. 3, pp. 493–513, 2020.
- [7] L. Yu, Q. Shi, Y. Jin, Z. Liu, J. Li, and W. Sun, "Blockage of AMPK-ULK1 pathway mediated autophagy promotes cell apoptosis to increase doxorubicin sensitivity in breast cancer (BC) cells: an in vitro study," *BMC Cancer*, vol. 21, no. 1, p. 195, 2021.
- [8] J. Zhang, G. Wu, C. P. Miller et al., "Whole-genome sequencing identifies genetic alterations in pediatric low-grade gliomas," *Nature Genetics*, vol. 45, pp. 602–612, 2013.
- [9] Q. T. Ostrom, L. Bauchet, F. G. Davis et al., "The epidemiology of glioma in adults: a "state of the science" review," *Neuro-Oncology*, vol. 16, no. 7, pp. 896–913, 2014.
- [10] O. Gussyatiner and M. E. Hegi, "Glioma epigenetics: from subclassification to novel treatment options," *Seminars in Cancer Biology*, vol. 51, pp. 50–58, 2018.
- [11] E. Parmigiani, V. Taylor, and C. Giachino, "Oncogenic and Tumor-suppressive functions of NOTCH signaling in glioma," *Cells*, vol. 9, 2020.
- [12] W. A. Flavahan, Y. Drier, B. B. Liau et al., "Insulator dysfunction and oncogene activation in IDH mutant gliomas," *Nature*, vol. 529, no. 7584, pp. 110–114, 2016.
- [13] K. Katsushima, A. Natsume, F. Ohka et al., "Targeting the notch-regulated non-coding RNA TUG1 for glioma treatment," *Nature Communications*, vol. 7, no. 1, Article ID 13616, 2016.
- [14] D. B. Buglak, E. J. Kushner, A. P. Marvin, K. L. Davis, and V. L. Bautch, "Excess centrosomes disrupt vascular lumenization and endothelial cell adherens junctions," *Angiogenesis*, vol. 23, no. 4, pp. 567–575, 2020.
- [15] F. Cao, M. L. Maguire, D. J. McAndrew et al., "Overexpression of mitochondrial creatine kinase preserves cardiac energetics without ameliorating murine chronic heart failure," *Basic Research in Cardiology*, vol. 115, no. 2, p. 12, 2020.
- [16] E. Eskilsson, G. V. Røslund, G. Solecki et al., "EGFR heterogeneity and implications for therapeutic intervention in glioblastoma," *Neuro-Oncology*, vol. 20, no. 6, pp. 743–752, 2018.

- [17] R. Stupp, W. P. Mason, M. J. van den Bent et al., "Radiotherapy plus concomitant and adjuvant temozolomide for glioblastoma," *New England Journal of Medicine*, vol. 352, no. 10, pp. 987–996, 2005.
- [18] K. Ludwig and H. I. Kornblum, "Molecular markers in glioma," *Journal of Neuro-Oncology*, vol. 134, no. 3, pp. 505–512, 2017.
- [19] C. K. Cheng, Q. W. Fan, and W. A. Weiss, "PI3K signaling in glioma-animal models and therapeutic challenges," *Brain Pathology*, vol. 19, no. 1, pp. 112–120, 2009.
- [20] I. Cuijpers, S. J. Simmonds, M. van Bilsen et al., "Microvascular and lymphatic dysfunction in HFpEF and its associated comorbidities," *Basic Research in Cardiology*, vol. 115, no. 4, p. 39, 2020.
- [21] C. Porta, C. Paglino, and A. Mosca, "Targeting PI3K/Akt/mTOR signaling in cancer," *Frontiers in Oncology*, vol. 4, p. 64, 2014.
- [22] M. Aoki and T. Fujishita, "Oncogenic roles of the PI3K/AKT/mTOR Axis," *Current Topics in Microbiology and Immunology*, vol. 407, pp. 153–189, 2017.
- [23] J. Chen, F. L. Lin, J. Y. K. Leung et al., "A drug-tunable Flt23k gene therapy for controlled intervention in retinal neovascularization," *Angiogenesis*, 2020.
- [24] N. Wen, B. Guo, H. Zheng et al., "Bromodomain inhibitor jq1 induces cell cycle arrest and apoptosis of glioma stem cells through the VEGF/PI3K/AKT signaling pathway," *International Journal of Oncology*, vol. 55, pp. 879–895, 2019.
- [25] Q. W. Fan and W. A. Weiss, "Targeting the RTK-PI3K-mTOR axis in malignant glioma: overcoming resistance," *Current Topics in Microbiology and Immunology*, vol. 347, pp. 279–296, 2010.
- [26] V. S. Tomar, V. Patil, and K. Somasundaram, "Temozolomide induces activation of Wnt/ β -catenin signaling in glioma cells via PI3K/Akt pathway: implications in glioma therapy," *Cell Biology and Toxicology*, vol. 36, no. 3, pp. 273–278, 2020.
- [27] D. V. C. de Jel, F. J. M. Disch, S. Kroon, J. J. Mager, and F. J. Verdam, "Intranasal efudix reduces epistaxis in hereditary hemorrhagic telangiectasia," *Angiogenesis*, vol. 23, no. 3, pp. 271–274, 2020.
- [28] R. A. Deckelbaum, I. B. Lobov, E. Cheung et al., "The potassium channel Kcne3 is a VEGFA-inducible gene selectively expressed by vascular endothelial tip cells," *Angiogenesis*, vol. 23, no. 2, pp. 179–192, 2020.
- [29] C. L. Depoix, A. Colson, C. Hubinont, and F. Debieve, "Impaired vascular endothelial growth factor expression and secretion during in vitro differentiation of human primary term cytotrophoblasts," *Angiogenesis*, vol. 23, no. 2, pp. 221–230, 2020.
- [30] M. R. Detter, R. Shenkar, C. R. Benavides et al., "Novel murine models of cerebral cavernous malformations," *Angiogenesis*, vol. 23, no. 4, pp. 651–666, 2020.
- [31] T. D. Le Cras, J. Goines, N. Lakes et al., "Constitutively active PIK3CA mutations are expressed by lymphatic and vascular endothelial cells in capillary lymphatic venous malformation," *Angiogenesis*, vol. 23, no. 3, pp. 425–442, 2020.
- [32] M. di Somma, M. Vliora, E. Grillo et al., "Role of VEGFs in metabolic disorders," *Angiogenesis*, vol. 23, no. 2, pp. 119–130, 2020.
- [33] M. T. Islam, "Angiostatic effects of ascorbic acid: current status and future perspectives," *Angiogenesis*, vol. 23, no. 3, pp. 275–277, 2020.
- [34] E. García-Martínez, A. Redondo, J. M. Piulats, A. Rodríguez, and A. Casado, "Are Antiangiogenics a Good 'Partner' for Immunotherapy in Ovarian Cancer?" *Angiogenesis*, vol. 23, no. 4, pp. 543–557, 2020.
- [35] M. Heimerl, I. Sieve, M. Ricke-Hoch et al., "Neuraminidase-1 promotes heart failure after ischemia/reperfusion injury by affecting cardiomyocytes and invading monocytes/macrophages," *Basic Research in Cardiology*, vol. 115, no. 6, p. 62, 2020.
- [36] D. J. Hausenloy, M. Ntsekhe, and D. M. Yellon, "A future for remote ischaemic conditioning in high-risk patients," *Basic Research in Cardiology*, vol. 115, no. 3, p. 35, 2020.
- [37] H. Jiang, D. Jia, B. Zhang et al., "Exercise improves cardiac function and glucose metabolism in mice with experimental myocardial infarction through inhibiting HDAC4 and upregulating GLUT1 expression," *Basic Research in Cardiology*, vol. 115, no. 3, p. 28, 2020.
- [38] H. Zhou, S. Toan, P. Zhu, J. Wang, J. Ren, and Y. Zhang, "DNA-PKcs promotes cardiac ischemia reperfusion injury through mitigating BI-1-governed mitochondrial homeostasis," *Basic Research in Cardiology*, vol. 115, no. 2, p. 11, 2020.
- [39] Y. J. Zhang, M. Zhang, X. Zhao et al., "NAD⁺ administration decreases microvascular damage following cardiac ischemia/reperfusion by restoring autophagic flux," *Basic Research in Cardiology*, vol. 115, no. 5, p. 57, 2020.
- [40] L. Zhang, X. Y. Zhu, Y. Zhao et al., "Selective intrarenal delivery of mesenchymal stem cell-derived extracellular vesicles attenuates myocardial injury in experimental metabolic renovascular disease," *Basic Research in Cardiology*, vol. 115, no. 2, p. 16, 2020.
- [41] M. Kirsch, G. Schackert, and P. M. Black, "Angiogenesis, metastasis, and endogenous inhibition," *Journal of Neuro-Oncology*, vol. 50, no. 1/2, pp. 173–180, 2000.
- [42] Y. Zhang, S. Wang, and A. C. Dudley, "Models and molecular mechanisms of blood vessel co-option by cancer cells," *Angiogenesis*, vol. 23, no. 1, pp. 17–25, 2020.
- [43] Q. K. Yang, T. Chen, S. Q. Wang, X. J. Zhang, and Z. X. Yao, "Apatinib as targeted therapy for advanced bone and soft tissue sarcoma: a dilemma of reversing multidrug resistance while suffering drug resistance itself," *Angiogenesis*, vol. 23, no. 3, pp. 279–298, 2020.
- [44] S. K. Lahiri, A. P. Quick, B. Samson-Couterie et al., "Nuclear localization of a novel calpain-2 mediated junctophilin-2 C-terminal cleavage peptide promotes cardiomyocyte remodeling," *Basic Research in Cardiology*, vol. 115, no. 4, p. 49, 2020.
- [45] Y. Lin, K. Liao, Y. Miao et al., "Role of asparagine endopeptidase in mediating wild-type p53 inactivation of glioblastoma," *JNCI: Journal of the National Cancer Institute*, vol. 112, no. 4, pp. 343–355, 2020.
- [46] N. Lubos, S. van der Gaag, M. Gerçek, S. Kant, R. E. Leube, and C. A. Krusche, "Inflammation shapes pathogenesis of murine arrhythmogenic cardiomyopathy," *Basic Research in Cardiology*, vol. 115, no. 4, p. 42, 2020.
- [47] J. Wang, Z. Liu, Y. Cui et al., "Evaluation of EZH2 expression, BRAF V600E mutation, and CDKN2A/B deletions in epithelioid glioblastoma and anaplastic pleomorphic xanthoastrocytoma," *Journal of Neuro-Oncology*, vol. 144, no. 1, pp. 137–146, 2019.
- [48] P. Wischmann, V. Kuhn, T. Suvorova et al., "Anaemia is associated with severe RBC dysfunction and a reduced circulating NO pool: vascular and cardiac eNOS are crucial for the adaptation to anaemia," *Basic Research in Cardiology*, vol. 115, no. 4, p. 43, 2020.
- [49] A. Winiewicz and P. Woltanowski, "Leopold auerbach's achievements in the field of vascular system," *Angiogenesis*, vol. 23, no. 4, pp. 577–579, 2020.

Retraction

Retracted: DNA Damage Response Genes in Osteosarcoma

Journal of Osteoporosis

Received 12 November 2022; Accepted 12 November 2022; Published 15 December 2022

Copyright © 2022 Journal of Oncology. This is an open access article distributed under the Creative Commons Attribution License, which permits unrestricted use, distribution, and reproduction in any medium, provided the original work is properly cited.

Journal of Oncology has retracted the article titled “DNA Damage Response Genes in Osteosarcoma” [1] due to concerns that the peer review process has been compromised.

Following an investigation conducted by the Hindawi Research Integrity team [2], significant concerns were identified with the peer reviewers assigned to this article; the investigation has concluded that the peer review process was compromised. We therefore can no longer trust the peer review process, and the article is being retracted with the agreement of the Chief Editor.

References

- [1] Y. Tang, Y.-X. Liu, X. Huang, and P. Li, “DNA Damage Response Genes in Osteosarcoma,” *Journal of Oncology*, vol. 2021, Article ID 9365953, 9 pages, 2021.
- [2] L. Ferguson, “Advancing Research Integrity Collaboratively and with Vigour,” 2022, <https://www.hindawi.com/post/advancing-research-integrity-collaboratively-and-vigour/>.

Research Article

DNA Damage Response Genes in Osteosarcoma

Ying Tang,¹ Yan-xia Liu,² Xiuning Huang,² and Peng Li¹ 

¹Trauma Center, State Key Laboratory of Trauma, Burns and Combined Injury, Institute of Surgery Research, Daping Hospital, Army Medical University, No. 10 Changjiang Zhi Road, Yuzhong District, Chong Qing 400042, China

²Department of Pharmacognosy and Traditional Chinese Medicine, College of Pharmacy and Laboratory Medicine, Army Medical University, No. 30 Gaotanyan Centre Street, Shapingba District, Chong Qing 400038, China

Correspondence should be addressed to Peng Li; pengli@tmmu.edu.cn

Received 13 September 2021; Revised 6 October 2021; Accepted 11 October 2021; Published 2 November 2021

Academic Editor: Yun-dai Chen

Copyright © 2021 Ying Tang et al. This is an open access article distributed under the Creative Commons Attribution License, which permits unrestricted use, distribution, and reproduction in any medium, provided the original work is properly cited.

Background. Improving the osteosarcoma (OS) patients' survival has long been a challenge, even though the disease's treatment is on the verge of progress. DNA damage response (DDR) has traditionally been associated with carcinogenesis, tumor growth, and genomic instability. No study has used DDR genes as a signature to identify the prognosis of OS. The goal of this work was to find an effective possible DDR gene biomarker for predicting OS prognosis, which may be useful in clinical diagnosis and therapy. **Methods.** To assess gene methylation, univariate and multivariate cox regression analyses were performed on data from OS patients. The data were retrieved from public databases, including the Therapeutically Applicable Research to Generate Effective Treatments (TARGET) and the Gene Expression Omnibus (GEO). **Results.** The DDR gene signature was chosen, which included seven genes (NHEJ1, RMI2, SWI5, ERCC2, CLK2, POLG, and MLH1). In the TARGET dataset, patients were categorized into two groups: high-risk and low-risk. Patients with a high-risk score revealed a shorter OS rate (hazard ratio (HR): 3.15, 95% confidence interval (CI): 1.38–4.34, $P < 0.001$) in comparison with the patients with a low-risk score in the TARGET as a training group. The validation of the prognostic signature accuracy was carried out in relapse and validation cohorts (TARGET, $n = 75$; GSE21257, $n = 53$). The signature was found to be an independent predictive factor for OS in multivariate cox regression analysis, and a nomogram model was developed to predict an individual's risk of OS. DDR gene signature involved in Fanconi anemia pathway, nonhomologous end-joining pathway, mismatch repair, and nucleotide excision repair pathway. **Conclusions.** Our study suggests that the identified novel DDR genes could be a powerful prognostic tool for prognosis evaluation and a valuable tool in predicting the risk factors in OS patients.

1. Introduction

The most common primary malignant tumour of bone is osteosarcoma, which occurs most frequently in teens and young adults during the pubertal growth spurt [1]. Despite advancements in chemotherapy, surgery, and radiotherapy, patients with osteosarcoma without metastases have a 5-year OS rate of 78% [2]. OS, on the other hand, still has a 30% mortality rate [3]. Even though numerous ways for diagnosing and treating osteosarcoma have been established, new approaches for the treatment and prevention are required to be developed. The pathophysiology of osteosarcoma progression is still a mystery. As a result, finding efficient diagnostic markers and researching the leading molecular etiology of osteosarcoma is critical.

In many solid tumors, defective alterations during DNA repair can result in a significant increase in the frequency of neoantigens [4]. As a result, poor DNA repair has been linked to better clinical responses to PD-1 inhibition. A weakened mismatch repair (MMR) gave better therapeutic benefits with pembrolizumab in individuals with colorectal cancer [5–7] and the study of various solid tumors [8]. These findings have led to the FDA's landmark approval of PD-1 inhibitors in MMR-deficient malignancies, signaling a paradigm shift toward oncologic therapy based on molecular proficiency [8]. Several different DNA repair mechanisms have been linked to the accumulation of neoantigens. In a study of patients with NSCLC, POLE, MSH2, and mutations in POLD1 were found in excessive tumor neoantigens burden, which was linked to enhanced PD-1 treatment

responsiveness. Additionally, polymerase epsilon (POLE) mutations in endometrial cancers had higher expression of neoantigen burden and PD-L1 [9], and these mutations have been linked to exceptional immunotherapy responders [10]. Changes in the homologous recombination apparatus including BRCA2 and BCRA1 mutations were also linked to increased neoantigen load and overall survival following the treatment with anti-PD-1 [11]. Somatic alterations affecting the DNA damage repair (DDR) pathways and/or cell cycle are found in multiple subsets of osteosarcomas, and clinical trials are being designed to test precision medicine approaches based on these aberrations. However, the biomarker of DDR genes in the prognosis of OS has not yet been explored.

In the current study, we have examined and validated candidate DNA damage repair signature as a marker to predict prognosis by utilizing the GEO and TARGET databases. Identification of DNA damage repair signature will allow patients to be separated into low-risk and high-risk groups. Moreover, the expression pattern of DDR genes could be used as an independent prognostic signature for OS patients, allowing for the development of new treatment targets and diagnostic biomarkers.

2. Materials and Methods

2.1. Dataset and Data Processing. The data generated by the OS project of the TARGET (<https://ocg.cancer.gov/programs/target>) were used as the training set. The TARGET osteosarcoma project was used for the important clinical information for osteosarcoma patients as well as level three RNA-Seq data. As a validation set, the GEO dataset GSE21257 was employed. The GEO database was used for collecting the survival information of dataset GSE21257 and mRNA data.

2.2. Screening of Survival-Related DDR Genes. The model was developed by employing the machine learning approach and statistics as described previously [12]. To analyze the link between the survival time, and statue, and the expression of each DDR gene in the training cohorts, the univariate cox proportional hazard regression analysis was used on the basis of earlier studies. To build a prognosis model, multivariate cox regression analysis was used to filter for the most powerful and reliable predictive prognostic methylation sites. On the basis of the model, the prognosis risk was calculated using the expression equation as follows:

$$\text{risk score (RS)} = \sum_{i=1}^N \text{Exp}_i * \text{Coef}_i, \quad (1)$$

the number of expression of DDR gene signature is indicated by N , the expression of the DDR genesis is indicated by Exp_i , and multivariate cox regression coefficient is indicated by Coef_i . The risk score (RS) was the multinode weighted sum of risk scores, calculated using the signature coefficient for each patient as reported earlier. The median risk score was utilized as the cutoff value for dividing the training, test, and validation cohorts into high- and low-risk groups. The log-

rank test was employed for comparing the prognoses between two groups using Kaplan–Meier (K–M) survival analysis. The independent survival prediction of the methylation fingerprints was investigated via multivariable cox regression analysis. The methylation genes and differential expression between surrounding tissues and tumors were screened using the Student's t -test.

2.3. Functional Enrichment Analyses. The pathway enrichment analysis was carried out for the genes on the basis of the Gene Ontology (GO) database (biological process, cellular component, and molecular function abbreviated as BP, CC, and MF, respectively) and Kyoto Encyclopedia of Genes and Genomes (KEGG). For multiple comparisons, the P values were adjusted using the false-discovery rate (FDR) approach. The R package clusterProfiler was used to conduct all of the analyses [13].

2.4. Construction of the Nomogram. A nomogram was developed incorporating the two independent clinical risk factors (metastasis and age) and the methylation sites signature to predict the 1-, 3-, and 5-year survival rate in clinical practice. On a point scale, the nomogram score was determined for each variable. Following the calculation of the overall nomogram score, we calculated the anticipated 1-, 3-, and 5-year survival rates for each patient, as previously discussed.

2.5. Statistical Evaluations. The statistical evaluations were carried out with R 3.5.1 (<https://www.r-project.org>). pROC and Bioconductor (<https://bioconductor.org>) were used for downloading all the survivals. The two-tailed t -test with Mann–Whitney U -test was employed to identify the statistical variations between the two groups. A threshold P value <0.05 was regarded as statistically considerable for different analyses and correlations. The Wilcoxon rank-sum test was employed to determine the significance of the comparisons, and the results are displayed as mean P values (** $P < 0.01$; ** $P < 0.05$).

3. Results

3.1. Evaluation of the Prognostic DDR Genes from the Training Cohort. We first obtained DDR genes list from the study of Knijnenburg et al., [2], and then we integrated the expression of DDR genes in TARGET database samples. The sample from the TARGET database as the training group, with complete clinical information, was used for collecting more information on the association of prognosis with 276 genes. Being the independent variables, the survival statue and survival time were initially conducted using univariate cox proportional hazards regression analysis of the 276 genes. 18 DDR genes were considerably linked with the patients prognosis ($P < 0.05$; Figure 1(a) and Table S1). Furthermore, to obtain the highly predictive prognostic DDR genes, a multivariate cox regression analysis was carried out for the seven identified DDR genes set (NHEJ1,

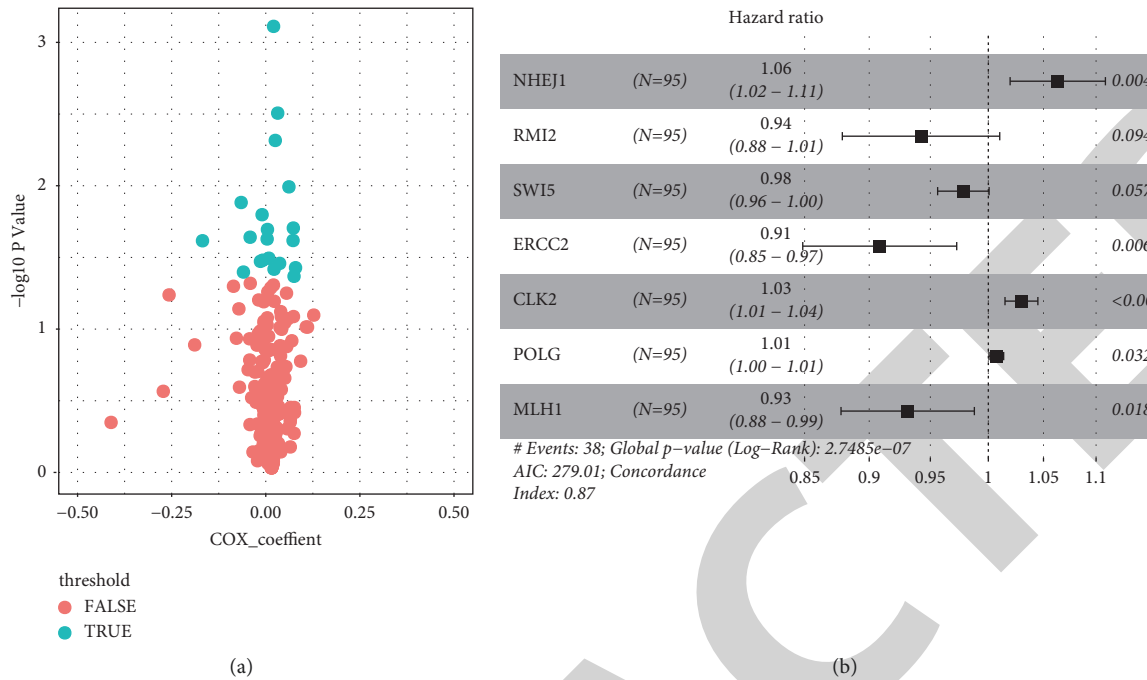


FIGURE 1: Develop DDR gene signature. (a) Univariate cox proportional hazards regression analysis of the DDR genes profiling data. (b) Multivariate cox regression analysis of the 18 DDR genes expression data. $P < 0.05$ was considered statistically significant in the group.

RMI2, SWI5, ERCC2, CLK2, POLG, and MLH1, Figure 1(b)) model to evaluate the prognosis risks for the patients. The risk score of the combination composed of NHEJ1, RMI2, SWI5, ERCC2, CLK2, POLG, and MLH1 (Table S2) was determined as follows:

$$\begin{aligned}
 RS = & (0.061 \times \text{Exp}_{\text{NHEJ1}}) + (0.06 \times \text{Exp}_{\text{RMI2}}) \\
 & + (-0.022 \times \text{Exp}_{\text{SWI5}}) \\
 & + (-0.096 \times \text{Exp}_{\text{ERCC2}}) + (0.029 \times \text{Exp}_{\text{CLK2}}) \\
 & + (0.007 \times \text{Exp}_{\text{POLG}}) + (-0.07 \times \text{Exp}_{\text{MLH1}}).
 \end{aligned} \quad (2)$$

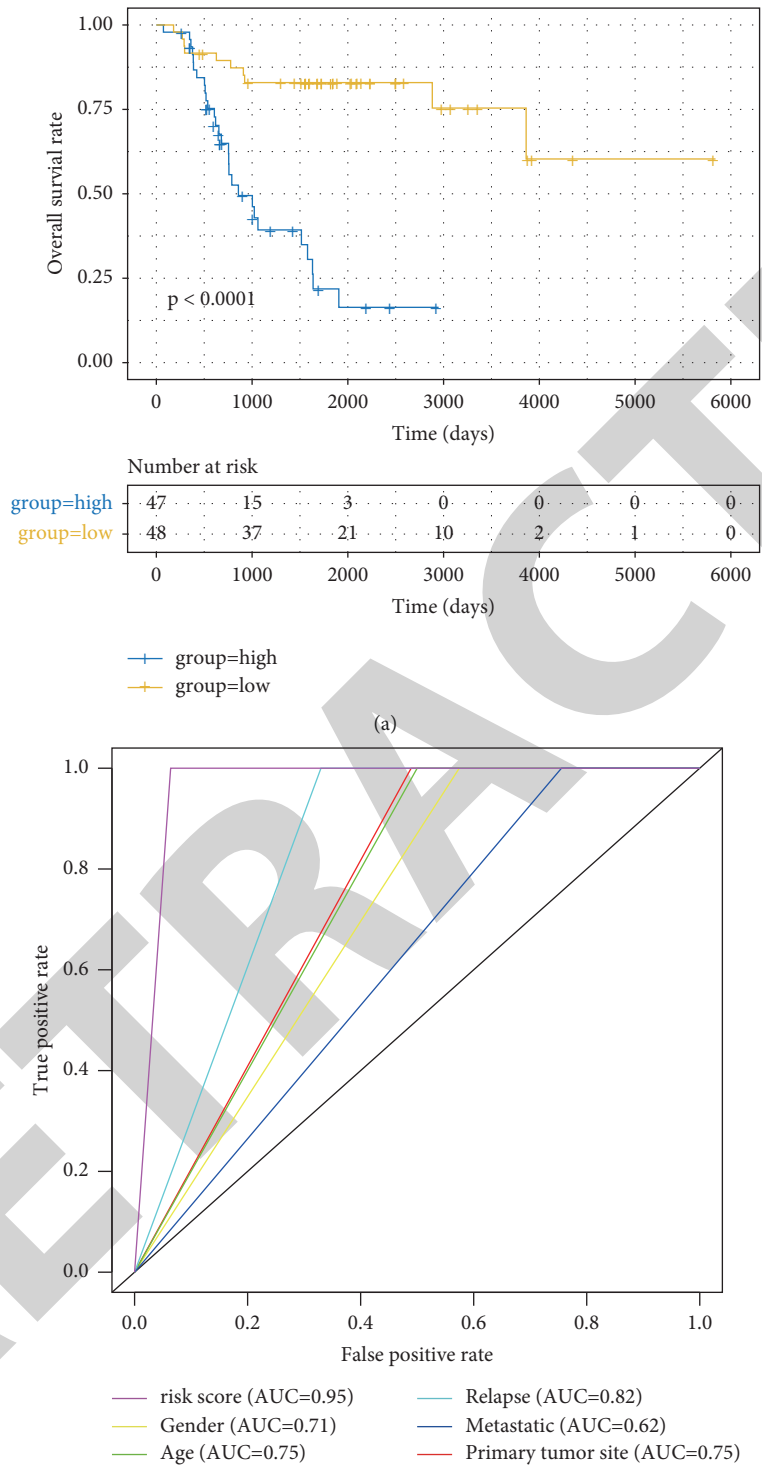
RS and Exp are the risk score and the expression value.

3.2. Confirmation of the Survival Status of the DDR Genes Signature in the TARGET Group. DDR genes signature was calculated in the risk score of all patients. To divide the training cohorts into high- ($n = 48$) and low-risk ($n = 47$) groups, the median risk score was used as the cutoff criterion. The survival rates were obtained using the K-M survival analysis. The low-risk scores patients had a 5-year survival rate of more than 75%, compared to less than 25% for the high-risk scores patients (HR: 3.15, 95% CI: 1.38–4.34, $P < 0.001$, Figure 2(a)). The receiver operating characteristic (ROC) curve was utilized to identify the prognostic model's accuracy. The model's ability to predict OS patients' prognosis improves as the area under the ROC curve increases. The prognostic signature's prediction precision was reliable in the training dataset (AUC Signature = 0.75, Figure 2(b)). Our results demonstrate that the DDR genes signature can be a potential novel and powerful accurate prognosis biomarker.

3.3. Confirmation of DDR Genes Signature's Ability to Survive in the Relapse Group. We collated relapse samples and follow-up data from the TARGET database. The relapse cohorts were classified into 39 (52%) high-risk and 36 (48%) low-risk groups using the established prognostic model. In the test group, the 5-year OS was more than 75% for the low-risk group and less than 25% for the high-risk group (HR: 2.65, 95% CI: 1.43–1.79; $P < 0.001$, Figure 2(c)).

3.4. The Robust DDR Gene Profile Validated in Different Validation Cohorts. The signature in GSE21257 was examined for the prognosis of OS patients to validate that the found seven DDR gene-based classifiers had equal predictive value in various patients. Employing the established coefficient of the module, the training cohorts were categorized into LR group (26 (49.1%)) and HR group (27 (50.9%)). The corresponding 5-year OS was 65% for the LR group and less than 50% for the HR group in GSE21257 (Figure 2(d)). The validation dataset also showed that the DDR gene profile used in this study was a reliable prognostic indicator.

3.5. Independent Prognostic Indicators and the Nomogram Development for Predicting the Prognosis of Patients. Multivariate cox regression analysis was carried out to evaluate the association between clinicopathological features (metastasis and age) and the signature risk score. In the training dataset, the association showed that the signature independently predicted the survival rate of patients (high- vs. low-risk group, HR = 0.15, 95% CI: 0.068–0.034, $P < 0.001$, Figure 3(a)). A nomogram incorporating the two clinical risk variables (metastasis and age) and the DDR



(b)
 FIGURE 2: Continued.

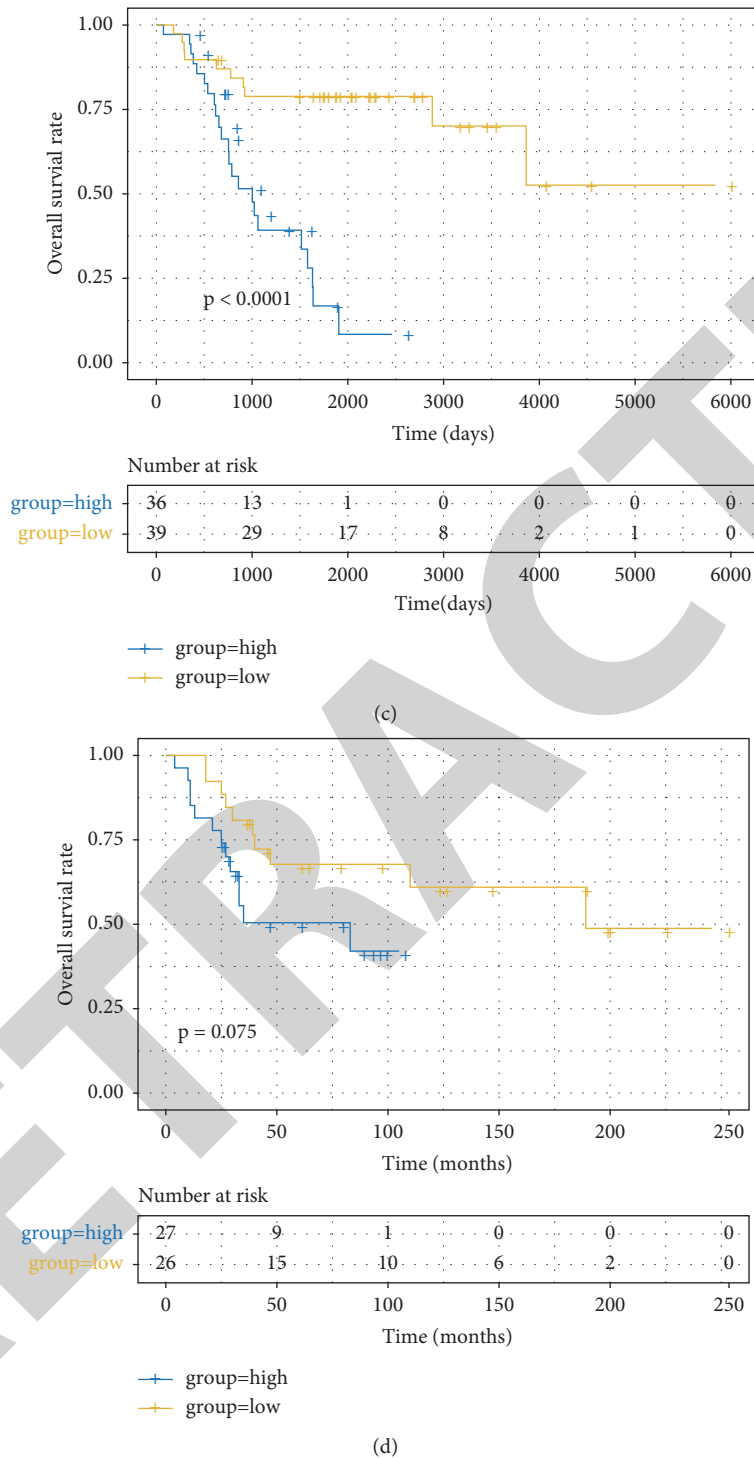


FIGURE 2: DDR gene signature predicts survival rate of patients with OS patients. (a) Kaplan–Meier survival curves divided OS patients into the high-risk group and low-risk group using the DDR genes signature in the TARGET groups. (b) Area under the curve (AUC) of receiver and the operating characteristic (ROC) curve to assess the sensitivity and specificity of the prognostic model. (c) DDR gene signature was validated in the relapse group. (d) DDR gene signature was validated in the GSE21257 group.

genes signature was developed for predicting the 1-, 2-, and 5-year survival rates in clinical practice. According to the point scale, the tool may calculate a nomogram score for each variable. We calculated the estimated probability of 1-,

3-, and 5-year survival for each patient after computing the overall nomogram score. The signature contributed the most to the 1-, 3-, and 5-year prognosis, according to the nomogram, followed by age and stage (Figure 3(b)).

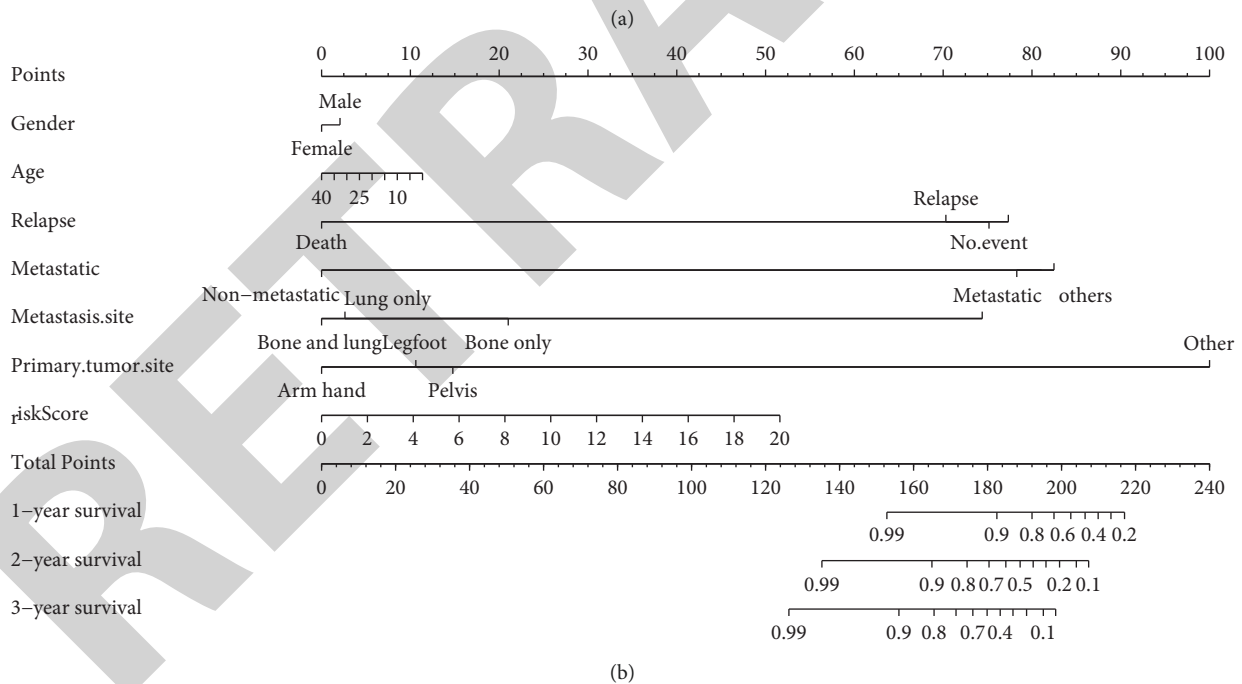
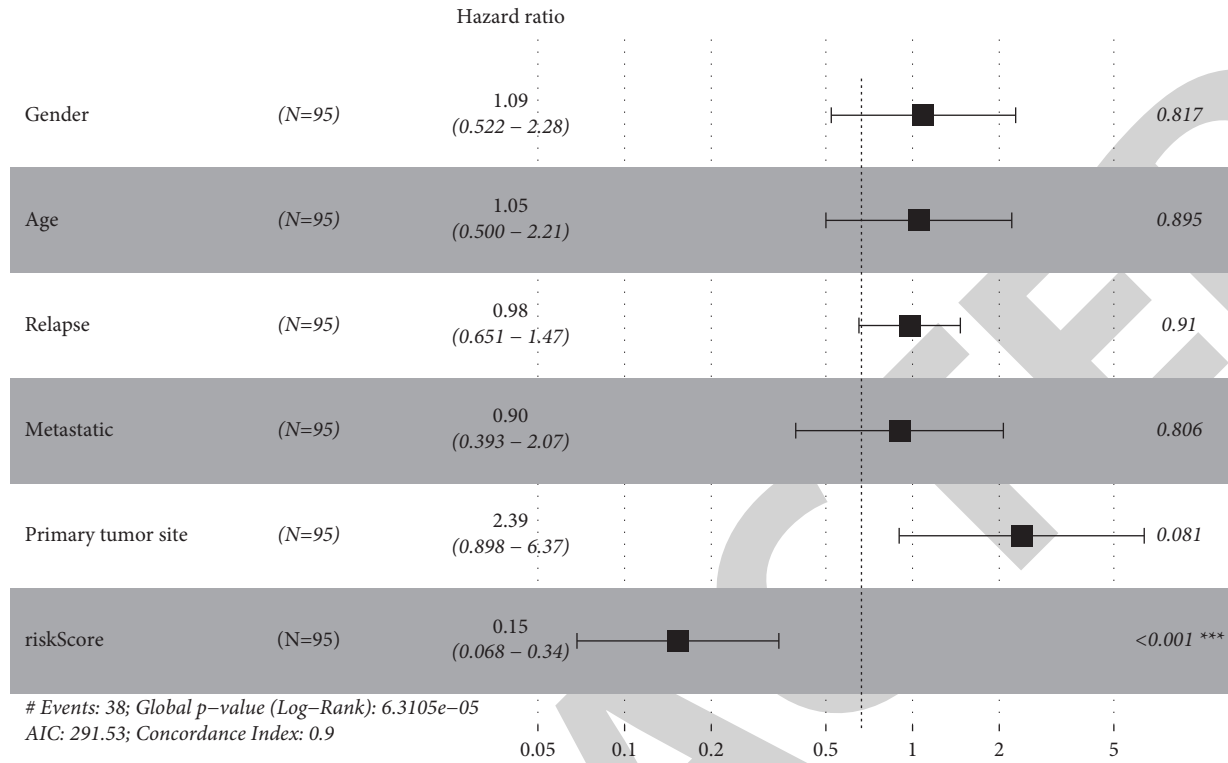


FIGURE 3: The DDR gene signature of independent prognostic factors and developed nomogram. (a) The signature-combined clinical information was used for multivariate cox regression analysis to study the correlation of prognosis of LUSC patients in the training group. (b) Nomogram-combined methylated gene sites signature and clinical-related variables predict patients' prognosis.

3.6. Functional Prediction of DDR Signature Genes. The possible participation of the DDR signature genes in biological processes involved with osteosarcoma development was investigated using GO and KEGG analyses. The functional analysis was performed with these genes. The GO findings showed that the DDR signature genes were related to DNA

recombination, chromosome segregation, double-strand break repair, and nonrecombinational repair (Figure 4(a)). We also found that DDR signature genes were involved in the Fanconi anemia pathway, NHEJ pathway, mismatch repair, and nucleotide excision repair pathway (Figure 4(b)) which is essential in single or double strands of DNA and their repair systems.

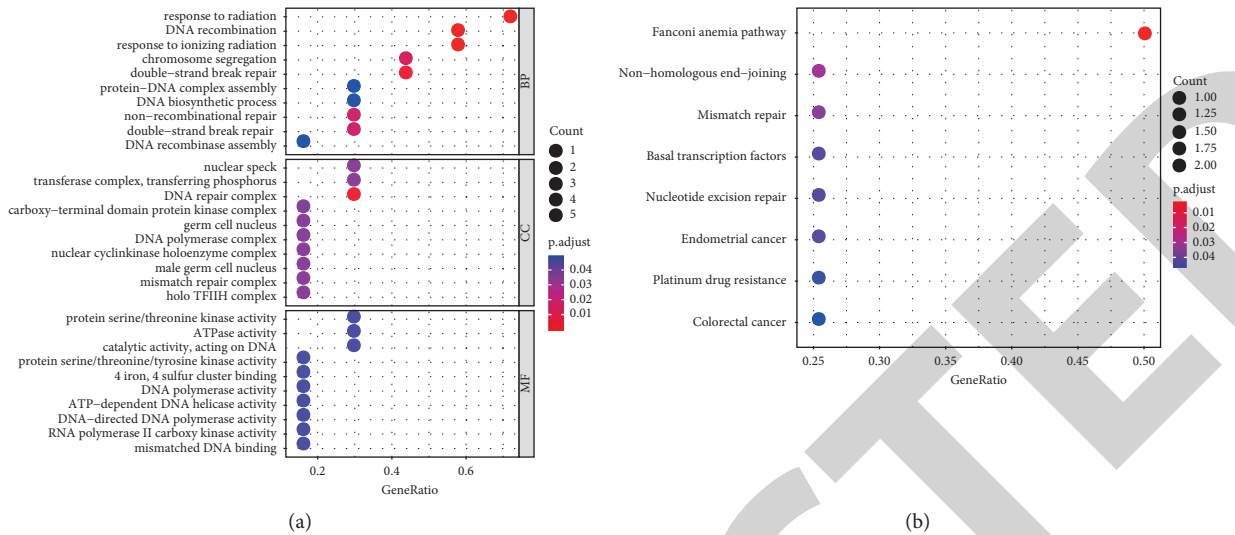


FIGURE 4: Functional analysis of the signature genes. (a) The results of GO analysis. (b) The results of KEGG analysis.

4. Discussion

One of the most common malignant tumors in the orthopedic area is osteosarcoma. It has been invasive, has a high rate of metastatic spread, and has a bad prognosis [14]. For OS patients, the absence of appropriate prognostic indicators has been the main concern. Somatic changes impacting the DDR pathways and/or cell cycle have been seen in multiple subsets of osteosarcomas, and clinical trials are being designed to test precision medicine strategies based on these aberrations. However, more precise DDR genes signatures and stable modules to predict prognosis is needed, which can make the individualized therapeutic decision for patients with OS patients. So, we are the first to study DDR-related prognosis signature in OS patients.

In our study, we evaluated 276 DDR genes from previous research which had opposite differential expressed patterns. By applying different statistical approaches, we identified seven DDR genes signature. Furthermore, we validated the DDR genes signature in the relapse group and external validation group which is a powerful tool in predicting the prognosis and was independently associated with the overall survival for OS patients. Finally, we established a DDR signature gene nomogram to predict prognosis. We found that DDR signature genes took part in the Fanconi anemia pathway, NHEJ cascades, mismatch repair, and nucleotide excision repair pathway. Our study implicates applications in precision therapy and then eventually leads to an enhancement in the prognosis of OS patients.

We determined a set of seven DDR genes consisting of NHEJ1, RMI2, and SWI5, ERCC2, CLK2, POLG, and MLH1 that predicts prognosis in two patient cohorts.

In colorectal cancer patients, the *MLH1* gene, like a number of other suppressor genes, is susceptible to being silenced by promoter methylation [15] and, for patients with stage II and III colorectal cancer, *MLH1* expression gives useful prognostic information [16]. *ERCC2* is a key

component of the nucleotide excision repair process, as well as cell cycle and apoptosis control and transcription initiation [17]. In colorectal and gastric cancers, *ERCC2* polymorphism predicts the clinical outcomes of oxaliplatin-based chemotherapies [18]. *POLG* is the sole DNA polymerase found in human mitochondria, and it is required for DNA repair and replication [19]. *POLG* gene was considerably linked with the prognosis of hepatocellular carcinoma patients in a dose-dependent manner [20]. In breast cancer, *CLK2*, a kinase that phosphorylates SR proteins implicated in splicing, functions as an oncogene [21], and highly expressed *CLK2* significantly enhances the proliferation of lung cancer cells, thereby promoting the occurrence and development of lung cancer [22].

In human cells, the nonhomologous end joining (NHEJ) DNA damage repair pathway is the most common pathway for DNA double-strand repair, and its abnormal activity has been linked to treatment resistance in a variety of cancers [23]. *NHEJ1* deficiencies may facilitate the accumulation of mutations in the setting of DNA mismatch repair deficiency in cancers [24]. *RMI2* is an important component of the BLM-TopoIIa-RMI1-RMI2 complex, which helps to keep the genome stable [25]. *RMI2* expression was linked to a poor prognosis and shorter survival time in patients with hepatocellular cancer [26] and is also important for lung cancer metastasis and growth [27]. *SWI5* facilitates the Rad51-dependent recombination repair cascade and is a component of the *SWI5-SFR1* heterodimers [28]. In both sporadic and familial breast cancer patients, *SWI5* proteins implicated in DNA damage response were expressed [29].

Taken together, we successfully obtained prognostic signatures which may predict the survival rate of OS patients. Importantly, we developed a seven-DDR gene nomogram to predict patients' prognosis. Our findings show that this signature has the potential to be a precise and reliable biomarker for predicting prognosis and tailoring therapy for OS patients.

Data Availability

All the data used to support the findings of this study are included within the article.

Ethical Approval

The contents of this article are data mining from the The Cancer Genome Atlas (TARGET) database. The TARGET database is open and shared.

Consent

Informed patient consent is not required.

Conflicts of Interest

The authors declare no conflicts of interest.

Authors' Contributions

Tang Ying and Yan-xia Liu collected the sample data and obtained the clinical information. Xiuning Huang and Peng Li performed data analysis and designed the study. Tang Ying and Peng Li integrated the results and drafted the manuscript.

Acknowledgments

The National Natural Science Foundation of China (grant number 81673098). Effect of epigenetic regulation of HMGA expression-related microRNA on the activation of NEPs cell group in neuronal regeneration of developing cerebellum after radiotherapy.

Supplementary Materials

Table S1: DDR genes of univariate cox regression analysis in the TARGET group. Table S2: the risk score of DDR gene signature in the TARGET group. (*Supplementary Materials*)

References

- [1] J. Gill and R. Gorlick, "Advancing therapy for osteosarcoma," *Nature Reviews Clinical Oncology*, vol. 18, no. 10, pp. 609–624, 2021.
- [2] T. A. Knijnenburg, L. Wang, M. T. Zimmermann et al., "Genomic and molecular landscape of DNA damage repair deficiency across the cancer genome Atlas," *Cell Reports*, vol. 23, no. 1, p. 239, 2018.
- [3] C.-D. Yin, Y.-L. Hou, X.-R. Liu et al., "Development of an immune-related prognostic index associated with osteosarcoma," *Bioengineered*, vol. 12, no. 1, pp. 172–182, 2021.
- [4] Y. K. Chae, J. F. Anker, M. S. Oh et al., "Mutations in DNA repair genes are associated with increased neoantigen burden and a distinct immunophenotype in lung squamous cell carcinoma," *Scientific Reports*, vol. 9, no. 1, p. 3235, 2019.
- [5] Y. Asaoka, H. Ijichi, and K. Koike, "PD-1 blockade in tumors with mismatch-repair deficiency," *New England Journal of Medicine*, vol. 373, no. 20, p. 1979, 2015.
- [6] D. T. Le, J. N. Uram, H. Wang et al., "PD-1 blockade in tumors with mismatch-repair deficiency," *New England Journal of Medicine*, vol. 372, no. 26, pp. 2509–2520, 2015.
- [7] L. A. Diaz Jr. and D. T. Le, "PD-1 blockade in tumors with mismatch-repair deficiency," *New England Journal of Medicine*, vol. 373, no. 20, p. 1979, 2015.
- [8] D. T. Le, J. N. Durham, K. N. Smith et al., "Mismatch repair deficiency predicts response of solid tumors to PD-1 blockade," *Science*, vol. 357, no. 6349, pp. 409–413, 2017.
- [9] B. E. Howitt, S. A. Shukla, L. M. Sholl et al., "Association of polymerase e-mutated and microsatellite-instable endometrial cancers with neoantigen load, number of tumor-infiltrating lymphocytes, and expression of PD-1 and PD-L1," *JAMA Oncology*, vol. 1, no. 9, pp. 1319–1323, 2015.
- [10] J. M. Mehnert, A. Panda, H. Zhong et al., "Immune activation and response to pembrolizumab in POLE-mutant endometrial cancer," *Journal of Clinical Investigation*, vol. 126, no. 6, pp. 2334–2340, 2016.
- [11] K. C. Strickland, B. E. Howitt, S. A. Shukla et al., "Association and prognostic significance of BRCA1/2-mutation status with neoantigen load, number of tumor-infiltrating lymphocytes and expression of PD-1/PD-L1 in high grade serous ovarian cancer," *Oncotarget*, vol. 7, no. 12, pp. 13587–13598, 2016.
- [12] N. Lee, X. Xia, H. Meng et al., "Identification of a novel CpG methylation signature to predict prognosis in lung squamous cell carcinoma," *Cancer Biomarkers*, vol. 30, no. 1, pp. 63–73, 2021.
- [13] G. Yu, L.-G. Wang, Y. Han, and Q.-Y. He, "clusterProfiler: an R package for comparing biological themes among gene clusters," *OMICS: A Journal of Integrative Biology*, vol. 16, no. 5, pp. 284–287, 2012.
- [14] Y. Prabowo, I. Setiawan, A. F. Kamal, E. Kodrat, and M. L. Labib Zufar, "Correlation between prognostic factors and the histopathological response to neoadjuvant chemotherapy in osteosarcoma: a retrospective study," *International Journal of Surgical Oncology*, vol. 2021, Article ID 8843325, 2021.
- [15] G. Lanza, R. Gafà, A. Santini, I. Maestri, L. Guerzoni, and L. Cavazzini, "Immunohistochemical test for MLH1 and MSH2 expression predicts clinical outcome in stage II and III colorectal cancer patients," *Journal of Clinical Oncology*, vol. 24, no. 15, pp. 2359–2367, 2006.
- [16] X. Li, X. Yao, Y. Wang et al., "MLH1 promoter methylation frequency in colorectal cancer patients and related clinicopathological and molecular features," *PLoS One*, vol. 8, no. 3, Article ID e59064, 2013.
- [17] S. Benhamou and A. Sarasin, "ERCC2/XPD gene polymorphisms and cancer risk," *Mutagenesis*, vol. 17, no. 6, pp. 463–469, 2002.
- [18] M. Yin, J. Yan, E. Martinez-Balibrea et al., "ERCC1 and ERCC2 polymorphisms predict clinical outcomes of oxaliplatin-based chemotherapies in gastric and colorectal cancer: a systemic review and meta-analysis," *Clinical Cancer Research*, vol. 17, no. 6, pp. 1632–1640, 2011.
- [19] S. S. L. Chan and W. C. Copeland, "DNA polymerase gamma and mitochondrial disease: understanding the consequence of POLG mutations," *Biochimica et Biophysica Acta (BBA)-Bioenergetics*, vol. 1787, no. 5, pp. 312–319, 2009.
- [20] X. Long, X. Wang, Y. Chen et al., "Polymorphisms in POLG were associated with the prognosis and mtDNA content in hepatocellular carcinoma patients," *Bulletin du Cancer*, vol. 104, no. 6, pp. 500–507, 2017.
- [21] T. Yoshida, J. H. Kim, K. Carver et al., "CLK2 is an oncogenic kinase and splicing regulator in breast cancer," *Cancer Research*, vol. 75, no. 7, pp. 1516–1526, 2015.

Retraction

Retracted: Development and Validation of a Novel Mitophagy-Related Gene Prognostic Signature for Hepatocellular Carcinoma Based on Immunoscore Classification of Tumor

Journal of Oncology

Received 10 October 2023; Accepted 10 October 2023; Published 11 October 2023

Copyright © 2023 Journal of Oncology. This is an open access article distributed under the Creative Commons Attribution License, which permits unrestricted use, distribution, and reproduction in any medium, provided the original work is properly cited.

This article has been retracted by Hindawi following an investigation undertaken by the publisher [1]. This investigation has uncovered evidence of one or more of the following indicators of systematic manipulation of the publication process:

- (1) Discrepancies in scope
- (2) Discrepancies in the description of the research reported
- (3) Discrepancies between the availability of data and the research described
- (4) Inappropriate citations
- (5) Incoherent, meaningless and/or irrelevant content included in the article
- (6) Peer-review manipulation

The presence of these indicators undermines our confidence in the integrity of the article's content and we cannot, therefore, vouch for its reliability. Please note that this notice is intended solely to alert readers that the content of this article is unreliable. We have not investigated whether authors were aware of or involved in the systematic manipulation of the publication process.

Wiley and Hindawi regrets that the usual quality checks did not identify these issues before publication and have since put additional measures in place to safeguard research integrity.

We wish to credit our own Research Integrity and Research Publishing teams and anonymous and named external researchers and research integrity experts for contributing to this investigation.

The corresponding author, as the representative of all authors, has been given the opportunity to register their agreement or disagreement to this retraction. We have kept a record of any response received.

References

- [1] H. Chen, J. Wang, R. Zeng et al., "Development and Validation of a Novel Mitophagy-Related Gene Prognostic Signature for Hepatocellular Carcinoma Based on Immunoscore Classification of Tumor," *Journal of Oncology*, vol. 2021, Article ID 5070099, 16 pages, 2021.

Research Article

Development and Validation of a Novel Mitophagy-Related Gene Prognostic Signature for Hepatocellular Carcinoma Based on Immunoscore Classification of Tumor

Hao Chen ¹, Jinghua Wang ², Ruijie Zeng ^{1,3}, Yujun Luo ¹, Kehang Guo ^{1,4},
Huihuan Wu ^{1,4}, Qi Yang ¹, Rui Jiang ^{1,5}, Weihong Sha ¹ and Zewei Zhuo ^{1,4,5}

¹Department of Gastroenterology, Guangdong Provincial People's Hospital, Guangdong Academy of Medical Sciences, Guangzhou 510080, China

²Department of Hematology, Guangdong Provincial People's Hospital, Guangdong Academy of Medical Sciences, Guangzhou 510080, China

³Shantou University Medical College, Shantou 515041, China

⁴School of Medicine, South China University of Technology, Guangzhou 510006, China

⁵School of Bioscience and Bioengineering, South China University of Technology, Guangzhou 510006, China

Correspondence should be addressed to Weihong Sha; shaweihong@gdph.org.cn and Zewei Zhuo; bizzw@mail.scut.edu.cn

Received 21 September 2021; Revised 3 October 2021; Accepted 6 October 2021; Published 25 October 2021

Academic Editor: Yun-dai Chen

Copyright © 2021 Hao Chen et al. This is an open access article distributed under the Creative Commons Attribution License, which permits unrestricted use, distribution, and reproduction in any medium, provided the original work is properly cited.

Emerging evidence suggested that mitophagy may play an important role in the progression of hepatocellular carcinoma (HCC), whereas the association between mitophagy-related genes and HCC patients' prognosis remains unknown. In this study, we aimed to investigate the potential prognostic values of mitophagy-related genes (MRGs) on HCC patients at the genetic level. According to median immunoscore, we categorized HCC patients from TCGA cohort into two immune score groups, while 39 differential expression MRGs were identified. By using univariate analysis, we screened out 18 survival-associated MRGs, and then, the least absolute shrinkage and selection operator (LASSO) analysis was applied to construct a prognosis model that consisted of 9 MRGs (ATG7, ATG9A, BNIP3L, GABARAPL1, HTRA2, MAP1LC3B2, TFE3, TIGAR, and TOMM70). In our prognostic model, overall survival in the high and low-risk groups was significantly different ($P < 0.001$), and the respective areas under the curve (AUC) of our prognostic model were 0.686 for 3-year survival in the TCGA cohort and 0.776 for 3-year survival in the ICGC cohort. Moreover, we identified the risk score as the independent factor for predicting the HCC patients' prognosis by using single and multifactor analyses, and a nomogram was also constructed for future clinical application. Further functional analyses showed that the immune status between two risk groups was significantly different. Our findings may provide a novel mitophagy-related gene signature, and these will be better used for prognostic prediction in HCC, thus improving patient outcome.

1. Introduction

Hepatocellular carcinoma (HCC) is the commonly diagnosed cancer, representing a significant proportion (75–85%) of cases in primary liver cancer. In 2020, approximately 906,000 new cases and 830,000 deaths occur in liver cancer, which has become an increasing threat to human health worldwide [1]. Large heterogeneity of tumor, frequent recurrence, and intrahepatic metastasis led to a poor 5-year survival rate (5–6%) of HCC, making prognostic

prediction challenging [2]. Despite some progresses made in HCC treatment, more new therapeutic targets are required to be implemented [3]. Hence, it is of significance to develop a novel biomarker and risk models to forecast HCC patients' prognosis and provide actionable targets for expanding therapeutic options.

Mitochondria are the dominating power sources of healthy cells. However, they produce lower energy in cancer cells, and the reprograms metabolism is one of the hallmarks of cancer [4]. Mitochondrial autophagy (mitophagy) can

remove dysfunctional or unneeded mitochondria by autophagy, which plays an essential process in cellular homeostasis [5]. Recently, mitophagy-related genes (MRGs) such as PINK1, Parkin, FUNDC1, PHB2, and BNIP3 have developed as a potential target for the development of novel therapeutic strategies for overcoming cancer resistance [6]. In 2020, Zhu et al. demonstrated that the abnormal expression of PINK1 can serve well as biomarker for prognosis of patients with HCC by pancancer analysis [7]. Yan et al. identified another novel mitophagy pathway, PHB2-PARL-PGAM5-PINK1 axis, involved in cancer proliferation and progression, which may become a promising target for the anticancer agent [8]. However, such investigations on MRGs are single or small combination studies, and they do not construct a predictive signature for HCC patients. Therefore, a comprehensive study of MRGs on HCC patients' prognosis at the genetic level is urgently needed.

Recently, immunoscore-based tumor classification has reliably estimated the risk and survival outcome in various tumors with improved guidance of diagnosis and prognosis in tumors [9]. Zheng et al. have also reported that immune-based signature can be used for forecasting HCC patients' prognosis, which offers new insight into treatment and prognosis [10]. Despite advances on the association between the immune score and the prognosis of tumor patients, individualized prognostic models using immunoscore-based tumor classification combined with MRGs have been seldomly reported.

Given the significant values of MRGs with a combination of immunoscore-based tumor classification on HCC patients, we developed and validated a novel mitophagy-related gene signature for forecasting HCC patients' prognosis, which may provide new insight into HCC treatment and prognosis.

2. Materials and Methods

2.1. Data Collection. RNA-sequencing (RNA-seq) information and clinical characteristics of 371 HCC cases were obtained from the TCGA database up to July 21st, 2021 (<https://portal.gdc.cancer.gov/repository>). The RNA-seq and their corresponding clinical information of 243 HCC samples were obtained as a validation cohort from the ICGC portal (<https://dcc.icgc.org/projects/LIRI-JP>). The immune score of HCC was retrieved from ESTIMATE (<https://bioinformatics.mdanderson.org/estimate>). 88 MRGs were selected from GeneCards (<https://www.genecards.org>) based on their relevance score (relevance score >2, Table S1) on July 21, 2021.

2.2. Immunoscore-Based Tumor Classification and Screening Differential MRGs. Using median immune score as the cutoff, 371 HCC cases were categorized into a high immune score group and a low immune score group. 88 MRGs expression profiles were extracted from the TCGA cohort's RNA-seq data, and then, the differentially expressed MRGs were screened out by using the "limma" R package between such two groups with a threshold of $P < 0.05$. Using the

"GOplot" package of R, GO enrichment visualization was employed to identify the main biological properties of these differentially expressed MRGs. Protein-protein interaction (PPI) networks of differentially expressed MRGs were obtained from a website called Search Tool for the Retrieval of Interacting Genes (STRING) (<https://string-db.org>), and the "igraph" package of R was used to analyze the correlation network of these differentially expressed MRGs [11].

2.3. Establishment and Verification of the Prognostic Model.

Univariate analysis was employed to evaluate overall survival (OS)-related genes, and we performed survival analysis on them. The LASSO algorithm (R package "glmnet") was further conducted on these OS-related genes to screen out the final gene signature for developing a prognostic model. Penalty parameter (λ) for the model was decided by the minimum criteria. Use the "scale" function of R to centralize and normalize the TCGA expression data for calculating the risk score. The formula is given as follows: risk score = sum (corresponding coefficient \times each gene's expression level). According to the median value of the risk score, we classified HCC cases into two risk groups (high-risk group and low-risk group). The training set (TCGA cohort) and validation set (ICGC cohort) were both applied to verify the validity of this risk model. Principal component analysis (PCA) was performed by the "prcomp" function in the "stats" R package. Survival analysis was performed to compare the OS time between two risk groups by "survminer" and "survival" packages of R. ROC curve analysis was performed by "survminer," "survival," and "time-ROC" of R to evaluate the performance of our prognostic risk score model.

2.4. Estimation of Independent Prognostic Value.

HCC patients' clinicopathological characteristics were extracted from the TCGA cohort. The relationship between the clinical variables (age, sex, tumor grade, T stage, N stage, M stage, and tumor stage) and risk model was performed by using univariate and multivariable Cox regression analyses. To better access the role of our risk score in HCC development, we further explore the association between the risk score and HCC patients' clinicopathological characteristics. Subsequently, R packages "rms" and "survival" were applied to develop a nomogram that included each MRG signature in the model to evaluate the role of the prognostic model. The calibration curve and its quantified data of each risk group were performed using the "riskRegression" and "survival" package.

2.5. Functional Enrichment Analysis.

DEGs between two risk groups were screened out by the criteria ($|\log_2FC| \geq 1$, $FDR < 0.05$). The "clusterProfiler" R package was applied to process Gene Ontology (GO) and Kyoto Encyclopedia of Genes and Genomes (KEGG) analyses [12]. The BH method was used to adjust P values. The most notably enriched GO terms and KEGG pathways were visualized by "GOplot" package of R. Tumor Immune Estimation Resource (TIMER) database was performed to analyze the

relationships between 9 MRGs expression and immune cell infiltration (<https://cistrome.shinyapps.io/timer/>). Single-sample gene set enrichment analysis (ssGSEA) enrichment score was performed by the “gsva” of R to assess the link between the immune activity and risk score.

2.6. Statistical Analysis. R (version 4.1.0) was used for all statistical analyses. Student’s *t*-test was employed to compare gene expression between high and low immune score groups. A log-rank test was applied to compare the OS between two risk groups. The independent predictors of OS were identified by implementing univariate and multivariate Cox regression analyses, while the categorical variables were compared by the chi-squared test. The BH method was used for *P* values adjusting. The Mann–Whitney test was applied to compare the ssGSEA enrichment scores between groups.

3. Results

3.1. Immune Score of HCC Samples and HCC Patients’ Baseline Information. We categorized the RNA expression data of HCC patients from the TCGA database (*n* = 371) into a high immune score group and low immune score group based on the median immune score, preparing for further screening differential genes. The immune score of each sample is given in Table S2. After excluding 6 tumor samples with missing data (follow up with 0 day), 365 HCC samples from the TCGA dataset were included as a training set. The validation set consisted of 243 HCC samples from the ICGC dataset (Table S3).

3.2. Identification of DEGs between High and Low Immune Score Groups. We presented a heatmap of normalized gene expression profiles of 88 MRGs between the high immune score group (*n* = 186) and low immune score group (*n* = 185) (Figure 1(a)). 39 MRGs were differentially expressed between two groups (FDR < 0.05). Figure 1(b) shows a boxplot of 39 MRGs expression between two immune score groups. GO enrichment analysis showed that these genes were mainly enriched in macroautophagy, autophagosome, mitochondrion, autophagosome membrane, and mitophagy, indicating their tight relationship with mitophagy (Figure 1(c)). Figure 1(d) shows the correlation network of the mitophagy-related DEGs between two immune score groups, and the colors intensity marked the degree of the relevance. Protein-protein interaction (PPI) analysis was performed to further explore the interactions of these mitophagy-related DEGs (interaction score = 0.700, high confidence). As shown in Figure 1(e), we could find that MAP1LC3A, MAP1LC3B, GABARAP, GABARAPL1, ATG7, ATG14, ATG9A, BNIP3, BNIP3L, OPTN, NBR1, TOMM20, PARK2, and TP53 were hub genes.

3.3. Establishment of the Prognostic Risk Model Based on MRG Signature. 18 MRGs were associated with patients’ survival after using univariate analysis (*P* < 0.05, Figure 2(a)). To further assess the influence of these genes on the

survival of HCC patients, we performed survival analyses and found that 9 MRGs (TFE3, PHB, HIF1A, TOMM70, HTRA2, ATG7, TIGAR, ATG9A, and MAP1LC3B2) were correlated with a poor prognosis (all adjusted *P* < 0.05, Figures 2(c)–2(k)), whereas GABARAPL1 was reversed (adjusted *P* < 0.05, Figure 2(b)). This well illustrated that using immunoscore-based tumor classification can be used to screen out most differentially expressed MRGs with a better survival and prognostic value, which laid a good foundation for developing a prognostic risk model. After LASSO regression analysis of these genes mentioned above, we obtained a 9-gene signature (ATG7, ATG9A, BNIP3L, GABARAPL1, HTRA2, MAP1LC3B2, TFE3, TIGAR, and TOMM70) based on the optimal value of λ (0.02719766) (Figures 3(a) and 3(b)). The multivariate Cox regression analysis of these 9 genes confirmed that GABARAPL1, HTRA2, and TOMM70 had significant prognostic values for patients with HCC from the TCGA cohort (*P* < 0.05, Figure 3(c)). The risk score model was established as follows: risk score = (0.345957 * MAP1LC3B2 + 0.145250 * TIGAR + 0.126953 * HTRA2 + 0.034558 * TOMM70 + 0.034531 * ATG9A + 0.020504 * BNIP3L + 0.002834 * ATG7 + 0.000903 * TFE3 – 0.014023 * GABARAPL1).

To offer a quantitative method to predict the survival rate of HCC patients, we developed a nomogram according to the risk score and 9-gene signature. The total nomogram score was calculated to predict HCC patients’ survival time at 1, 3, and 5 years (Figure 3(d)). The point of each gene was obtained via drawing a line straight upward from each gene to the point scale in the nomogram. Sum each point to the total points and then locate them in the total points scale to further convert to survival probability. The results indicated that the nomogram-predicted risk generally coincided with the estimated actual risk (Figure 3(e)). Quantitation data of the calibration curve has also shown that these values of predicted risk were close to that of the values of estimated actual risk in each risk group (Figure 3(f)). This suggested that our signature-based nomogram could provide a high value to predict the prognosis of HCC patients. According to the median risk score, we classified the HCC cases into a high-risk group (*n* = 182) and a low-risk group (*n* = 183) (Figure 4(a)). Figure 4(b) shows that the patients in the low-risk group possessed longer survival times and fewer deaths than in the high-risk group. PCA plot demonstrated that patients can be well separated into two clusters according to the risk score (Figure 4(c)). The survival time of the low-risk group was notably better than that of the high-risk group (*P* < 0.001, Figure 4(d)). In addition, to test the reliability of the prognostic model, we performed ROC analysis. As shown in Figure 4(e), the area under the ROC curve (AUC) was 0.743 for 1-year, 0.686 for 3-year, and 0.684 for 5-year survival, indicating that MRGs could be used as a predictor in the prognosis of HCC. Furthermore, a heatmap of the 9-gene signature was drawn between two risk groups in combination with clinical features from the TCGA cohort (Figure 4(f)). We could find that 8 genes (ATG7, ATG9A, BNIP3L, HTRA2, MAP1LC3B2, TFE3, TIGAR, and TOMM70) were upregulated in the high-risk group except for GABARAPL1 (*P* < 0.05).

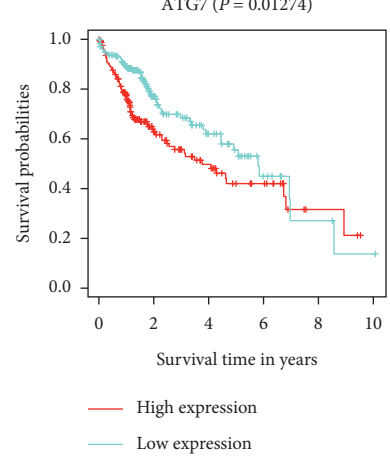
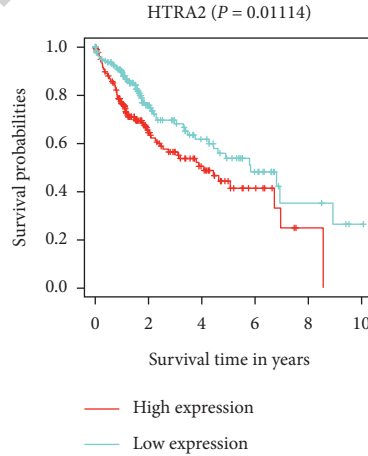
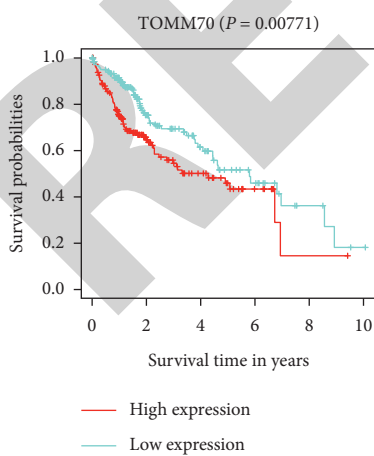
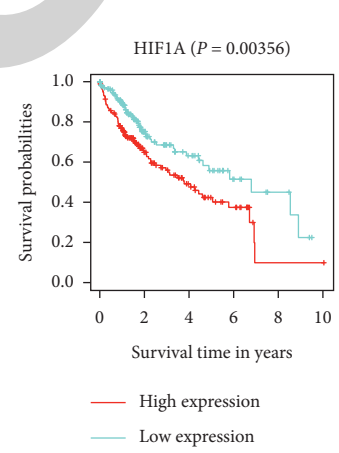
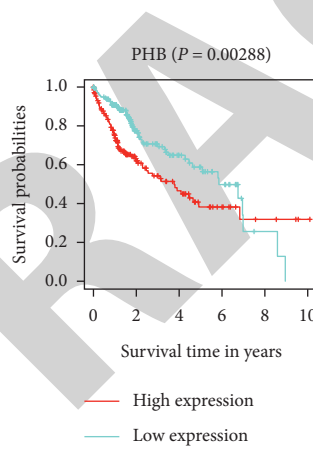
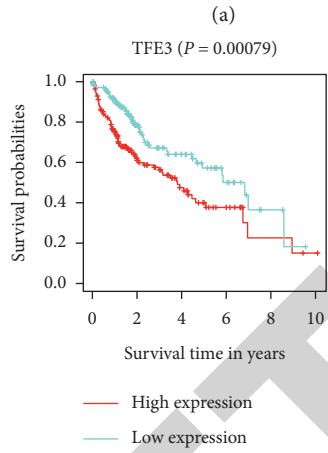
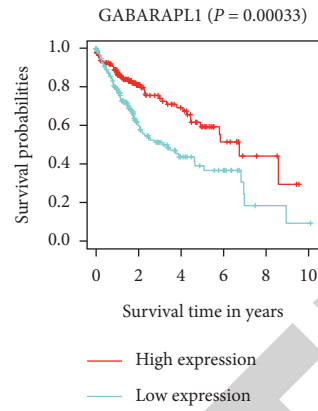
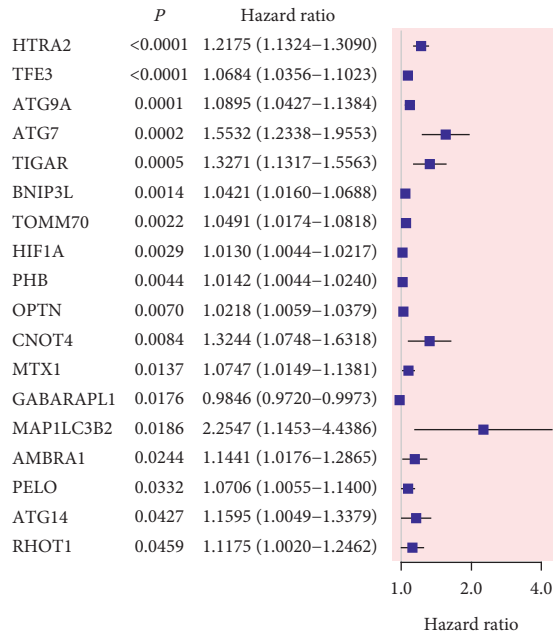


FIGURE 2: Continued.

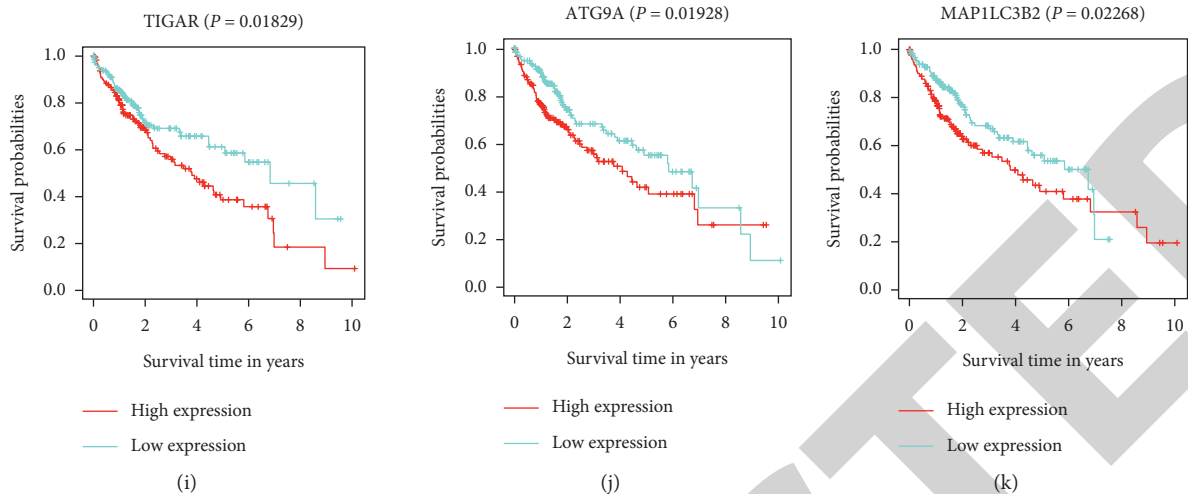


FIGURE 2: Survival analysis of 39 MRGs. (a) A forest plot of prognosis-related mitophagy genes after univariate analysis, and 18 genes were with $P < 0.05$; when the HR > 1 , the gene was regarded as a high-risk gene. HR, hazard ratio. (b)–(k) Survival analysis of 10 significantly different genes. High expression of TFE3, PHB, HIF1A, TOMM70, HTRA2, ATG7, TIGAR, ATG9A, and MAP1LC3B2 was correlated with a poor prognosis, whereas GABAPAPL1 was opposite (all $P < 0.05$).

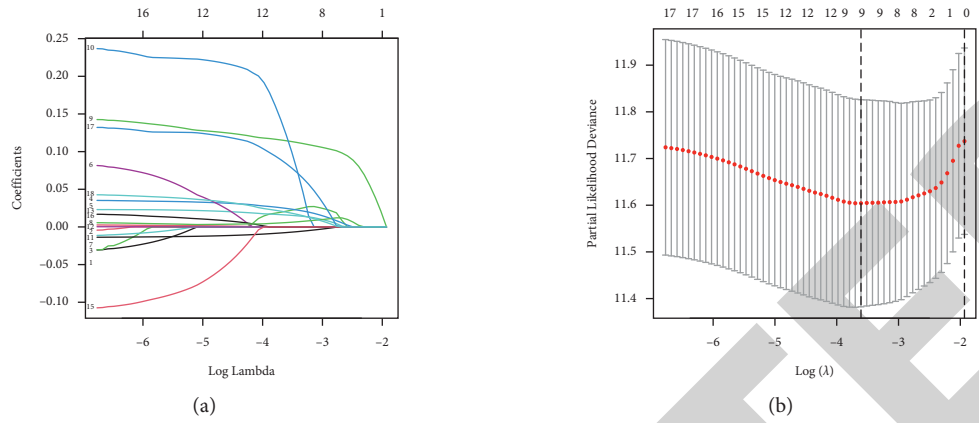
Similar to the results of the previous TCGA cohort, shorter survival times and more deaths occurred in the high-risk group compared to the low-risk group (Figure 4(h)). As expected, PCA plot demonstrated that HCC patients can be well separated into two clusters according to the risk score (Figure 4(i)). Likewise, compared to the high-risk group, the low-risk group showed a better survival ($P < 0.001$, Figure 4(j)). Moreover, the area under the ROC curve was 0.733 for 1-year, 0.769 for 2-year, and 0.776 for 3-year survival (Figure 4(k)), implying that 9-gene signature could be used to predict HCC patients' prognosis from the ICGC cohort as well. Figure 4(l) shows a heatmap of the expression level of 9-gene signature based on the risk score and corresponding clinical features from the ICGC cohort. The expression level of 9 genes between two risk groups was the same as the result of the TCGA cohort.

3.5. Independent Prognostic Analyses of HCC Patients Based on the Risk Score Model. We combined the clinical parameters of patients' age, sex, tumor grade, T stage, N stage, M stage, and tumor stage to assess whether the risk score was the independent prognostic factor. Univariate Cox regression analysis of HCC cases from the TCGA cohort revealed that tumor stage, T stage, M stage, and risk score had a significant influence on patients' prognosis ($P < 0.05$, Figure 6(a)). In the multivariate Cox regression analysis, risk score was the only independent predictor of HCC patients ($P < 0.05$, Figure 6(b)). Results of the ICGC cohort were consistent with the TCGA cohort after univariate and multivariate Cox regression analyses (Figures 5(b) and 5(c)). Subsequently, we observed the association between the risk score and the clinicopathological features of HCC patients in the TCGA cohort. Status (alive vs. dead, $P < 0.001$), T stage (T1 vs. T4, $P = 0.0172$), and tumor stage (stage I; vs. stage III, $P < 0.001$) were strongly associated with our risk score (Figure 6(c)). A gradual increase of the probability of

progression to the late-stage tumor is observed with the increased risk score indicating that our risk model may function in the progression of HCC.

3.6. Functional Analyses based on the Risk Model. DEGs were screened out by our risk model in the TCGA cohort (Table S4) and the ICGC cohort (Table S5). The result of GO enrichment showed that DEGs were mainly enriched in the olfactory receptor activity, G-protein coupled receptor activity, and detection of chemical stimulus involved in sensory perception of smell in the TCGA cohort, whereas DEGs from the ICGC cohort were significantly enriched in aromatase activity, mitotic nuclear division, and anaphase-promoting complex binding ($P_{\text{adjust}} < 0.05$, Figures 7(a) and 7(c)). In addition, DEGs from both two cohorts were all associated with the extracellular region ($P_{\text{adjust}} < 0.05$, Figures 7(a) and 7(c)). In KEGG pathway analysis, DEGs were primarily enriched in cell cycle and the retinol metabolism in both cohorts ($P < 0.05$, Figures 7(b) and 7(d)), indicating that DEGs obtained from our risk model were associated with the energy metabolism and cellular homeostasis.

3.7. Relationship between the Risk Score Model and Immune Activity. We analyzed the associations between 9 prognostic genes expression and six immune infiltration cells by the TIMER database. Among the 9 genes, ATG7, ATG9A, BNIP3L, HTRA2, MAP1LC3B2, TFE3, TIGAR, and TOMM70 were significantly correlated with B cell, CD8⁺ T cell, CD4⁺ T cell, macrophage, neutrophil, and dendritic cell infiltrations in HCC, while GABARAPL1 was inversely correlated with these six immune infiltration cells (Figure 8). For the further purposes of exploring the relationship between risk score and immune activity, ssGSEA was used to analyze the infiltration level of 16 immune cells and 13



	<i>p</i>	Hazard ratio
ATG7	0.9870	1.0028 (0.7140-1.4086)
ATG9A	0.2063	1.0351 (0.9812-1.0921)
BNIP3L	0.2631	1.0207 (0.9847-1.0580)
GABARAPL1	0.0259	0.9861 (0.9740-0.9983)
HTRA2	0.0058	1.1354 (1.0374-1.2426)
MAP1LC3B2	0.3979	1.4133 (0.6338-3.1519)
TFE3	0.9676	1.0009 (0.9582-1.0455)
TIGAR	0.1995	1.1563 (0.9262-1.4436)
TOMM70	0.0412	1.0352 (1.0014-1.0701)

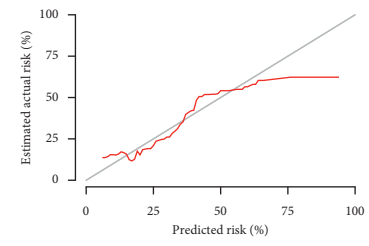
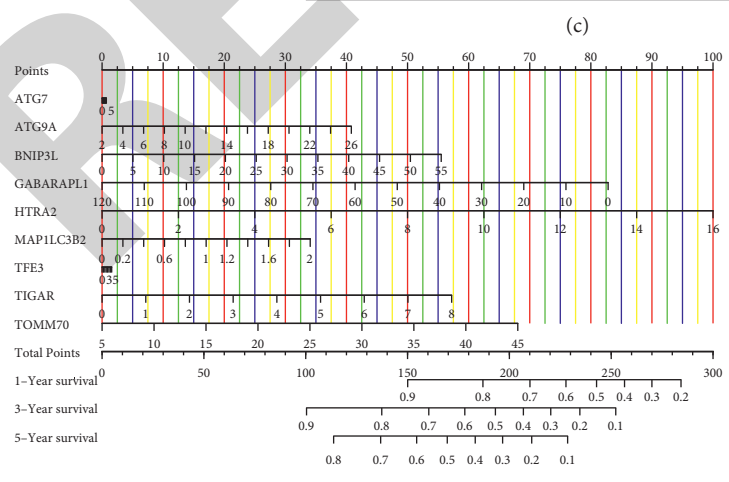


FIGURE 3: Continued.

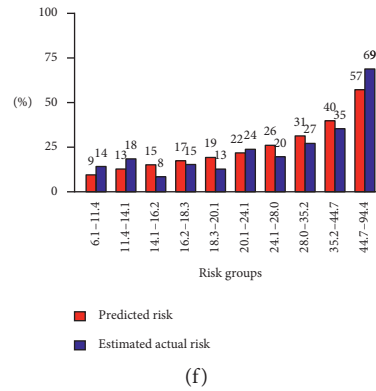


FIGURE 3: Establishment of the prognosis model according to mitophagy-related gene signature in the TCGA cohort. (a) LASSO regression of the 18 mitophagy genes with the prognosis value. (b) Cross-validation for tuning the parameter selection in the LASSO regression. (c) A forest plot of 9 MRGs by multivariate Cox regression, and GABARAPL1, HTRA2, and TOMM70 were with $P < 0.05$. (d) Nomogram for predicting the survival rate of HCC patients based on 9-gene signature. (e) Calibration curve of a nomogram. (f) Bar graph of predicted risk data and estimated actual risk data in each risk group.

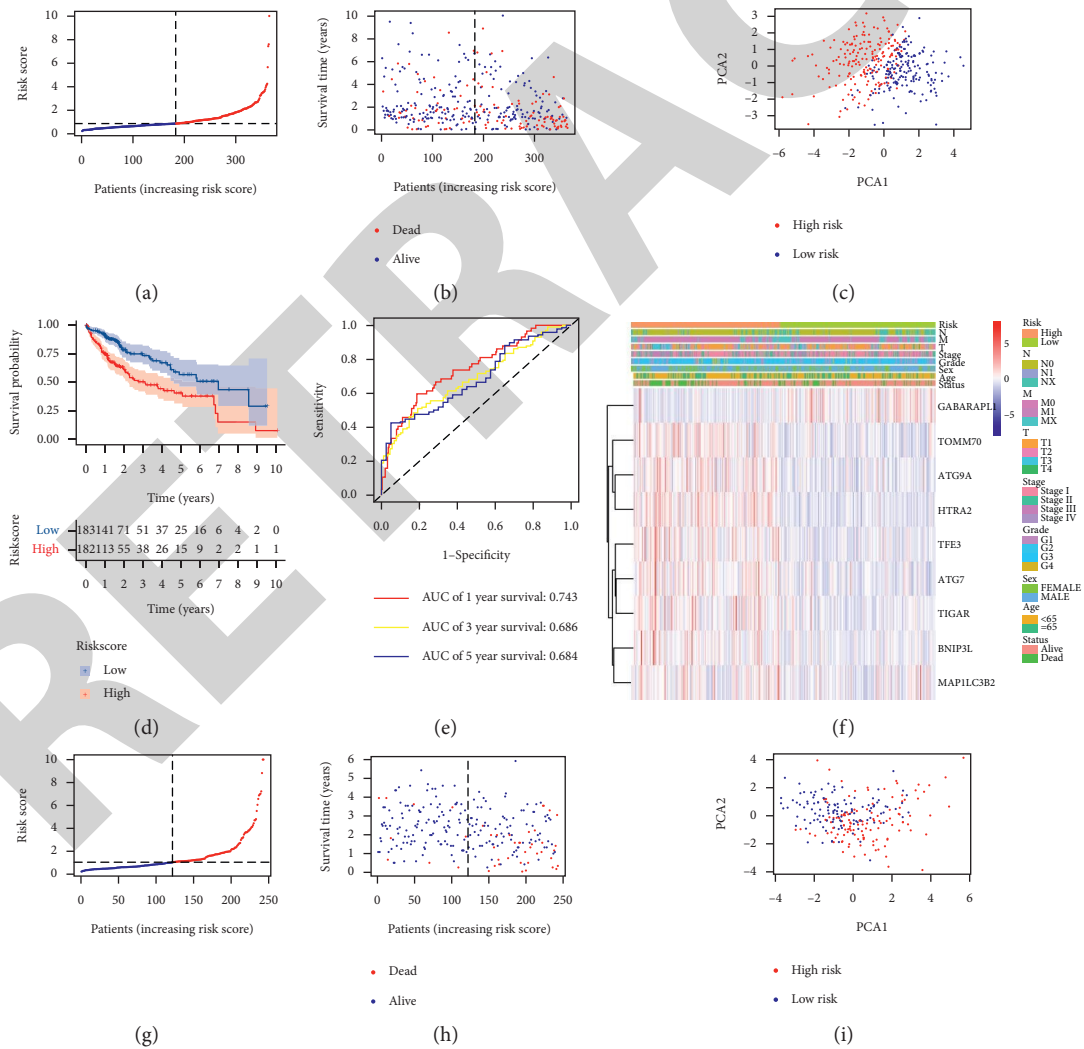


FIGURE 4: Continued.

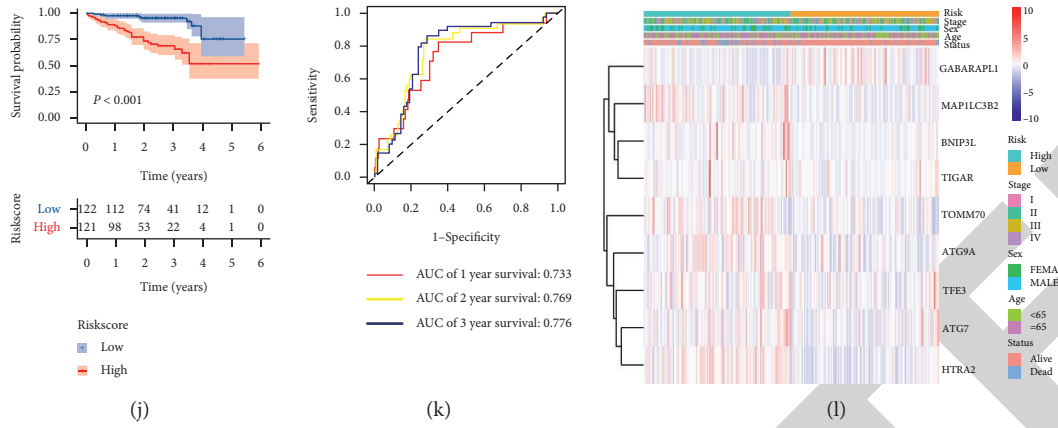
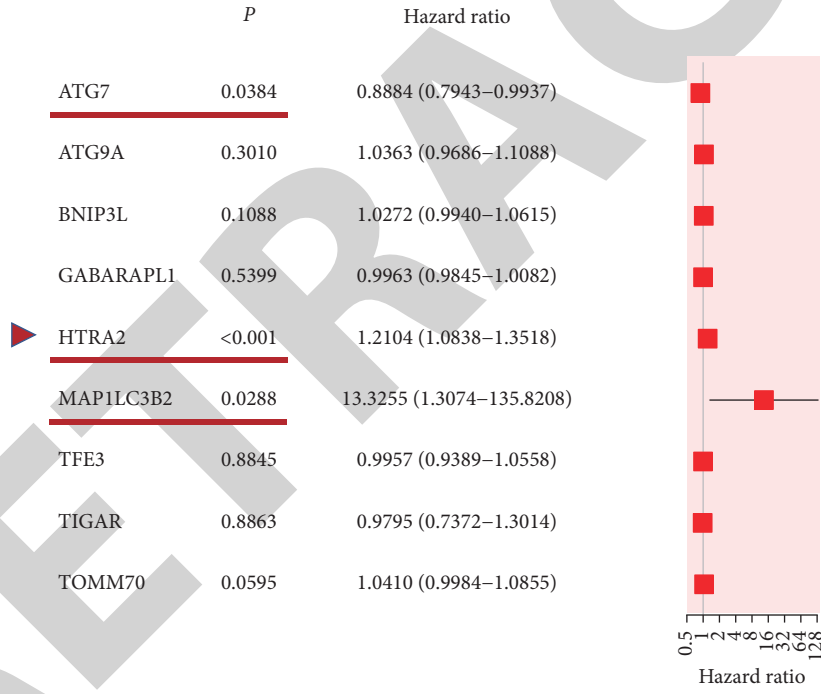
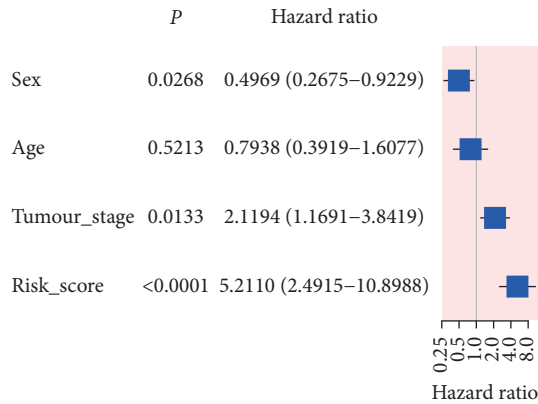


FIGURE 4: Prognostic risk model in HCC patients from the training set and validation set. Distribution of HCC patients based on the risk score in the training set (a) and validation set (g). Survival time and survival outcomes for each HCC patient in the training set (b) and validation set (h). PCA plot according to the risk score in the training set (c) and validation set (i). Kaplan-Meier curves for the survival of HCC patients between two risk groups in the training set (d) and validation set (j). ROC curves of HCC patients in the training set (e) and validation set (k). Heatmap of the training set (f) and validation set (l).

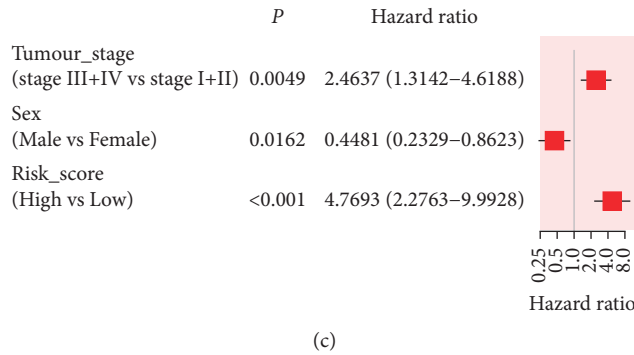


(a)



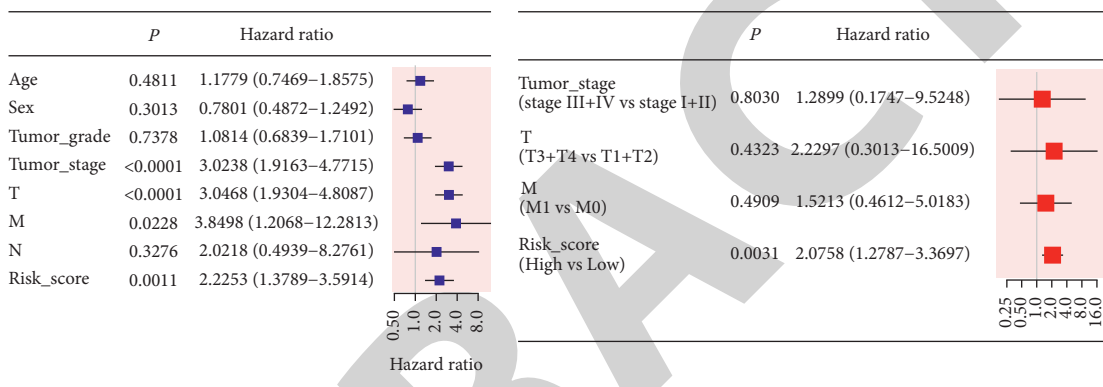
(b)

FIGURE 5: Continued.



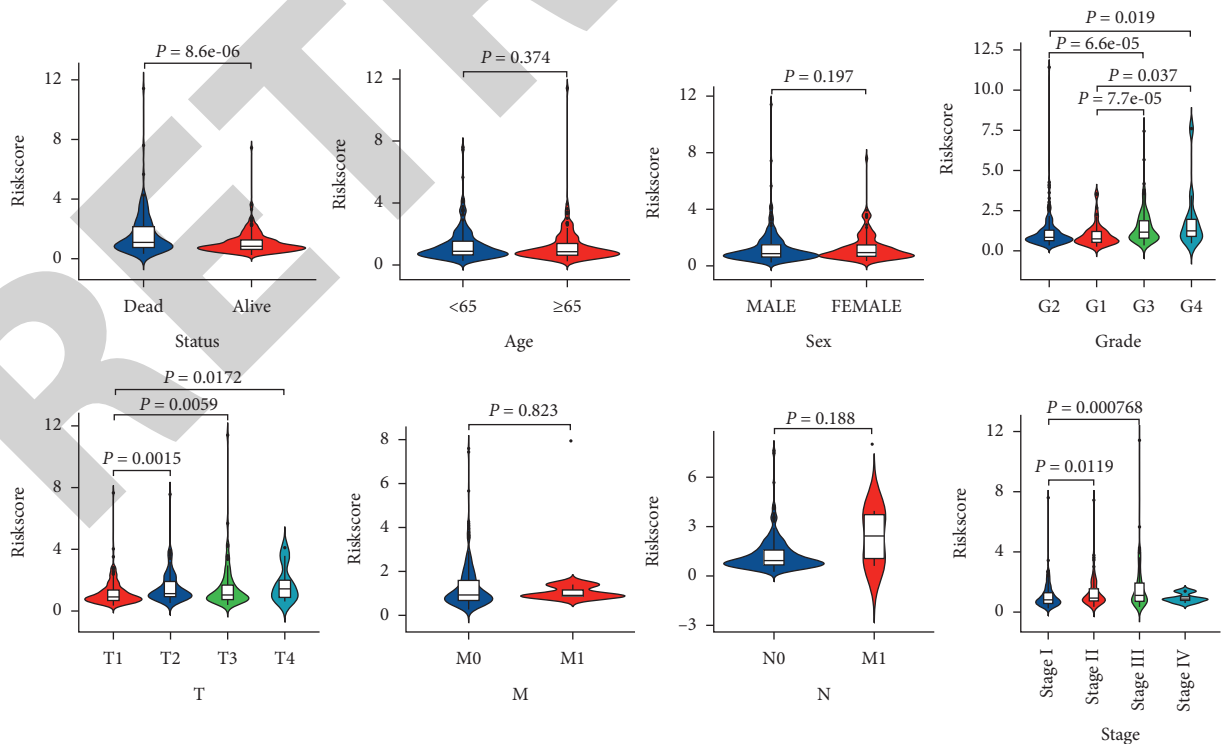
(c)

FIGURE 5: Univariate and multivariate Cox regression analyses of MRGs and clinical paraments in the ICGC cohort. (a) A forest plot of 9 MRGs by univariate Cox regression, and ATG7, HTRA2, and MAP1LC3B2 were with $P < 0.05$ Univariate (b) and multivariate analyses (c) of clinical paraments in the ICGC cohort.



(a)

(b)



(c)

FIGURE 6: Univariate and multivariate Cox regression analyses for the risk score. (a) Univariate and (b) multivariate analyses for the TCGA cohort. (c) Correlation of the risk score with status, age, sex, grade, T stage, N stage, M stage, and TNM stage of HCC.

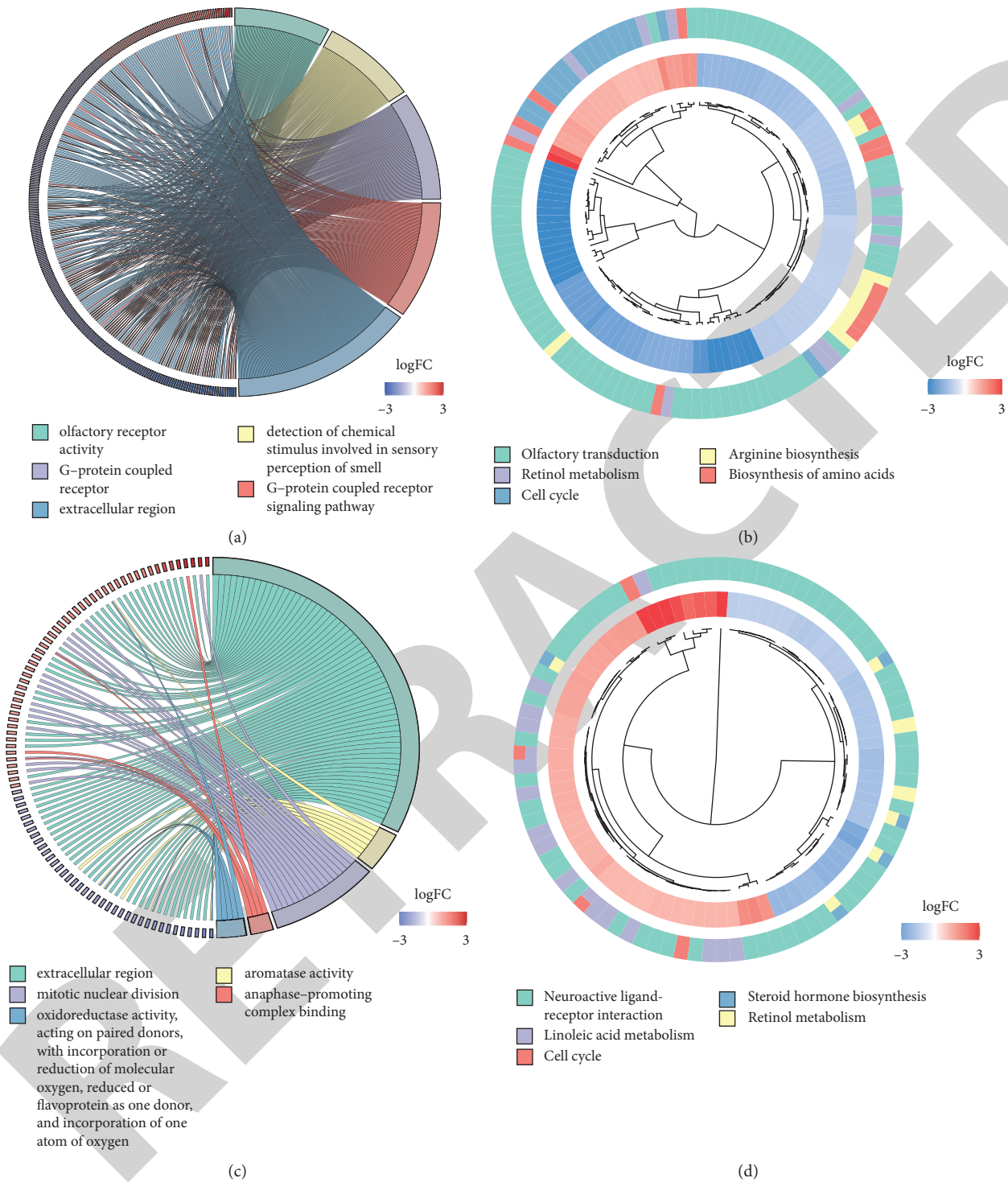
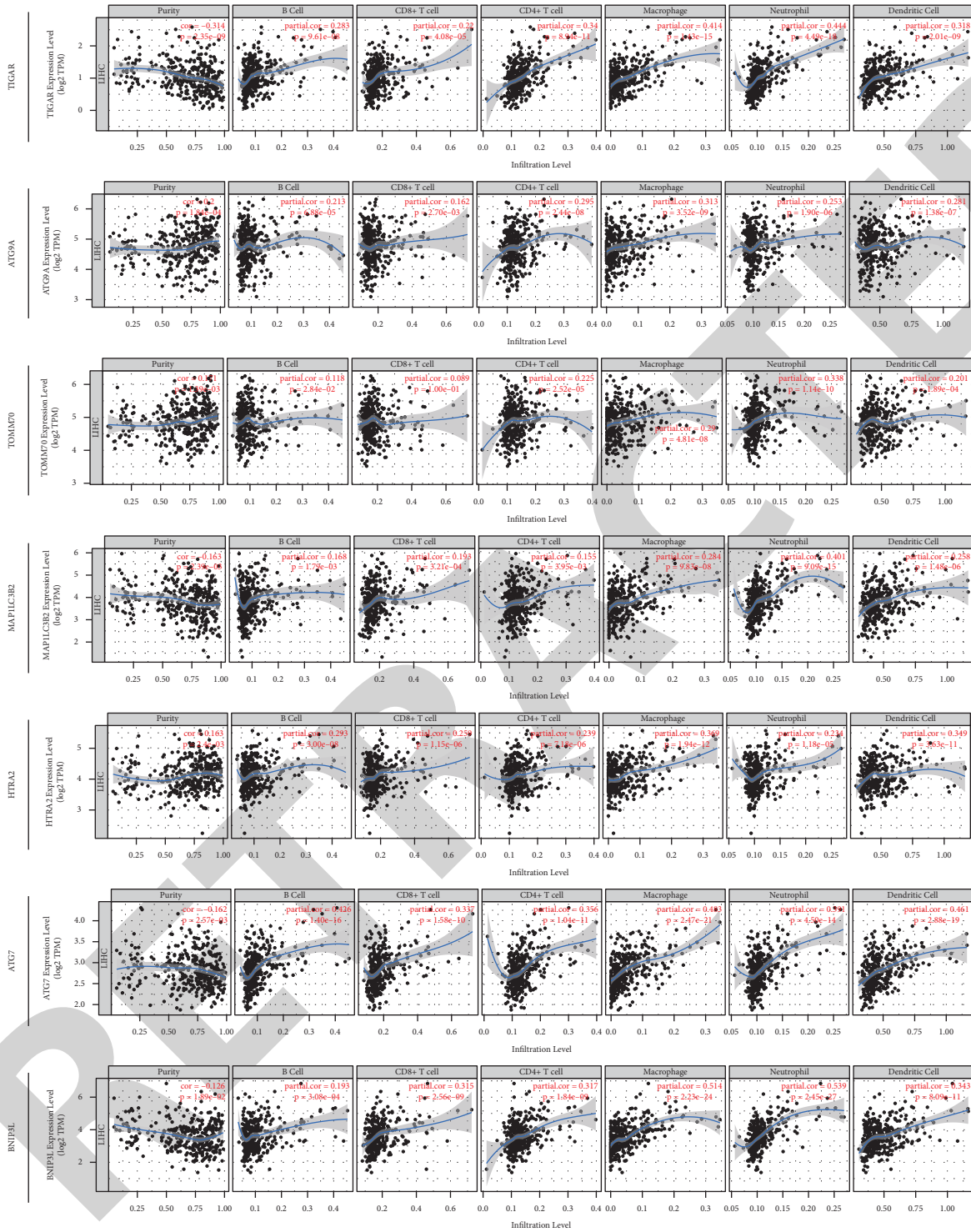


FIGURE 7: Functional analyses of DEGs that were screened between the two risk groups. GO enrichment (a) and KEGG pathways (b) in the training set. GO enrichment (c) and KEGG pathways (d) in the validation set.

immune-related pathways. The score of B cells, mast cells, natural killer (NK) cells, and plasmacytoid dendritic cells (pDCs) of the high-risk group were significantly lower compared to the low-risk group in the TCGA cohort, whereas the score of activated dendritic cells (aDCs) and macrophages is reversed (all adjusted $P < 0.05$, Figure 9(a)). Besides, the expression level of cytolytic activity, type I IFN

response, and type II IFN response was also hyporesponsive in the high-risk group compared to the low-risk group from the TCGA cohort, while the MHC class I pathway was opposite (all adjusted $P < 0.05$, Figure 9(b)). Likewise, except for the macrophages cell, the score of B cells, CD8⁺ T cells, neutrophils, NK cells, pDCs, T follicular helper (Tfh), and tumor infiltrating lymphocyte (TIL) was also decreased in



(a)

FIGURE 8: Continued.

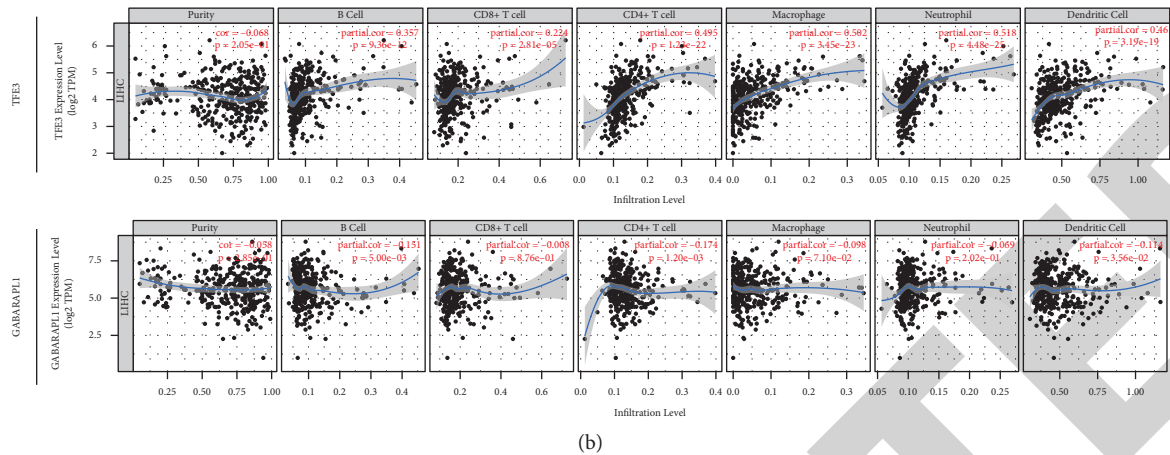


FIGURE 8: The correlation between 9 MRGs expression and immune cell infiltration using the TIMER database.

the high-risk group from the ICGC cohort (all adjusted $P < 0.05$, Figure 9(c)). Additionally, the expression level of antigen-presenting cell (APC) costimulation, cytokine-cytokine receptor (CCR), cytolytic activity, T cell costimulation, type I IFN response, and type II IFN response were all reduced in the high-risk group compared to the low-risk group of the ICGC cohort (all adjusted $P < 0.05$, Figure 9(d)).

4. Discussion

Mitophagy accounts for the maintenance of cellular homeostasis and energy metabolism in cancers [13]. Despite efforts in investigating the role of mitophagy in cancer recurrence or acquired resistance anticancer therapeutics [14, 15], the precise effect of mitophagy in predicting HCC patients' prognosis is still unknown. Herein, we combined MRGs with immunoscore-based tumor classification to construct a 9-gene risk signature for HCC. Both the training set (TCGA cohort) and validation set (ICGC cohort) work well to verify our risk model by comparing OS and ROC curve between groups. Our functional analyses showed that the DEGs between two risk groups were primarily enriched in the extracellular region process, cell cycle, and metabolism-related pathways. Further immune activity analysis had indicated that the high-risk group had a generally reduced level of antitumor immune activity.

The prognostic model proposed in this study was composed of 9 MRGs (ATG7, ATG9A, BNIP3L, GABARAPL1, HTRA2, MAP1LC3B2, TFE3, TIGAR, and TOMM70). Compared with single or small combination study on MRGs, our study performed a comprehensive study on MRGs for HCC prognosis at the genetic level by using whole transcriptome datasets. Previous studies have also established the prognostic model for predicting HCC patients' survival such as m6A methylation-related [16] or ferroptosis-related gene signature [17] by harnessing gene expression profiles. However, these results lack external datasets [16] and thorough investigation of prognostic signature [17]. Compared to traditional subtype (normal groups versus tumor groups), our MRG

signature combined the MRGs with the immunoscore tumor classification to select more stable specific prognostic markers, which has a better prognostic value for the clinical diagnosis and prognosis.

To date, mitophagy has not been fully researched. This is because initiation and progression of a tumor is not a series of isolated mitophagy pathways but instead is a complex process coexisting and interacting with multiple modes of cell death. Therefore, we could find that these 9 genes are also associated with mitochondria regulators (BNIP3L, HTRA2, TFE3, TOMM70), autophagy (ATG7, ATG9A, GABARAPL1, and MAP1LC3B2), apoptosis (HTRA2), and antioxidant activity (TIGAR). BCL-2 interacting protein 3 like (BNIP3L), transcription factor E3 (TFE3), and translocase of outer mitochondrial membrane 70 (TOMM70) have been implicated in modulation of mitochondrial function. BNIP3L can directly target mitochondria by binding to Bcl-2 and promote cancer stemness of HCC by glycolysis metabolism reprogramming [18], whereas TFE3 are involved in PINK1 and Parkin-dependent mitophagy and can promote the proliferation of renal cell carcinoma [19]. Translocase of outer mitochondrial membrane 70 (TOMM70) is a key receptor of hydrophobic preproteins for binding to mitochondria, which can induce apoptosis of hepatoma cells [20]. HTRA2 is a nuclear-encoded mitochondrial serine protease that has been shown to have a dual function including regulation of cellular apoptosis and mitochondrial homeostasis [21]. A recent study has revealed that inhibition of HTRA2 releasing from the mitochondrion can suppress HCC cell apoptosis [22]. Autophagy-related 7 (ATG7), autophagy-related protein 9A (ATG9A), gamma-aminobutyric acid receptor-associated protein-like 1 (GABARAPL1), and microtubule-associated proteins 1A/1B light chain 3 beta 2 (MAP1LC3B2) are mainly involved in autophagosome formation, whereas the absence of them can lead to a reduction of mitochondrial clearance [23–26]. TP53-induced glycolysis regulatory phosphatase (TIGAR), also named C12 or f5, has antioxidant activity and can protect cells from metabolic stress-induced cell death. Previous

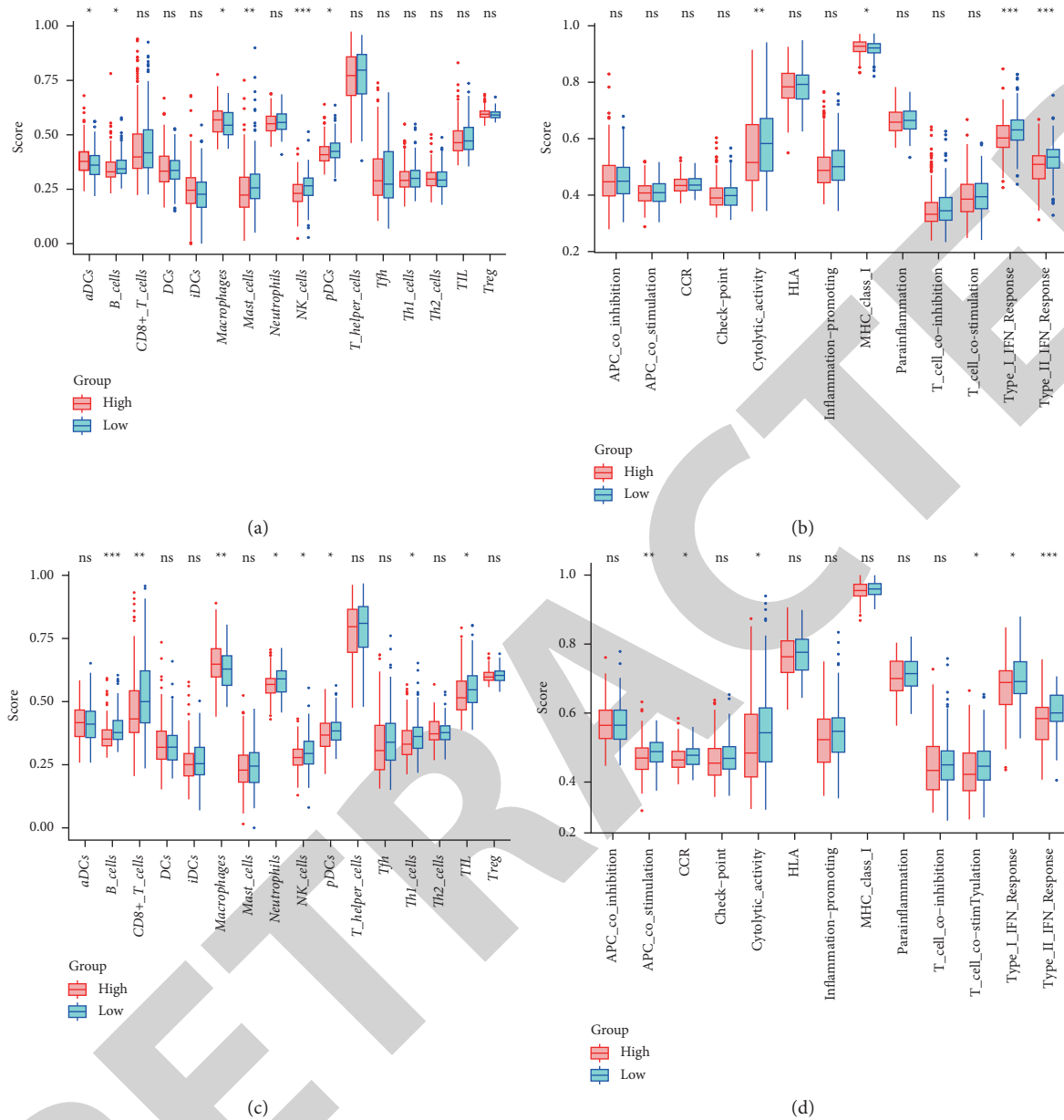


FIGURE 9: The association between immune activity and two risk groups. Enrichment score of immune cells (a) and immune-related pathways (b) in the training set. Enrichment score of immune cells (c) and immune-related pathways (d) in the validation set. Red box represents the high-risk group. Green box represents the low-risk group (the below is the same). Adjusted *P* values: ns, not significant; **P* < 0.05; ***P* < 0.01; ****P* < 0.001.

studies indicated that the expressions of BNIP3L, TFE3, TOMM70, HTRA2, ATG7, ATG9A, MAP1LC3B2, and TIGAR are overexpressed in tumor tissues, and the knockout of them can significantly inhibit tumor outgrowth [20, 22, 27–32]. In contrast, GABARAPL1 expressions were downregulated in cancer, and our survival analysis of GABARAPL1 showed that high GABARAPL1 expression had a better survival outcome in HCC. The same trend goes as their correlations with immune cell infiltration. Except for GABARAPL1, the remaining 8 genes were positively correlated with B cell, CD8⁺ T cell, CD4⁺ T cell, macrophage, neutrophil, and dendritic cell

infiltrations in HCC by using the TIMER database, which indicated that these mitophagy signature may play a vital role in immune activity.

We also analyzed the DEGs between two risk groups and found that DEGs were associated with the extracellular region process, cell cycle, and energy metabolism pathways. Moreover, compared to the low-risk group, the contents of B cells, NK cells, and pDCs were relatively minimal in the high-risk group in both two cohorts, indicating a decreased antitumor immune response in HCC patients' high-risk group. Emergent evidence has indicated the significance of mitochondrial dynamics in these immune cells [33].

Immune cells proliferation and activation lead to increased metabolic demands, and thus, the reduction activity of antitumor activity of these cells may be associated with mitophagy dysfunction [34]. How mitophagy exerts its action in the regulation of immune cells' activation in different stages is worth to be further explored. In addition, the expression level of macrophages was significantly increased in the high-risk group compared to the low-risk group in both two cohorts. Increased macrophages are correlated with poor prognosis because of their important function in innate immunity [35]. Moreover, a high-risk score may link to compromised immune function. In this study, the components of immune-related functions such as cytolytic activity, type I IFN response, and type II IFN response were also reduced in the high-risk group in both two cohorts. Thus, unfavorable prognosis in the high-risk group of HCC patients may be related to lower immune infiltration levels.

There are several limitations of this study as well. Our analytical data are mainly obtained from the public dataset, and it is necessary to search for more prospective clinical data to prove the practicability of our prognostic risk model. In addition, further *in vitro* and *in vivo* verifications are required to elucidate the specific role of MRGs on HCC. In the future, we can pay more attention in the exploration of the specific mechanism of MRGs on progression of HCC, which may provide novel opportunities for the treatment of HCC.

5. Conclusions

In summary, we found that MRGs were associated with HCC patients' prognosis and used them to develop and validate a valid prognostic risk model based on 9-gene signature. Risk score calculated by 9-gene signature was confirmed as an independent prognosis risk factor in both the TCGA cohort and ICGC cohort. Risk score calculated by 9-gene signature was confirmed as an independent prognosis risk factor in both two cohorts. The result of our study may be of significance to develop novel prognostic biomarkers and actionable targets for expanding therapeutic options of HCC patients.

Data Availability

The datasets are available in the TCGA database (<https://portal.gdc.cancer.gov/repository>) and ICGC portal (<https://dcc.icgc.org/projects/LIRI-JP>).

Conflicts of Interest

The authors declare that they have no conflicts of interest.

Authors' Contributions

HC, JHW, and RJZ acquired the data, performed the analysis, and wrote the manuscript. YJL and KHG participated in data analysis. HHW, QY, and RJ are responsible for data curation. WHS and ZWZ involved in study design, supervision, and acquiring funding. HC, JHW, RJZ, and YJL contributed equally to this work.

Acknowledgments

The authors would like to acknowledge the TCGA and the ICGC for providing data and graphical abstract created with BioRender.com. This work was supported by the National Natural Science Foundation of China (82171698, 82170561, 82100238, 81300279, and 81741067), the Natural Science Foundation for Distinguished Young Scholars of Guangdong Province (2021B1515020003), and the Climbing Program of Introduced Talents and High-Level Hospital Construction Project of Guangdong Provincial People's Hospital (DFJH201923, DFJH201803, KJ012019099, KJ012021143, and KY012021183).

Supplementary Materials

Supplementary Table S1. MRGs included in analysis. Supplementary Table S2. The immune score of each HCC sample from TCGA cohort. Supplementary Table S3. Clinicopathologic characteristics of HCC patients. Supplementary Table S4. Differentially expressed genes between the risk groups in the TCGA cohort. Supplementary Table S5. Differentially expressed genes between the risk groups in the ICGC cohort. (*Supplementary Materials*)

References

- [1] H. Sung, J. Ferlay, R. L. Siegel et al., "Global cancer statistics 2020: globocan estimates of incidence and mortality worldwide for 36 cancers in 185 countries," *CA: A Cancer Journal for Clinicians*, vol. 71, no. 3, pp. 209–249, 2021.
- [2] L. Buonaguro, A. Petrizzo, M. Tagliamonte, M. L. Tornesello, and F. M. Buonaguro, "Challenges in cancer vaccine development for hepatocellular carcinoma," *Journal of Hepatology*, vol. 59, no. 4, pp. 897–903, 2013.
- [3] T. B. Toh, J. J. Lim, L. Hooi, M. B. M. A. Rashid, and E. K.-H. Chow, "Targeting Jak/Stat pathway as a therapeutic strategy against SP/CD44+ tumorigenic cells in Akt/ β -catenin-driven hepatocellular carcinoma," *Journal of Hepatology*, vol. 72, no. 1, pp. 104–118, 2020.
- [4] J. P. Morris, J. J. Yashinski, R. Koche et al., " α -Ketoglutarate links p53 to cell fate during tumour suppression," *Nature*, vol. 573, no. 7775, pp. 595–599, 2019.
- [5] L. Shu, C. Hu, M. Xu et al., "ATAD3B is a mitophagy receptor mediating clearance of oxidative stress-induced damaged mitochondrial DNA," *The EMBO Journal*, vol. 40, no. 8, Article ID e106283, 2021.
- [6] Y. Guan, Y. Wang, B. Li et al., "Mitophagy in carcinogenesis, drug resistance and anticancer therapeutics," *Cancer Cell International*, vol. 21, no. 1, Article ID 350, 2021.
- [7] L. Zhu, W. Wu, S. Jiang et al., "Pan-cancer analysis of the mitophagy-related protein PINK1 as a biomarker for the immunological and prognostic role," *Frontiers in Oncology*, vol. 10, Article ID 569887, 2020.
- [8] C. Yan, L. Gong, L. Chen et al., "PHB2 (prohibitin 2) promotes PINK1-PRKN/parkin-dependent mitophagy by the PARL-PGAM5-PINK1 axis," *Autophagy*, vol. 16, no. 3, pp. 419–434, 2020.
- [9] F. Pagès, B. Mlecnik, F. Marliot et al., "International validation of the consensus immunoscore for the classification of colon cancer: a prognostic and accuracy study," *Lancet*, vol. 391, pp. 2128–2139, 2018.

Retraction

Retracted: Yap-Hippo Signaling Activates Mitochondrial Protection and Sustains Breast Cancer Viability under Hypoxic Stress

Journal of Oncology

Received 10 October 2023; Accepted 10 October 2023; Published 11 October 2023

Copyright © 2023 Journal of Oncology. This is an open access article distributed under the Creative Commons Attribution License, which permits unrestricted use, distribution, and reproduction in any medium, provided the original work is properly cited.

This article has been retracted by Hindawi following an investigation undertaken by the publisher [1]. This investigation has uncovered evidence of one or more of the following indicators of systematic manipulation of the publication process:

- (1) Discrepancies in scope
- (2) Discrepancies in the description of the research reported
- (3) Discrepancies between the availability of data and the research described
- (4) Inappropriate citations
- (5) Incoherent, meaningless and/or irrelevant content included in the article
- (6) Peer-review manipulation

The presence of these indicators undermines our confidence in the integrity of the article's content and we cannot, therefore, vouch for its reliability. Please note that this notice is intended solely to alert readers that the content of this article is unreliable. We have not investigated whether authors were aware of or involved in the systematic manipulation of the publication process.

In addition, our investigation has also shown that one or more of the following human-subject reporting requirements has not been met in this article: ethical approval by an Institutional Review Board (IRB) committee or equivalent, patient/participant consent to participate, and/or agreement to publish patient/participant details (where relevant).

Wiley and Hindawi regrets that the usual quality checks did not identify these issues before publication and have since put additional measures in place to safeguard research integrity.

We wish to credit our own Research Integrity and Research Publishing teams and anonymous and named external researchers and research integrity experts for contributing to this investigation.

The corresponding author, as the representative of all authors, has been given the opportunity to register their agreement or disagreement to this retraction. We have kept a record of any response received.

References

- [1] C. Shi, S. Zhang, C. Guo, and J. Tie, "Yap-Hippo Signaling Activates Mitochondrial Protection and Sustains Breast Cancer Viability under Hypoxic Stress," *Journal of Oncology*, vol. 2021, Article ID 5212721, 10 pages, 2021.

Research Article

Yap-Hippo Signaling Activates Mitochondrial Protection and Sustains Breast Cancer Viability under Hypoxic Stress

Chen Shi, Siyuan Zhang, Changkuo Guo, and Jian Tie 

Department of Radiation Oncology, Key Laboratory of Carcinogenesis and Translational Research (Ministry of Education/Beijing), Peking University Cancer Hospital and Institute, Beijing 100142, China

Correspondence should be addressed to Jian Tie; jiantie@bjcancer.org

Received 25 July 2021; Revised 31 August 2021; Accepted 2 September 2021; Published 17 September 2021

Academic Editor: Yun-dai Chen

Copyright © 2021 Chen Shi et al. This is an open access article distributed under the Creative Commons Attribution License, which permits unrestricted use, distribution, and reproduction in any medium, provided the original work is properly cited.

Yes-associated protein (Yap) is a transcriptional regulator that upregulates oncogenes and downregulates tumor repressor genes. In this study, we analyzed protein expression, RNA transcription, and signaling pathways to determine the function and mechanism of Yap in breast cancer survival during hypoxic stress. Yap transcription was drastically upregulated by hypoxia in a time-dependent manner. siRNA-mediated Yap knockdown attenuated breast cancer viability and impaired cell proliferation under hypoxic conditions. Yap knockdown induced mitochondrial stress, including mitochondrial membrane potential reduction, mitochondrial oxidative stress, and ATP exhaustion after exposure to hypoxia. It also repressed mitochondrial protective systems, including mitophagy and mitochondrial fusion upon exposure to hypoxia. Finally, our data showed that Yap knockdown suppresses MCF-7 cell migration by inhibiting F-actin transcription and promoting lamellipodium degradation under hypoxic stress. Taken together, Yap maintenance of mitochondrial function and activation of F-actin/lamellipodium signaling is required for breast cancer survival, migration, and proliferation under hypoxic stress.

1. Introduction

Breast cancer is the most commonly diagnosed cancer in women, with an estimated 268,600 newly diagnosed women with invasive disease in 2019 in the United States [1]. Approximately 42,000 women are expected to die in the US from breast cancer each year, making it as the second-leading cause of cancer-related death among US women after lung cancer [2]. Although breast cancer generally has been identified as a single disease, there are up to 21 distinct histological subtypes and at least four different molecular subtypes [3]. Most cases (80%) are invasive, or infiltrating, and while black and white women in the US are diagnosed at roughly the same rate, the relative survival rate was 83% for black women and 92% for white women [4].

Yes-associated protein (Yap) was originally reported as a transcriptional regulator that upregulates the transcription of oncogenes and reduces the levels of tumor suppressors. Under physiological conditions, Yap is primarily found

unphosphorylated in the cytoplasm. After stimulation by hypoxia and inflammation, Yap is phosphorylated at Ser127 [5] and translocates into the nucleus, where it regulates gene expression related to tumor development with the help of transcriptional coactivators with a PDZ-binding motif (TAZ) [6]. Accordingly, several researchers have proposed that Yap is a critical factor in cancer genesis and development. Our previous study [7] revealed a link between Yap activation and hepatocellular carcinoma invasion. We found that Yap inhibited JNK phosphorylation and thus sustained the levels of mitochondria-generated ATP, favoring cancer migration and mobilization. In addition to liver cancer, abundant expression of Yap modulates the activity of macrophage stimulating 4 (MST4) kinase and is also associated with gastric tumorigenesis [6]. The metabolic reprogramming in neural crest is also controlled by Yap signaling [8]. In colorectal cancer, the level of intracellular total Yap rather than its phosphorylation status has been used as a prognostic biomarker [9]. In breast cancer, recent

studies have shown that Yap activates the ubiquitin ligase RNF187 and is a potential target for the treatment of triple negative breast cancer [10]. Moreover, anti-HER2 treatment resistance in breast cancer seems to be also associated with Yap.

Tumor hypoxia occurs when tumor cells rapidly outgrow their blood supply, reducing oxygen concentration in the tumor. Although excessive hypoxia would impair cancer metabolism and thus induce cancer cell death or proliferation arrest, the presence of hypoxic regions is one of the negative independent prognostic factors for human cancer [11, 12]. Under hypoxic conditions, hypoxia-induced factor 1 (HIF1) is activated to upregulate the transcription of genes that are involved in angiogenesis, cell survival, and glucose metabolism. For example, overexpression of HIF1 promotes cancer metastasis [13]. HIF-1 promotes the Warburg effect, the tumor-related metabolic switch, which helps cancer cells create energy largely by disintegration of glucose in a non-oxidative manner rather than typical oxidative phosphorylation. Due to decreased oxygen delivery, VEGF expression is upregulated by HIF1 activation and contributes to the formation of blood vessels [14]. HIF1 appears to play a critical role in preventing cell death and promoting cancer proliferation through upregulation of the transcription and expression of cell-cycle-related proteins such as Cyclin D and p21 [15]. Notably, the relationship between Yap and HIF1 has been reported in gastric cancer [16], liver cancer [17], and pancreatic cancer [18], but not in breast cancer. Therefore, the aim of our study was to explore the role of Yap in breast cancer survival and determine whether Yap affects breast cancer cell death through HIF1 under a hypoxic environment.

2. Materials and Methods

2.1. Cell Culture and Treatment. Human breast cancer cell line MCF-7 was purchased from the American Type Culture Collection (ATCC, Manassas, VA, USA) [19]. We cultured cells in RPMI 1640 medium supplemented with 10% FBS (ExCell Bio, China), 100 mg/ml streptomycin, and 100 U/ml penicillin (Gibco; Thermo Fisher Scientific, Inc., Grand Island, NY) in an incubator at 37°C with 5% CO₂ [20]. Hypoxia treatment was induced in the hypoxic incubator at 37°C with 1% O₂.

2.2. Quantitative Real-Time- (qRT-) PCR. Reverse transcription was performed using qScript microRNA cDNA Synthesis Kit (Quanta). PCR was performed using an ABI PRISM Sequence Detector System 7500 (Applied Biosystems) with SYBR Green (Quanta) as the fluorescent dye and ROX (Quanta) as the passive reference dye [21]. The cycle number at which the reaction crossed an arbitrarily-placed threshold (CT) was determined for each gene, and the relative amount of each gene to 18S rRNA was used to quantify cellular RNA [22].

2.3. Western Blot. Western blotting was conducted with minor modifications. Briefly, cells infected with siRNA were lysed in ice-cold lysis buffer (50 mmol/L Tris-HCl

[pH 8.0], 150 mmol/L NaCl, 0.1% Triton X-100, 10 mmol/L EDTA, complete protease inhibitor (Roche), and 20 mmol/L N-ethylmaleimide). For Western blot analysis, approximately 50 µg of protein from each sample was separated by SDS-PAGE and transferred to PVDF membranes (Schleicher & Schuell) [23]. The membranes were blocked with 5% non-fat milk and then incubated with primary antibodies at 4°C overnight. The membranes were incubated with secondary antibodies conjugated to horseradish peroxidase (Jackson ImmunoResearch) and then developed with a chemiluminescent substrate (Perkin Elmer) [24].

2.4. Immunofluorescence and Confocal Microscopy. Cells were collected and fixed with 4% paraformaldehyde for 30 minutes at room temperature. Prior to staining, fixed vessels were rinsed with PBS, permeabilized with PBST (PBS with 0.1% Triton X-100) for 10 minutes, and then blocked for nonspecific binding using 5% goat serum for 2 hours at 4°C on a rocker plate [25]. Once blocked, samples were incubated overnight with primary antibodies in PBS [26]. Images were captured using an inverted confocal fluorescence microscope Olympus IX81 with a Hamamatsu C11440 ORCAFlash4.0 digital camera [27].

2.5. Mitochondrial Respiration Assays. Respiration was assessed in isolated mitochondria by measuring O₂ consumption using an Oroboros Oxygraph (Oroboros Instruments, Innsbruck, Austria) [28]. Standardized instrumental and chemical calibrations were performed to correct for backdiffusion of O₂ into the chamber from leakage, consumption by the chemical medium and sensor consumption [29]. Measurements were taken from 50 µg of mitochondria or 120,000 cells in suspension (2 mL) gently agitated at 37°C. State 2 respiration (mito only) was assessed with the addition of glutamate (10 mM), malate (2 mM), and succinate (10 mM) as the complex I and II substrates, and then State 3 respiration (mito only) was assessed by the addition of ADP (0.5 mM) [30]. State 4 (leak) respiration was assessed with the complex V inhibitor oligomycin (2 µg/mL). Respiration due to reactive oxygen species formation was assessed with Antimycin A (2.5 µM) [31]. O₂ flux was measured by Datlab2 software (Oroboros Instruments, Innsbruck, Austria), capable of converting nonlinear changes in the negative time derivative of the oxygen concentration signal [32].

Mitochondrial respiration was also assessed in plated cells by measuring O₂ consumption using the Seahorse XF24 e Analyzer. Cells were grown on a plastic 24-well plate, cultured with Claycomb media and allowed to grow to confluence [33]. Before experimentation, cells were washed with supplemented XF assay media (Seahorse Bioscience, North Billerica, MA) and allowed to equilibrate for 1 h. ATP production, maximal respiration, and nonmitochondrial respiration were assessed by treating cells with oligomycin (1 µM), FCCP (1 µM), and a rotenone (1 µM)/antimycin (1 µM) mixture, respectively [32].

2.6. Mitochondrial Membrane Potential/ROS Assessment.

Cells were loaded in 96 well plates and then stained with 5 μ m MitoSox for 10 min to quantify ROS and 10 nm TMRM for 30 min to quantify changes in mitochondrial membrane potential [34]. Cells were imaged in a widefield fluorescence microscope (ImageXpress Micro, Molecular Devices, Sunnyvale, CA), and changes in intensity means were quantified using Imaris software [35].

2.7. Mitochondrial Isolation.

Mitochondria were isolated from cells by first detaching cells with 0.05% Trypsin/EDTA for 10 min, washing with Claycomb media and resuspending cells in a minimal volume of isolation buffer. Cells were then lysed by passing through a 27-gauge syringe (15 strokes) [36]. Cell lysates were centrifuged at 500 \times g for 10 min, and the resulting supernatants were centrifuged at 10,000 \times g for 15 min. The mitochondrial pellet was washed once with isolation buffer and the final pellet resuspended in a minimal volume of isolation buffer and kept on ice for functional assays [37]. If samples were used for Western blot, mitochondria were solubilized in isolation buffer containing 1% Triton X and stored at -80°C . Purity of mitochondrial fractions is confirmed by the absence of the cytosolic protein enolase [38].

2.8. Generation of Yap Knockout Cell Line.

siRNA against Yap was purchased from Addgene. Cells (1×10^5 cells) were plated in a 24-well plate and transfected with siRNA. Forty-eight hours after transfection, FACS (BD FACSAria TM II, BD) was performed to isolate GFP-positive cells [39]. Following isolation, cells were plated in a 96-well plate by limiting dilution for a single-cell cloning. Western blots were used to validate the knockdown efficiency of Yap siRNA [40].

2.9. Statistical Analysis.

All experiments are presented as mean \pm SEM. Statistical analysis was performed using Prism 6 (GraphPad) or SPSS (IBM). Shapiro–Wilk test was used for normality test. Statistical significance was determined by either unpaired *t*-test, one-way ANOVA, or two-way ANOVA followed by Tukey multiple comparison test. If the normality assumption was violated, nonparametric tests were conducted. $p < 0.05$ denotes statistical significance.

3. Results

3.1. Yap Knockdown Induces Breast Cancer Cell Death and Proliferation Arrest under Hypoxia.

After exposure to hypoxic stress, the viability of MCF-7 cells was significantly reduced in a time-dependent manner (Figure 1(a)), suggesting that prolonged hypoxia may cause MCF-7 death. This hypothesis was validated by analyzing TUNEL staining and caspase-3 activity. As shown in Figure 1(b), compared to the control group, the number of TUNEL-positive cells was progressively increased in response to hypoxia treatment, an effect that was followed by an increase in the activity of caspase-3 *in vitro* (Figure 1(c)). These results indicate that

excessive hypoxia is a proapoptotic signal for MCF-7 cells *in vitro*. To analyze the role of Yap in hypoxia-related cell damage, siRNA against Yap was transfected into MCF-7 cells as we previously described [7]. Knockdown efficiency was confirmed through qPCR (Figure 1(d)). Then, cell death was analyzed through MTT assay and TUNEL staining. As shown in Figure 1(a), baseline knockdown of Yap had no influence on cell viability but significantly augmented hypoxia-mediated cell death. Similar results were also observed using TUNEL staining (Figure 1(b)), indicating that hypoxia-induced breast cancer cell damage may be amplified due to Yap deficiency.

CCK-8 assay was used to analyze MCF-7 growth under hypoxic stress. As shown in Figure 1(e), compared to the control group, hypoxia slightly reduced the proliferation rate in MCF-7, and this effect could be further augmented by Yap knockdown. The transcription levels of VEGF and *p21* were moderately downregulated after exposure to hypoxic stress, while Yap knockdown further reduced the levels of VEGF and *p21* (Figures 1(f) and 1(g)), suggesting that breast cancer cell proliferation is negatively affected by hypoxia and further reduced by Yap deficiency. Notably, since hypoxia for 24 hours caused a statistically significant reduction in MCF-7 viability (Figure 1(a)) and proliferation (Figure 1(e)), 24-hour hypoxia was used in the following experiments.

3.2. Yap Knockdown Reduces Mitochondrial Function in Hypoxia-Treated Breast Cancer.

Our previous studies [7] showed that mitochondria function downstream of Yap in liver cancer. Loss of Yap induced a decline in mitochondrial ATP production and thus caused intracellular calcium overload, resulting into cancer cell mobilization impairment. Based on these studies [7], we questioned whether mitochondrial dysfunction also occurred downstream as a result of Yap knockdown. Mitochondrial ATP production was reduced slightly by hypoxia and largely by Yap knockdown (Figure 2(a)). Intracellular ATP levels are determined by mitochondrial membrane potential, which converts chemical potential energy to kinetic energy [41, 42]; the latter is used by mitochondria to generate ATP. After exposure to hypoxia, mitochondrial membrane potential was reduced (Figures 2(b) and 2(c)), and this action was further augmented in Yap-knocked down MCF-7 cells, suggesting that Yap is required to sustain mitochondrial potential under hypoxia stimulus. Furthermore, due to a loss of mitochondrial potential, the levels of mitochondrial ROS were also increased under hypoxia, while Yap knockdown multiplied ROS formation (Figures 2(d) and 2(e)).

In addition to mitochondrial dysfunction, we also found that the mitochondrial autophagy system, termed mitophagy, was enhanced during the period of hypoxia (Figure 2(f)), which is in accordance with previous studies [43, 44]. Interestingly, without Yap, mitophagy was significantly reduced, consistent with our previous findings [7], reconfirming that Yap is an activator of mitophagy during hypoxia that enhances mitochondrial self-repair. Additionally, the mitochondrial fusion system attenuates mitochondrial damage through generation of a long, shared

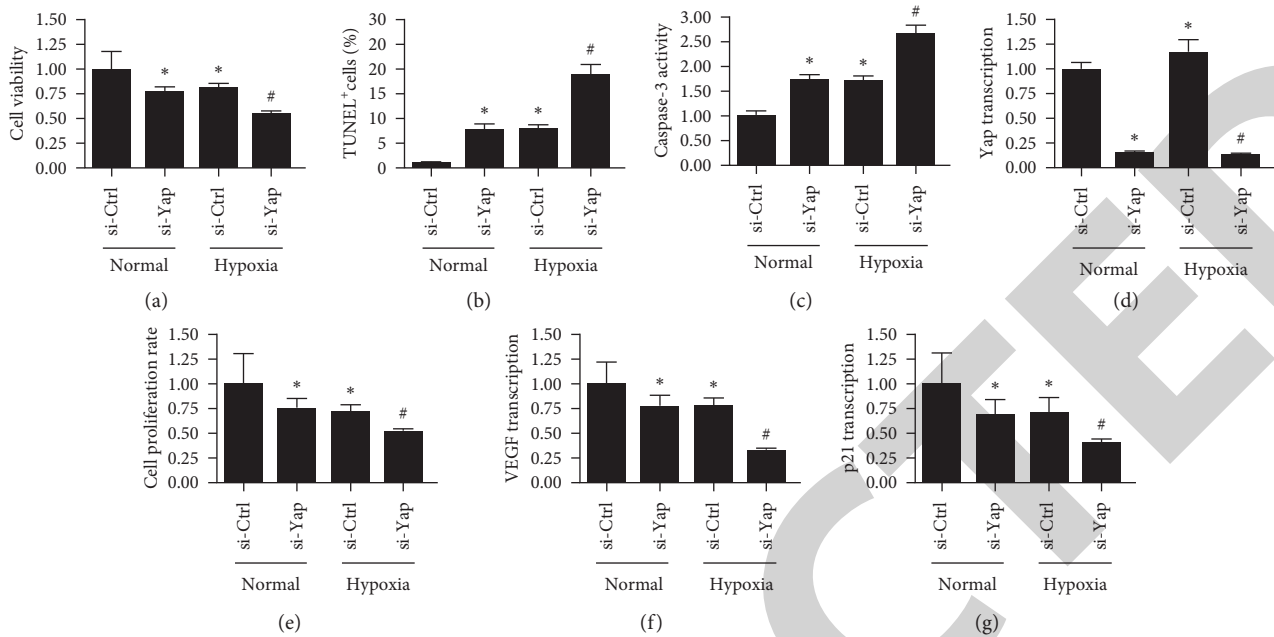


FIGURE 1: Yap knockdown induces breast cancer cell death and proliferation arrest under hypoxia stress. (a) MTT assay for cell viability in MCF-7 cells. siRNA against Yap (si-Yap) was transfected into cell before 24–48 hours hypoxia. (b) TUNEL staining was used to observe the cell apoptotic rate. siRNA against Yap (si-Yap) was transfected into cell before 24–48 hours hypoxia. (c) Caspase-3 activity was measured through ELISA. (d) qPCR was used to determine the efficiency of knockdown after si-Yap transfection. (e) CCK-8 assay was used to observe the cell proliferation capacity in MCF-7 cells under hypoxia. (f, g) qPCR assay was used to detect the transcription of VEGF and *p21* in MCF-7 cells transfected with si-Yap. * $p < 0.05$.

electrochemical potential within the mitochondrial network [45, 46]. Mitochondrial fusion also equilibrates mitochondrial proteins, lipids, metabolites, and mtDNA, which is thought to alleviate the local stress response and restore mitochondrial homeostasis [47, 48]. Although mitochondrial fusion parameters were unregulated by hypoxia (Figures 2(g) and 2(h)), Yap knockdown inhibited the activity of mitochondrial fusion in MCF-7 cells.

3.3. Yap Activates HIF1 under Hypoxia and Maintains Mitochondrial Homeostasis. To explain the regulatory role played by Yap in mitochondrial homeostasis under hypoxia, we focused on HIF1, which has been identified as a key transcriptional factor activated by hypoxia and contributes to transcription of protective genes [49]. Firstly, we found that the transcription of HIF1 was rapidly increased in response to hypoxia treatment, whereas this trend was reversed by Yap knockdown, suggesting that HIF1 activation requires Yap under hypoxia condition (Figure 3(a)), which is in accordance with the previous studies [50]. This finding was further supported via Figure 3(b). Compared to the control group, HIF expression was augmented by hypoxia, as evidenced by abundant expression of HIF1 in the cytoplasm. However, in MCF-7 cells transfected with Yap siRNA, the levels of intracellular HIF1 were apparently downregulated (Figure 3(b)). These data indicate that hypoxia activates HIF1 through Yap.

To understand whether HIF1 is involved in Yap-related mitochondrial dysfunction, HIF1 adenovirus was transfected into Yap-knockdown cells. Then, mitochondrial

function and cell viability were measured again. As shown in Figure 3(c), compared to the control group, intracellular ATP generation was reduced in response to Yap knockdown, and this effect could be attenuated by HIF1 overexpression. Additionally, Yap deletion-mediated ROS overproduction was ameliorated by HIF1 overexpression (Figure 3(d)), reconfirming that HIF1 may function downstream of Yap and sustain mitochondrial homeostasis in MCF-7 cells.

3.4. Overexpression of HIF1 Abolishes Yap Knockdown-Mediated Breast Cancer Death and Proliferation Arrest. Next, we explored whether HIF1 overexpression attenuates Yap knockdown-induced breast cancer cell death and proliferation arrest. As shown in Figure 4(a), compared to the control group, Yap knockdown augmented hypoxia-initiated cell death, as evidenced by MTT assay, whereas overexpression of HIF1 maintained MCF-7 cell viability. Similar to these results, TUNEL assay demonstrated that the number of apoptotic cells was increased by Yap knockdown; this effect could be abolished by HIF1 overexpression (Figure 4(b)). In addition to cell death, CCK-8 assay also illustrated that the proliferative capacity of MCF-7 cells was impaired by Yap knockdown, whereas HIF1 overexpression could sustain cancer cell proliferation (Figure 4(c)). This finding was also supported by qPCR for the analysis of cell-cycle-related genes. As shown in Figures 4(d) and 4(e), compared to the control group, the transcription levels of VEGF and *p21* were reduced by hypoxia, whereas this action could be abolished by HIF1 overexpression.

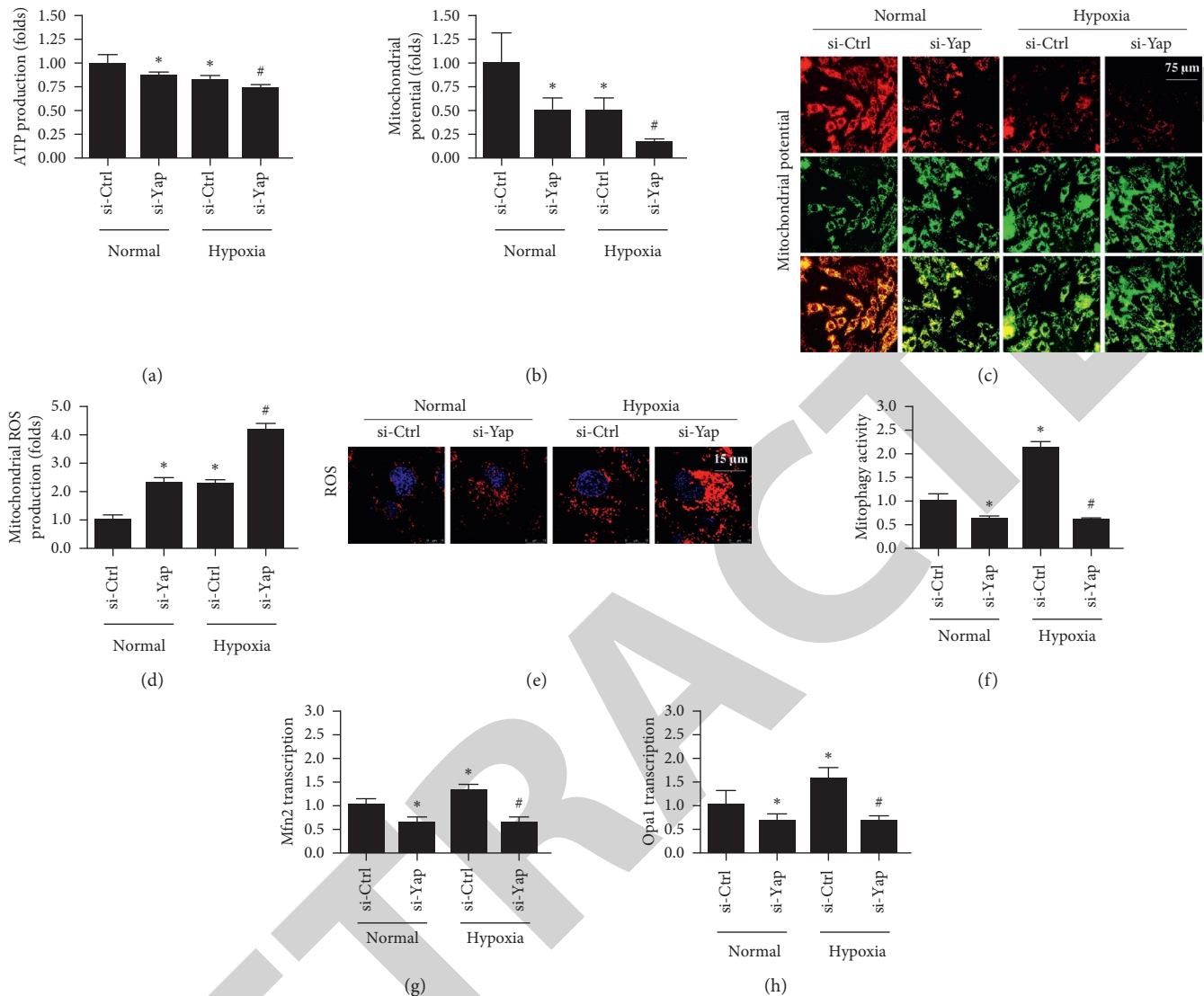


FIGURE 2: Yap knockdown reduces mitochondrial function in hypoxia-treated breast cancer. (a) ATP production was measured through ELISA. (b, c) Mitochondrial membrane potential was determined in MCF-7 cells. siRNA against Yap (si-Yap) was transfected into cells before 24 hours hypoxia. (d, e) ROS production was detected in response to Yap knockdown. (f) Mitophagy activity was determined through the mt-Kemia assay. (g, h) qPCR assay was used to detect the transcription of Mfn2 and Opa1 in MCF-7 cells transfected with si-Yap. * $p < 0.05$.

3.5. F-Actin/Lamellipodium Signaling Pathway Is Impaired by Yap Knockdown under Hypoxia. In addition to cancer cell survival and proliferation, invasion is vital for cancer development and progression. Our previous study [7] reported that F-actin and lamellipodium are vital for cancer mobilization. At the molecular level, F-actin multimerizes at the membrane and then forms the lamellipodium, which induces cellular deformation and migration [51]. In this study, immunofluorescence was used to observe alterations in the lamellipodium. As shown in Figures 5(a)–5(c), compared to the control group, the number and length of lamellipodia were significantly reduced in response to hypoxia. After knockdown of Yap, the number and length of lamellipodia further decreased; these effects could be reversed by HIF1 overexpression. Lamellipodium degradation may be a result

of F-actin downregulation [52]. Therefore, qPCR was used to analyze the alterations of F-actin. As shown in Figure 5(d), compared to the control group, F-actin transcription was inhibited by hypoxia, and this effect was augmented by Yap deletion. Interestingly, HIF1 overexpression restored F-actin transcription in MCF-7 cells under hypoxia treatment. F-actin downregulation and lamellipodium degradation may impair cancer cell migration [53]. Thus, transwell assay was used to analyze the migratory response of MCF-7 in response to hypoxia and/or Yap knockdown. As shown in Figure 5(e), compared to the control group, the number of migrating MCF-7 cells was reduced after exposure to hypoxic stimulus. Although Yap knockdown further reduced the migratory response in hypoxia-treated MCF-7 cells, HIF1 overexpression could normalize MCF-7 mobility.

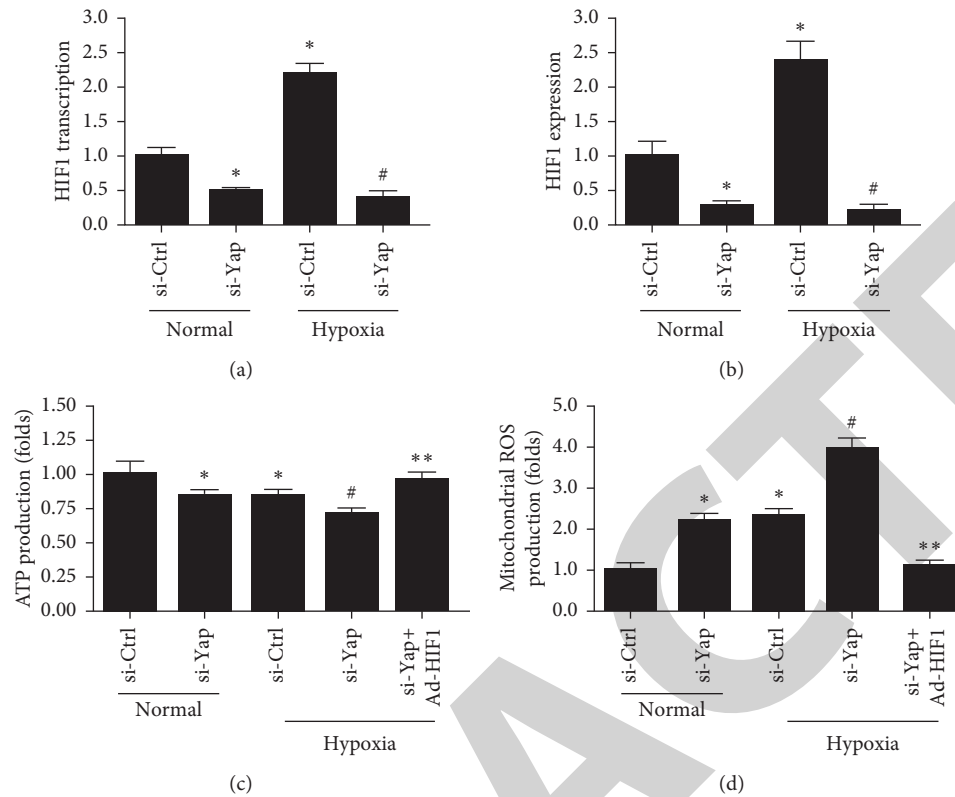


FIGURE 3: Yap maintains mitochondrial homeostasis through activating HIF1 in MCF-7 cells under hypoxia. (a) The transcription of HIF1 was determined via qPCR in MCF-7 cells under hypoxia. (b) HIF1 expression was detected in response to Yap knockdown in the presence of hypoxia in MCF-7 cells. (c) ATP production was measured through ELISA. (d) ROS production was measured in response to Yap knockdown in the presence of hypoxia. * $p < 0.05$.

Overall, this result indicates that Yap knockdown weakens breast cancer mobilization through inhibiting the F-actin/lamellipodium signaling pathway in a manner dependent on HIF1.

4. Discussion

In this study, we found that Yap expression is increased in MCF-7 breast cancer cells under hypoxia stimulus. Higher levels of Yap contribute to the survival, proliferation, and migration of MCF-7 breast cancer cells by activating HIF1. Loss of Yap activated apoptosis and limited proliferation in MCF-7 cells through induction of mitochondrial dysfunction. Yap knockdown also blunted the F-actin/lamellipodium signaling pathway, thereby attenuating the MCF-7 migratory response. Mechanistically, Yap knockdown dissipated mitochondrial membrane potential, resulting in ATP undersupply and ROS overproduction. Moreover, Yap knockdown also impaired mitophagy and mitochondrial fusion through an undefined mechanism. Moderately damaged mitochondria fail to produce ATP for cell metabolism and mobilization, whereas excessively injured mitochondria are a trigger for cellular apoptosis. To the best of our knowledge, this is the first study to identify Yap as the master of breast cancer survival through protection of mitochondrial function in the setting of hypoxic stress. This finding defines Yap and its downstream effector, HIF1, as

potential targets to prevent breast cancer growth and invasion.

Yap activation plays an important role in decreasing the immune system response [54] and accelerating cancer cell type transition [55]. Tumor cell senescence or reduced stemness is also associated with a drop in the expression of Yap [56]. Interestingly, chemotherapy or radiotherapy resistance mechanisms in prostate cancer [57], gastric cancer [58], bone pediatric cancer [59], and breast cancer [60] are linked to Yap activation or overexpression. We found that hypoxic stress was a critical factor that induces Yap transcription and activation in a time-dependent manner. Considering the tumor-promoting property of Yap, increased levels of Yap may offset the adverse impacts induced by hypoxia, such as apoptosis, migration inhibition, and proliferation arrest. In our study, we found that Yap was required for MCF-7 cell survival and proliferation under hypoxic conditions since knockdown of Yap augmented hypoxia-induced apoptosis [61].

Mechanistically, we found that Yap deficiency was associated with mitochondrial dysfunction including mitochondrial membrane potential reduction, mitochondrial metabolic impairment, and oxidative stress injury. In addition, mitochondrial protective mechanisms such as mitophagy and fusion were also inhibited by Yap knockdown. Our previous studies [7] showed that Yap deletion reduces mitochondrial ATP production and thus impairs

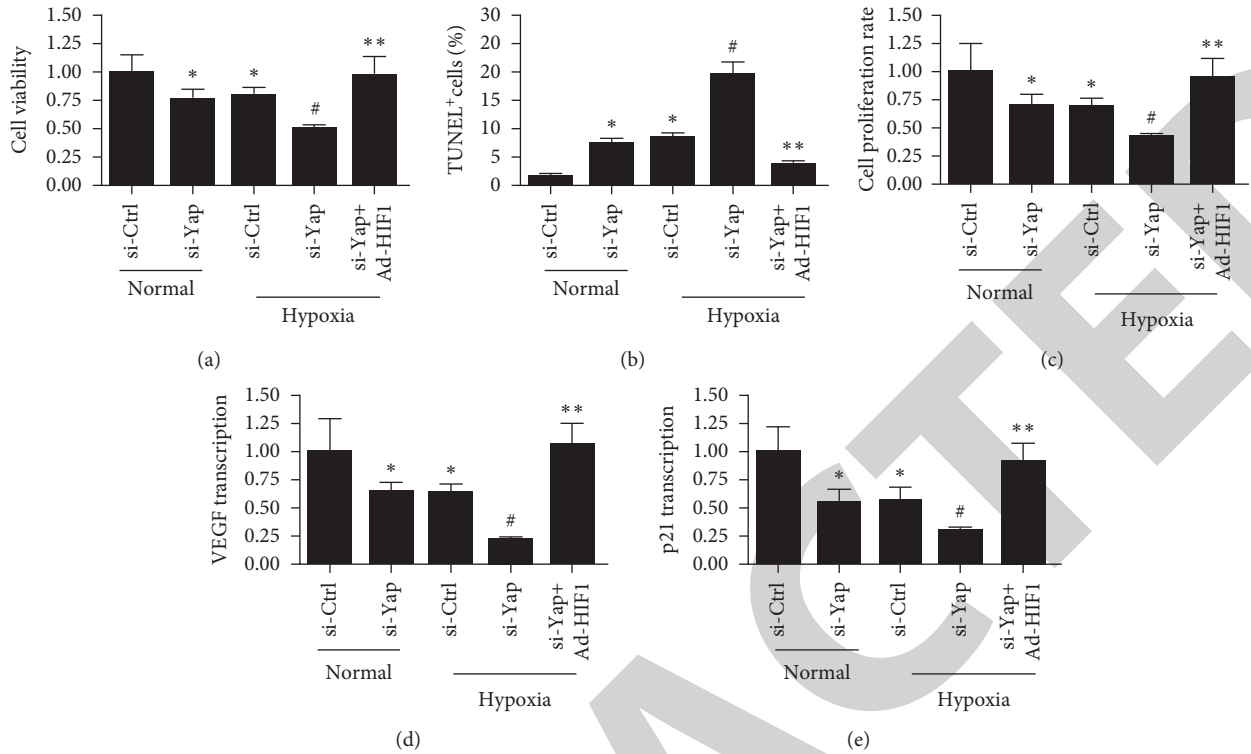


FIGURE 4: Overexpression of HIF1 abolishes Yap knockdown-mediated breast cancer cell death and proliferation arrest. (a) MTT assay for cell viability in MCF-7 cells. siRNA against Yap (si-Yap) was transfected into cells before 24 hours hypoxia. HIF1 adenovirus (ad-HIF1) was transfected into Yap-deleted MCF-7 cells before 24 hours hypoxia. (b) TUNEL staining was used to observe the cell apoptotic rate. (c) CCK-8 assay was used to observe the cell proliferation capacity in MCF-7 cells under hypoxia. (d, e) qPCR assay was used to detect the transcription of VEGF and p21 in MCF-7 cells transfected with si-Yap. * $p < 0.05$.

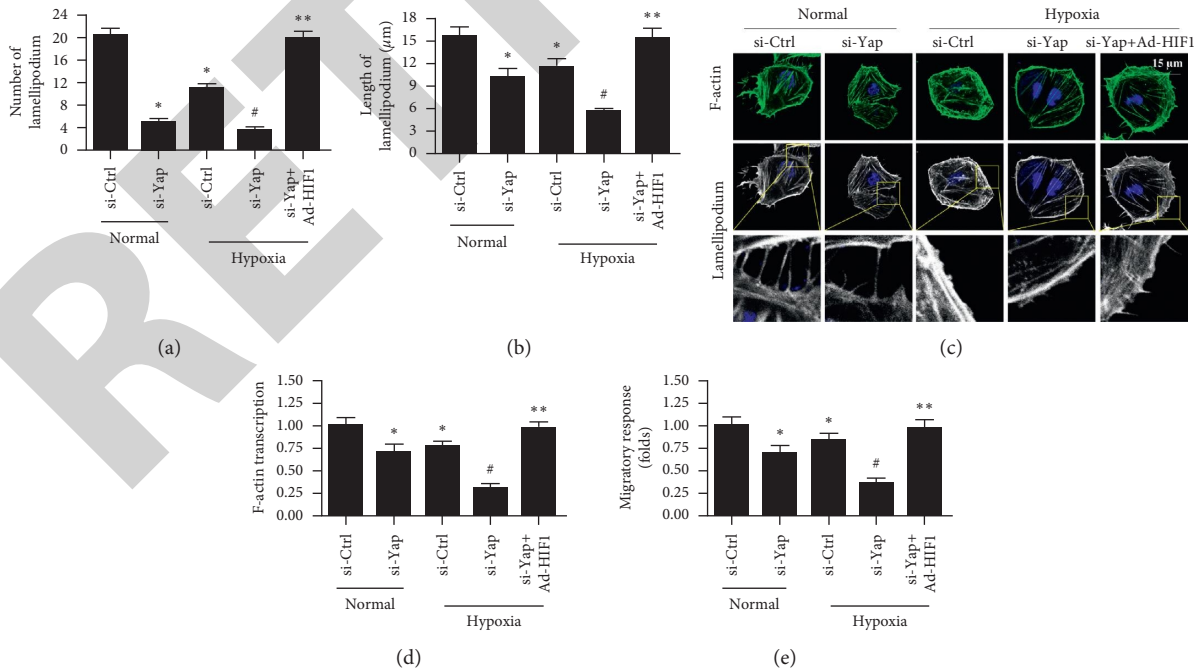


FIGURE 5: F-actin/lamellipodium signaling pathway is impaired by Yap knockdown under hypoxia. (a-c) Immunofluorescence for lamellipodium. The average length and number of lamellipodia was determined. siRNA against Yap (si-Yap) was transfected into cells before 24 hours hypoxia. HIF1 adenovirus (ad-HIF1) was transfected into Yap-deleted MCF-7 cells before 24 hours hypoxia. (d) qPCR was used to detect the alterations of F-actin in response to hypoxia, si-Yap transfection, and ad-HIF1 infection. (e) Transwell assay was used to observe the migratory response of MCF-7 cells. * $p < 0.05$.

liver cancer migration, which is highly dependent on intracellular energy supply. In glioblastoma A172 cells, the loss of Yap prevents the activation of AMPK, a sensor of cellular ATP status [62, 63]. In breast cancer, pharmacologic blockade of Yap through administration of curcumin induces oxidative stress damage in breast cancer and thus limits cell growth rate *in vitro* [63]. In septic cardiomyopathy, Yap deficiency activates mitochondrial stress through inhibiting ERK pathway, resulting into cardiomyocyte death in a manner dependent on mitochondria-initiated apoptotic pathway [64]. In cerebral hypoxia-reoxygenation injury, knockdown of Yap reduces gliocyte-mediated tissue regeneration through inhibiting the ROCK1/F-actin pathway [65].

Finally, we found that the F-actin/lamellipodium signaling is also modulated by Yap under hypoxic conditions. F-actin-mediated lamellipodium formation has been identified as a necessary step for cancer migration and invasion. We observed that lamellipodium degradation, partly due to F-actin transcriptional downregulation, was induced by hypoxia [66]. Interestingly, this effect could be enhanced by Yap knockdown, suggesting that Yap favors breast cancer mobilization under hypoxic stress. Similar to our finding, lamellipodium-related gastric cancer migration is also governed by Yap through the SIRT1-Mfn2 pathway [67]. In squamous cell carcinomas [68] and endometrial cancer [69], F-actin homeostasis is also sustained by Yap. Therefore, our results provide a novel insight into the molecular mechanism underlying breast cancer migration. Targeting the Yap/F-actin/lamellipodium pathway could be a promising approach to control breast metastasis.

Data Availability

The datasets used and/or analyzed during the current study are available from the corresponding author on reasonable request.

Conflicts of Interest

The authors declare that there are no conflicts of interest.

Authors' Contributions

Chen Shi and Jian Tie conceived the research; Chen Shi conducted the experiments; Siyuan Zhang and Changkuo Guo analyzed the data; Chen Shi wrote the manuscript; all authors participated in discussing and revising the manuscript.

Acknowledgments

The study was supported by the grant from the Open Project funded by Key laboratory of Carcinogenesis and Translational Research, Ministry of Education/Beijing (2017 Open Project-9).

References

- [1] G. N. Hortobagyi, "Breast cancer: 45 years of research and progress," *Journal of Clinical Oncology*, vol. 38, no. 21, pp. 2454–2462, 2020.
- [2] N. M. Tung, J. C. Boughey, L. J. Pierce et al., "Management of hereditary breast cancer: American society of clinical oncology, American society for radiation oncology, and society of surgical oncology guideline," *Journal of Clinical Oncology*, vol. 38, no. 18, pp. 2080–2106, 2020.
- [3] J. S. Vaidya, M. Bulsara, C. Saunders et al., "Effect of delayed targeted intraoperative radiotherapy vs whole-breast radiotherapy on local recurrence and survival: long-term results from the TARGIT-a randomized clinical trial in early breast cancer," *JAMA Oncology*, vol. 6, no. 7, Article ID e200249, 2020.
- [4] N. Kunst, J. B. Long, X. Xu et al., "Use and costs of breast cancer screening for women in their 40s in a US population with private insurance," *JAMA Internal Medicine*, vol. 180, no. 5, pp. 799–801, 2020.
- [5] B. Zhao, L. Li, K. Tumaneng, C.-Y. Wang, and K.-L. Guan, "A coordinated phosphorylation by Lats and CK1 regulates YAP stability through SCF-TRCP," *Genes & Development*, vol. 24, no. 1, pp. 72–85, 2010.
- [6] L. An, P. Nie, M. Chen et al., "MST4 kinase suppresses gastric tumorigenesis by limiting YAP activation via a non-canonical pathway," *Journal of Experimental Medicine*, vol. 217, no. 6, 2020.
- [7] C. Shi, Y. Cai, Y. Li et al., "Yap promotes hepatocellular carcinoma metastasis and mobilization via governing cofilin/F-actin/lamellipodium axis by regulation of JNK/Bnip3/SERCA/CaMKII pathways," *Redox Biology*, vol. 14, pp. 59–71, 2018.
- [8] D. Bhattacharya, A. P. Azambuja, and M. Simoes-Costa, "Metabolic reprogramming promotes neural crest migration via yap/tead signaling," *Developmental Cell*, vol. 53, no. 2, pp. 199.e6–211.e6, 2020.
- [9] C. Koulis, R. Yap, R. Engel et al., "Personalized medicine-current and emerging predictive and prognostic biomarkers in colorectal cancer," *Cancers*, vol. 12, no. 4, p. 812, 2020.
- [10] Z. Wang, Q. Kong, P. Su et al., "Regulation of hippo signaling and triple negative breast cancer progression by an ubiquitin ligase RNF187," *Oncogenesis*, vol. 9, no. 3, p. 36, 2020.
- [11] X. Jing, F. Yang, C. Shao et al., "Role of hypoxia in cancer therapy by regulating the tumor microenvironment," *Molecular Cancer*, vol. 18, no. 1, p. 157, 2019.
- [12] S. Li, H.-X. Xu, C.-T. Wu et al., "Angiogenesis in pancreatic cancer: current research status and clinical implications," *Angiogenesis*, vol. 22, no. 1, pp. 15–36, 2019.
- [13] H. Zhong, A. M. De Marzo, E. Laughner et al., "Overexpression of hypoxia-inducible factor 1alpha in common human cancers and their metastases," *Cancer Research*, vol. 59, pp. 5830–5835, 1999.
- [14] D. C. Rigracciolo, A. Scarpelli, R. Lappano et al., "Copper activates HIF-1α/GPER/VEGF signalling in cancer cells," *Oncotarget*, vol. 6, no. 33, pp. 34158–34177, 2015.
- [15] H. Kumar and D. K. Choi, "Hypoxia inducible factor pathway and physiological adaptation: a cell survival pathway?" *Mediators of Inflammation*, vol. 2015, Article ID 584758, 11 pages, 2015.
- [16] Y. Li, Q. Xu, W. Yang, T. Wu, and X. Lu, "Oleanolic acid reduces aerobic glycolysis-associated proliferation by inhibiting yes-associated protein in gastric cancer cells," *Gene*, vol. 712, Article ID 143956, 2019.
- [17] X. Zhang, Y. Li, Y. Ma et al., "Yes-associated protein (YAP) binds to HIF-1α and sustains HIF-1α protein stability to promote hepatocellular carcinoma cell glycolysis under hypoxic stress," *Journal of Experimental & Clinical Cancer Research*, vol. 37, no. 1, p. 216, 2018.

- [18] B. Yan, Z. Jiang, L. Cheng et al., "Paracrine HGF/c-MET enhances the stem cell-like potential and glycolysis of pancreatic cancer cells via activation of YAP/HIF-1 α ," *Experimental Cell Research*, vol. 371, no. 1, pp. 63–71, 2018.
- [19] A. C. Fender, S. Kleeschulte, S. Stolte et al., "Thrombin receptor PAR4 drives canonical NLRP3 inflammasome signaling in the heart," *Basic Research in Cardiology*, vol. 115, no. 2, p. 10, 2020.
- [20] D. B. Buglak, E. J. Kushner, A. P. Marvin, K. L. Davis, and V. L. Bautch, "Excess centrosomes disrupt vascular lumenization and endothelial cell adherens junctions," *Angiogenesis*, vol. 23, no. 4, pp. 567–575, 2020.
- [21] A. Daiber and T. Münzel, "Interplay of the red blood cell and vascular endothelial nitric oxide synthase system to combat cardiac complications of anemia," *Basic Research in Cardiology*, vol. 115, no. 4, p. 44, 2020.
- [22] A. R. Ednie and E. S. Bennett, "Intracellular O-linked glycosylation directly regulates cardiomyocyte L-type Ca²⁺ channel activity and excitation-contraction coupling," *Basic Research in Cardiology*, vol. 115, no. 6, p. 59, 2020.
- [23] A. Grogan, A. Coleman, H. Joca et al., "Deletion of obscurin immunoglobulin domains Ig58/59 leads to age-dependent cardiac remodeling and arrhythmia," *Basic Research in Cardiology*, vol. 115, no. 6, p. 60, 2020.
- [24] S. Díaz Del Moral, S. Barrena, R. Muñoz-Chápuli, and R. Carmona, "Embryonic circulating endothelial progenitor cells," *Angiogenesis*, vol. 23, no. 4, pp. 531–541, 2020.
- [25] A. Umaphathy, L. W. Chamley, and J. L. James, "Reconciling the distinct roles of angiogenic/anti-angiogenic factors in the placenta and maternal circulation of normal and pathological pregnancies," *Angiogenesis*, vol. 23, no. 2, pp. 105–117, 2020.
- [26] L. C. Dieterich, C. Tacconi, F. Menzi et al., "Lymphatic MAFB regulates vascular patterning during developmental and pathological lymphangiogenesis," *Angiogenesis*, vol. 23, no. 3, pp. 411–423, 2020.
- [27] A. Sanchez, M. Kuras, J. R. Murillo et al., "Novel functional proteins coded by the human genome discovered in metastases of melanoma patients," *Cell Biology and Toxicology*, vol. 36, no. 3, pp. 261–272, 2020.
- [28] D. Unterleuthner, P. Neuhold, K. Schwarz et al., "Cancer-associated fibroblast-derived WNT2 increases tumor angiogenesis in colon cancer," *Angiogenesis*, vol. 23, no. 2, pp. 159–177, 2020.
- [29] M.-M. Vaeyens, A. Jorge-Peñas, J. Barrasa-Fano et al., "Matrix deformations around angiogenic sprouts correlate to sprout dynamics and suggest pulling activity," *Angiogenesis*, vol. 23, no. 3, pp. 315–324, 2020.
- [30] S. Liu, J. Chen, J. Shi et al., "M1-like macrophage-derived exosomes suppress angiogenesis and exacerbate cardiac dysfunction in a myocardial infarction microenvironment," *Basic Research in Cardiology*, vol. 115, no. 2, p. 22, 2020.
- [31] A. Vasseur, L. Cabel, O. Tredan et al., "Prognostic value of CEC count in HER2-negative metastatic breast cancer patients treated with bevacizumab and chemotherapy: a prospective validation study (UCBG COMET)," *Angiogenesis*, vol. 23, no. 2, pp. 193–202, 2020.
- [32] M. Lobo-Gonzalez, C. Galán-Arriola, X. Rossello et al., "Metoprolol blunts the time-dependent progression of infarct size," *Basic Research in Cardiology*, vol. 115, no. 5, p. 55, 2020.
- [33] P. Villacampa, S. E. Liyanage, I. P. Klaska et al., "Stabilization of myeloid-derived HIFs promotes vascular regeneration in retinal ischemia," *Angiogenesis*, vol. 23, no. 2, pp. 83–90, 2020.
- [34] H. Wang, A. Ramshekar, E. Kunz, D. B. Sacks, and M. E. Hartnett, "IQGAP1 causes choroidal neovascularization by sustaining VEGFR2-mediated Rac1 activation," *Angiogenesis*, vol. 23, no. 4, pp. 685–698, 2020.
- [35] X. Lu, Y. He, C. Tang et al., "Triad3A attenuates pathological cardiac hypertrophy involving the augmentation of ubiquitination-mediated degradation of TLR4 and TLR9," *Basic Research in Cardiology*, vol. 115, no. 2, p. 19, 2020.
- [36] J. Wang, S. Toan, and H. Zhou, "New insights into the role of mitochondria in cardiac microvascular ischemia/reperfusion injury," *Angiogenesis*, vol. 23, no. 3, pp. 299–314, 2020.
- [37] N. Lubos, S. van der Gaag, M. Gerçek, S. Kant, R. E. Leube, and C. A. Krusche, "Inflammation shapes pathogenesis of murine arrhythmogenic cardiomyopathy," *Basic Research in Cardiology*, vol. 115, no. 4, p. 42, 2020.
- [38] E. Watanabe, T. Wada, A. Okekawa et al., "Stromal cell-derived factor 1 (SDF1) attenuates platelet-derived growth factor-B (PDGF-B)-induced vascular remodeling for adipose tissue expansion in obesity," *Angiogenesis*, vol. 23, no. 4, pp. 667–684, 2020.
- [39] J. Lyu, M. Wang, X. Kang et al., "Macrophage-mediated regulation of catecholamines in sympathetic neural remodeling after myocardial infarction," *Basic Research in Cardiology*, vol. 115, no. 5, p. 56, 2020.
- [40] A. Wincewicz and P. Woltanowski, "Leopold auerbach's achievements in the field of vascular system," *Angiogenesis*, vol. 23, no. 4, pp. 577–579, 2020.
- [41] H. Zhou, D. Li, P. Zhu et al., "Melatonin suppresses platelet activation and function against cardiac ischemia/reperfusion injury via PPAR γ /FUNDC1/mitophagy pathways," *Journal of Pineal Research*, vol. 63, 2017.
- [42] H. Zhou, Y. Zhang, S. Hu et al., "Melatonin protects cardiac microvasculature against ischemia/reperfusion injury via suppression of mitochondrial fission-VDAC1-HK2-mPTP-mitophagy axis," *Journal of Pineal Research*, vol. 63, 2017.
- [43] Q. Jin, R. Li, N. Hu et al., "DUSP1 alleviates cardiac ischemia/reperfusion injury by suppressing the Mff-required mitochondrial fission and Bnip3-related mitophagy via the JNK pathways," *Redox Biology*, vol. 14, pp. 576–587, 2018.
- [44] R. Li, T. Xin, D. Li, C. Wang, H. Zhu, and H. Zhou, "Therapeutic effect of sirtuin 3 on ameliorating nonalcoholic fatty liver disease: the role of the ERK-CREB pathway and Bnip3-mediated mitophagy," *Redox Biology*, vol. 18, pp. 229–243, 2018.
- [45] P. Zhu, S. Hu, Q. Jin et al., "Ripk3 promotes ER stress-induced necroptosis in cardiac IR injury: a mechanism involving calcium overload/XO/ROS/mPTP pathway," *Redox Biology*, vol. 16, pp. 157–168, 2018.
- [46] H. Zhou, P. Zhu, J. Guo et al., "Ripk3 induces mitochondrial apoptosis via inhibition of FUNDC1 mitophagy in cardiac IR injury," *Redox Biology*, vol. 13, pp. 498–507, 2017.
- [47] H. Zhou, P. Zhu, J. Wang, H. Zhu, J. Ren, and Y. Chen, "Pathogenesis of cardiac ischemia reperfusion injury is associated with CK2 α -disturbed mitochondrial homeostasis via suppression of FUNDC1-related mitophagy," *Cell Death & Differentiation*, vol. 25, no. 6, pp. 1080–1093, 2018.
- [48] H. Zhou, S. Wang, S. Hu, Y. Chen, and J. Ren, "ER-mitochondria microdomains in cardiac ischemia-reperfusion injury: a fresh perspective," *Frontiers in Physiology*, vol. 9, p. 755, 2018.
- [49] Y. Li, V. Kasim, X. Yan et al., "Yin Yang 1 facilitates hepatocellular carcinoma cell lipid metabolism and tumor progression by inhibiting PGC-1 β -induced fatty acid oxidation," *Theranostics*, vol. 9, no. 25, pp. 7599–7615, 2019.
- [50] O. Vetrovoy, K. Sarieva, E. Lomert et al., "Pharmacological HIF1 inhibition eliminates downregulation of the pentose

Retraction

Retracted: Mst2 Overexpression Inhibits Thyroid Carcinoma Growth and Metastasis by Disrupting Mitochondrial Fitness and Endoplasmic Reticulum Homeostasis

Journal of Oncology

Received 10 October 2023; Accepted 10 October 2023; Published 11 October 2023

Copyright © 2023 Journal of Oncology. This is an open access article distributed under the Creative Commons Attribution License, which permits unrestricted use, distribution, and reproduction in any medium, provided the original work is properly cited.

This article has been retracted by Hindawi following an investigation undertaken by the publisher [1]. This investigation has uncovered evidence of one or more of the following indicators of systematic manipulation of the publication process:

- (1) Discrepancies in scope
- (2) Discrepancies in the description of the research reported
- (3) Discrepancies between the availability of data and the research described
- (4) Inappropriate citations
- (5) Incoherent, meaningless and/or irrelevant content included in the article
- (6) Peer-review manipulation

The presence of these indicators undermines our confidence in the integrity of the article's content and we cannot, therefore, vouch for its reliability. Please note that this notice is intended solely to alert readers that the content of this article is unreliable. We have not investigated whether authors were aware of or involved in the systematic manipulation of the publication process.

Wiley and Hindawi regrets that the usual quality checks did not identify these issues before publication and have since put additional measures in place to safeguard research integrity.

We wish to credit our own Research Integrity and Research Publishing teams and anonymous and named external researchers and research integrity experts for contributing to this investigation.

The corresponding author, as the representative of all authors, has been given the opportunity to register their agreement or disagreement to this retraction. We have kept a record of any response received.

References

- [1] H. Zhang, X. Qu, L. Han, and X. Di, "Mst2 Overexpression Inhibits Thyroid Carcinoma Growth and Metastasis by Disrupting Mitochondrial Fitness and Endoplasmic Reticulum Homeostasis," *Journal of Oncology*, vol. 2021, Article ID 1262291, 10 pages, 2021.

Research Article

Mst2 Overexpression Inhibits Thyroid Carcinoma Growth and Metastasis by Disrupting Mitochondrial Fitness and Endoplasmic Reticulum Homeostasis

Haichao Zhang, Xin Qu, Lu Han, and Xu Di 

Department of Thyroid and Breast Surgery, Tianjin Fourth Central Hospital, The Fourth Central Hospital Affiliated to Nankai University, The Fourth Center Clinical College of Tianjin Medical University, Tianjin 300140, China

Correspondence should be addressed to Xu Di; 5020200897@nankai.edu.cn

Received 12 July 2021; Revised 27 July 2021; Accepted 31 August 2021; Published 14 September 2021

Academic Editor: Yun-dai Chen

Copyright © 2021 Haichao Zhang et al. This is an open access article distributed under the Creative Commons Attribution License, which permits unrestricted use, distribution, and reproduction in any medium, provided the original work is properly cited.

Although the incidence of thyroid carcinoma has increased over the past several decades, it has an excellent prognosis and overall 5-year survival, with a stable mortality rate, except in cases with advanced stages or rare malignant tumor types. Biomarkers have emerged as effective targets of molecular therapy against thyroid carcinoma due to their rapid and convenient detection; however, there has been little clinical application. Macrophage stimulating 2 (Mst2) is a proapoptotic protein with implications in carcinogenesis and metastasis. We found that Mst2 overexpression-induced endoplasmic reticulum (ER) stress in MDA-T32 thyroid carcinoma cells, accompanied by elevated caspase-12 activity, increased apoptotic rate, and reduced cell viability. In addition, Mst2 overexpression contributed to mitochondrial damage, as evidenced by increased mitochondrial oxidative stress and activated the mitochondrial apoptotic pathway. Inhibition of the JNK pathway abolished these effects. These results show Mst2 to be a novel tumor suppressor that induces mitochondrial dysfunction and ER stress via the JNK pathway. Thus, Mst2 could potentially serve as a biomarker for developing targeted therapy against thyroid carcinoma.

1. Introduction

The incidence of thyroid carcinoma has been increasing worldwide; however, its mortality rate has largely remained stable. Thyroid carcinoma can be categorized into differentiated (papillary and follicular), poorly differentiated, and rarely occurring medullary and anaplastic tumor types. Approximately 80% of the patients are diagnosed with poorly differentiated thyroid carcinoma. Although surgery, chemotherapy, and targeted therapy have proved to be effective in patients with early detection, those with advanced metastatic thyroid carcinoma have few treatment choices and poor prognosis. In addition, despite the initial response to cytotoxic therapy being favorable in 30–40% of patients, a majority of them experience progression during or after treatment. The most common cause of progression to advanced stages is the dysregulation of oncogenes and tumor suppressor genes.

Mitochondria function as a cellular powerhouse to provide a constant supply of ATP for performing numerous biological processes such as metabolism, proliferation, growth, metastasis, differentiation, angiogenesis, and apoptosis [1]. Their involvement in the development and progression of thyroid carcinoma is evident from the fact that mitochondrial proteins serve as potential targets of chemotherapeutic receptor tyrosine kinase inhibitor drugs such as vandetanib and cabozantinib [2, 3]. Moreover, the inhibition of mitochondrial function via disruption of oxidative phosphorylation has been shown to enhance the response to chemotherapy [4]. Endoplasmic reticulum (ER) facilitates the processing of newly formed prosurvival and proliferation proteins required for tumor growth and metastasis. Impaired ER activity or ER stress has been shown to contribute to thyroid carcinoma metastasis [5, 6]. Another study reported that ER stress reduced the radiosensitivity of thyroid carcinoma cells and inhibited apoptosis [7, 8]. In

contrast, a study demonstrated that impaired protein folding and ER activity promoted thyroid carcinoma cell apoptosis [9, 10]. Although the common upstream regulator of mitochondrial fitness and ER integrity has not been elucidated, the above findings show that mitochondrial dysfunction and ER stress are potential therapeutic targets for thyroid cancer.

Macrophage stimulating 2 (Mst2), also known as mammalian sterile 20 kinase 2, is a serine protease that regulates posttranscriptional phosphorylation of several proteins. For example, Mst2 strengthens the immune system by promoting the activation of the IL-2/Stat5 signaling pathway [11, 12]. Mst2 controls the activity of the Akt prosurvival pathway, a downstream event in Mst2 upregulation [13, 14]. In addition, Mst2 is known to control the differentiation of the epididymal initial segment via the MEK-ERK pathway [15]. Recent studies have implicated Mst2 in regulating mitochondrial ROS production, suggesting a link between Mst2 and mitochondrial dysfunction [16]. In addition, upregulated levels of ER stress markers, such as CHOP, caspase-9, and GRP94, following Mst2 activation in a rat model of diabetic cardiomyopathy [17] highlight its function in maintaining ER homeostasis. Based on these findings, we speculate Mst2 as a common upstream mediator of mitochondrial function and ER stabilization.

2. Materials and Methods

2.1. Cell Culture and Treatment. Human thyroid carcinoma MDA-T32 (ATCC® CRL-3351™) cells were maintained in Dulbecco's modified Eagle's medium (DMEM) supplemented with 10% fetal bovine serum (FBS) and 1% antibiotics in 5% CO₂ at 37°C [18]. To overexpress Mst2, MDA-T32 cells were transfected with adenovirus-expressing Mst2 constructs [19].

2.2. Cell Proliferation Assay. A CCK8 assay was conducted following the manufacturer's instructions (DH343-2, Beijing Dongsheng Biotechnology, China). Briefly, cells with or without Mst2 overexpression were seeded in 96-well plates (2,000 cells/well) and cultured for 5 days [20]. Next, 10 μL of CCK8 (5 mg/mL) was added to the culture medium, and cells were further cultured for 2 h. Finally, the OD was measured at 490 nm (BioTek ELx800, USA) [21].

2.3. Western Blotting. The total protein was extracted from the cells following the standard protocol (Beyotime Biotechnology Co., Ltd.), and the protein concentration was determined using a bicinchoninic acid (BCA) protein assay kit. The total protein (40 μg) was subjected to 15% SDS-PAGE, and the separated proteins were transferred to nitrocellulose membranes [22]. After blocking in fresh 5% nonfat milk at room temperature for 2 h, membranes were incubated overnight at 4°C with the primary antibodies, followed by incubation with the secondary antibody at room temperature for 2 h. An enhanced chemiluminescence (ECL) kit (Thermo Fisher Scientific, Inc.) was used to visualize the signals [23]. The antibodies (Affinity Biosciences Ltd.) used included anti-SIRT1 (FD6033; 1:1000), anti-p-

AMPK (AF3423; 1:1000), anti-AMPK (AF6423; 1:1000), anti-Cox-2 (AF7003; 1:1000), anti-iNOS (AF0199; 1:1000), anti-Bcl-2 (AF6139; 1:1000), anti-Bax (AF0120; 1:1000), anticlaved caspase-3 (AF7022; 1:1000), anticlaved caspase-9 (AF5240; 1:1000), anti-GAPDH (AF7021; 1:5000), and goat anti-rabbit IgG (S0001; 1:5000). The protein expression was semiquantified using ImagePro Plus software, version 6.0 (Roper Technologies, Inc.) [24].

2.4. MTT Assay. A suspension of ~5,000 MDA-T32 cells was seeded in 96-well plates. MTT (Sigma) was added to the wells, and cells were incubated for 4 h in 5% CO₂ at 37°C [25]. Next, 150 μL of dimethyl sulfoxide (DMSO) was added to each well for 10 min, and the absorbance of formazan was measured at 490 nm from 0 to 72 h [26].

2.5. Reverse Transcription-Quantitative PCR. The total RNA was extracted from cells using the TRIzol reagent (Invitrogen). We used 1 μg of total RNA to generate cDNAs using the PrimeScript RT reagent kit (Takara) [27]. Reverse transcription-quantitative polymerase chain reaction (RT-qPCR) was performed using the SYBR Green I Master Mix kit. The relative gene expression was calculated using the 2^{-ΔΔCt} method [28].

2.6. Immunofluorescence Assay. Cells were cultured on glass coverslips and transfected with Mst2-overexpressing adenovirus constructs. Afterward, cells were washed twice with phosphate-buffered saline (PBS), fixed in 4% formaldehyde for 10 min, and quenched with 50 mM NH₄Cl in PBS for 10 min [29]. After three washes with PBS, cells were permeabilized with 0.1% Triton X-100 in PBS for 5 min at 4°C. The excess binding sites were blocked with SuperBlock Blocking Buffer in PBS (Thermo Fisher Scientific, #37517) for 1 h at room temperature. The cells were incubated with primary antibodies overnight at 4°C, followed by incubation with secondary antibody for 1 h at room temperature [30]. Cells were washed thrice with PBS containing 1% BSA, and coverslips were mounted onto glass slides using Vectashield containing DAPI (Vector Laboratories, Burlingame, CA, USA). Images were captured using the Zeiss Axio Imager M1 automated microscope (Zeiss, Oberkochen, Germany) [31].

2.7. Propidium Iodide Staining. MDA-T32 cells were incubated in a medium containing a 1:500 dilution of PI (Thermo Fisher Scientific) at 37°C [32]. After 30 min, PI was removed, and the cells were washed twice with the medium [33]. The number of PI-positive cells was determined using fluorescence microscopy with an excitation of 535 nm and emission of 617 nm at 200x magnification [34].

2.8. ATP Assay and Mitochondrial ROS Production. Cellular ATP levels were measured using a commercial kit (Abcam) [35]. Mitochondrial ROS production was measured using the MitoSOX red mitochondrial superoxide indicator (Molecular Probes, USA) [36].

2.9. Cell Transfection. Adenovirus constructs overexpressing human Mst2 (Ad-Mst2) used for cell transfection (Vigene Biosciences Co., Ltd., Shandong, China) [37]. In brief, MDA-T32 cells were transfected with Ad-Mst2 and control adenovirus (ad-Cont) at a multiplicity of infection (MOI) of 100 for 8 h in a serum-free medium [38]. Next, the medium was discarded, and cells were grown in a complete medium for 48 h. Mst2-expressing cells were selected using puromycin (5 μ g/mL). The Mst2 expression was verified by qPCR and Western blotting [39].

2.10. Statistical Analysis. All data are presented as mean \pm standard error of the mean (SEM). Differences between the groups were analyzed using Student's *t*-tests or one-way analysis of variance (ANOVA). $P < 0.05$ was considered significant [40]. All experiments were conducted at least in triplicate.

3. Results

3.1. Mst2 Overexpression Induces ER Stress. We first overexpressed Mst2 in MDA-T32 cells to study its effect on ER homeostasis. As shown in Figures 1(a)–1(c), compared with the control group, Mst2 overexpression upregulated the transcription of CHOP, GRP78, and PERK, the markers of ER stress. In addition, we found elevated expression of CHOP, GRP78, and PERK proteins (Figures 1(d)–1(f)), suggesting that ER stress is induced by Mst2 overexpression. Irreversible ER damage activates caspase-12—an essential step in the cell apoptosis pathway. The enzyme-linked immunosorbent assay (ELISA) demonstrated that Mst2 overexpression enhanced the activity of caspase-12 in MDA-T32 cells (Figure 1(g)) when compared with the control group. Altogether, our results illustrate that Mst2 overexpression is associated with ER stress.

3.2. Mst2 Overexpression Promotes Mitochondrial Damage. We next studied the effects of Mst2 overexpression on mitochondrial function and structure. As shown in Figures 2(a) and 2(b), the immunofluorescence assay revealed the reduced number of mitochondria in Mst2-overexpressing MDA-T32 cells compared with the control group, suggesting that Mst2 overexpression decreased the mitochondrial mass. In addition, MitoSOX red staining revealed elevated mitochondrial ROS production in MDA-T32 cells (Figures 2(c) and 2(d)), accompanied by reduced levels of glutathione (GSH) and decreased activity of superoxide dismutase (SOD) and glutathione peroxidase (GPX) (Figures 2(e)–2(g)). This finding confirmed that oxidative stress was triggered by Mst2 overexpression in MDA-T32 cells. Next, we found that the mitochondria-related apoptotic pathway was activated, as evident by increased activities of Bax and caspase-9 (Figures 2(h) and 2(i)), when compared with the control group. Altogether, our results demonstrate that mitochondrial function is hindered by Mst2 overexpression in MDA-T32 cells.

3.3. Mst2 Inhibits the Viability of Thyroid Carcinoma Cells. Impaired mitochondrial function and ER stress ultimately activate tumor cell death [41]. Therefore, we next studied whether Mst2-induced mitochondrial damage and ER stress were associated with increased MDA-T32 cell apoptosis. First, we determined the cell viability using the MTT assay. As shown in Figure 3(a), MDA-T32 cell viability was highly reduced. Moreover, the lactate dehydrogenase (LDH) release assay revealed elevated LDH content in the medium, suggesting increased cell membrane disintegration in Mst2-overexpressing MDA-T32 cells (Figure 3(b)). Because mitochondrial damage and ER stress-induced cell death is primarily executed by apoptosis, we further analyzed the number of apoptotic cells. Thus, propidium iodide (PI) staining was performed. As shown in Figures 3(c) and 3(d), ~40% of Mst2-overexpressing MDA-T32 cells were apoptotic compared with only ~6% PI-positive cells in the control group. Overall, our results confirm that Mst2 overexpression activates apoptosis by impairing mitochondrial function and inducing ER stress.

3.4. Thyroid Carcinoma Proliferation Is Impaired by Mst2 Overexpression. Rapid proliferation rate is one of the hallmarks of malignant cancer cells [42, 43]. Therefore, we wanted to understand whether tumor proliferation of thyroid carcinoma cells was controlled by Mst2. The CCK8 assay demonstrated highly reduced growth rate of MDA-T32 cells following Mst2 overexpression (Figure 4(a)). At the molecular level, cyclin-related proteins have been reported to participate in cancer proliferation. Western blotting showed that the protein expression of cyclin D and cyclin E1 was markedly reduced by Mst2 overexpression when compared with the control group (Figures 4(b) and 4(c)). Altogether, these results confirm our hypothesis that thyroid carcinoma proliferation was inhibited by Mst2 overexpression.

3.5. Mst2 Impairs Mitochondrial and ER Functions through the JNK Pathway. The above results showed that Mst2 overexpression suppressed mitochondrial and ER functions and thus promoted MDA-T32 cell apoptosis and proliferation arrest. Recent studies have revealed an intricate link between Mst2 overexpression and JNK activation. In addition, the JNK pathway has been reported to function upstream of mitochondrial damage and ER stress pathways. Therefore, we investigated the involvement of JNK in Mst2-induced mitochondrial and ER damage. Treatment of Mst2-overexpressing MDA-T32 cells with SP600125, a JNK inhibitor, reversed the reduction in mitochondrial number as compared with the control group (Figures 5(a) and 5(b)). Furthermore, Mst2-induced mitochondrial ROS production was attenuated by SP600125 (Figures 5(c) and 5(d)), suggesting that Mst2-induced oxidative stress was dependent on the JNK pathway. Similarly, SP600125 treatment reduced Mst2 overexpression-induced transcription of CHOP, GRP78, and PERK (Figures 5(e)–5(g)). Altogether, our results demonstrate that Mst2 disrupts mitochondrial function

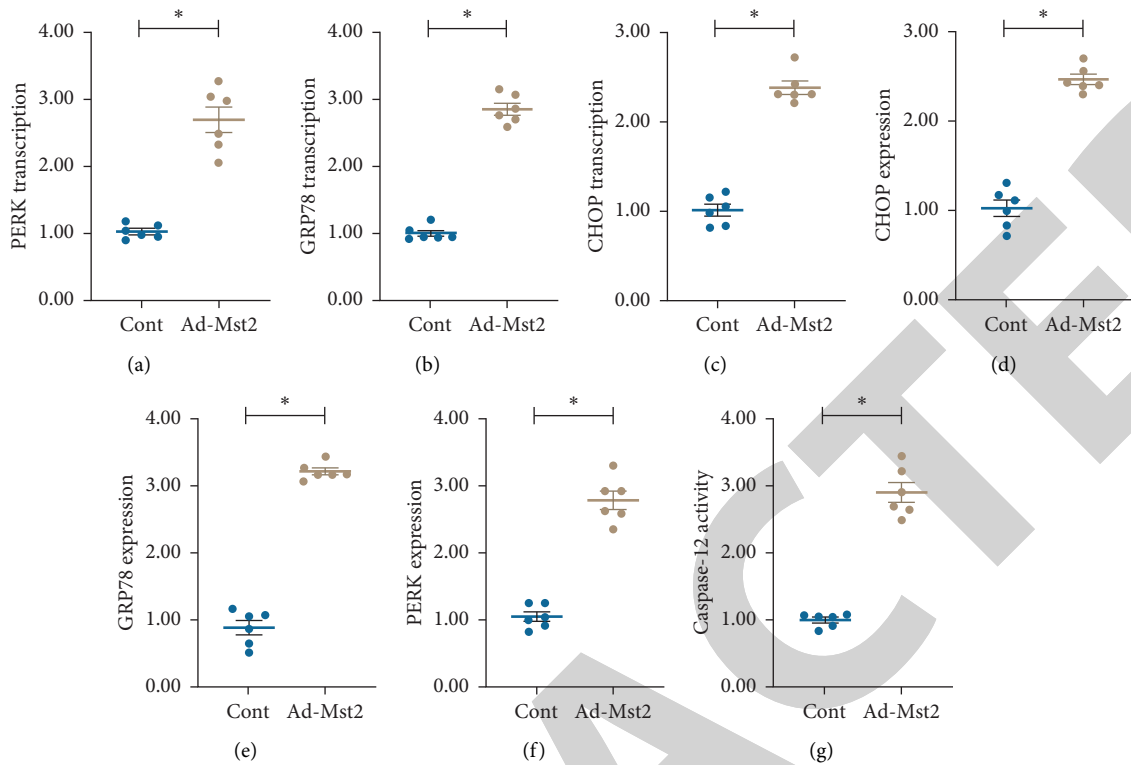


FIGURE 1: Mst2 overexpression induces ER stress. (a)–(c) MDA-T32 cells transfected with Mst2 adenovirus (Ad-Mst2) constructs. Next, a qPCR assay was used to analyze the transcription of CHOP, GRP78, and PERK. (d)–(f) Western blots showing the expression of CHOP, PERK, and GRP78. (g) ELISA performed to analyze the activity of caspase-12. * $P < 0.05$.

and induces ER stress in MDA-T32 cells through the JNK pathway.

4. Discussion

Thyroid carcinoma is one of the most common endocrine cancers with a high cure rate. Several factors contribute to thyroid carcinoma, including genetic, environmental, and lifestyle-related. Recent advances in medical imaging have led to early diagnosis and treatment of thyroid carcinoma [44]. The standard treatment includes surgery and radioactive iodine therapy; targeted therapies using specific biomarkers [45], such as tyrosine kinase inhibitors, have been recently introduced and appear to be promising due to their rapid and convenient detection. However, their clinical application is less, indicating the need to explore new effective biomarkers to improve the diagnostic efficiency, prognosis, and treatment outcomes. We showed that Mst2 overexpression in thyroid carcinoma cells induced mitochondrial damage and ER stress resulting in apoptosis and cell proliferation arrest [46]. Therefore, therapeutic approaches targeting Mst2 activity can further enhance the response of thyroid carcinoma to chemotherapy and radiotherapy.

The Mst family includes Mst1 and Mst2, and anticancer effects of Mst activation have been reported by several studies. For example, Mst1 activation induced oxidative stress and suppressed pancreatic cancer progression by promoting pyroptosis [47, 48]. Similarly, reduced serum

levels of Mst1 and Mst2 have been correlated with the development of liver cancer due to the increased proliferation of tumor cells [49, 50]. Moreover, overexpressed Mst1 reduced the invasiveness and proliferation of lung cancer cells [51, 52]. In breast cancer, reduced expression of Mst1 is associated with increased tumor proliferation and migration [53]. Mst1 and Mst2 are known to suppress colonic tumorigenesis and tumor stem cell proliferation by inhibiting Yes-associated protein (Yap) [54, 55]. Similar to these findings, we found that Mst2 overexpression suppressed the development of thyroid carcinoma by promoting cancer apoptosis and inhibiting cell proliferation.

Numerous studies have investigated the function of Mst family proteins in regulating mitochondrial function in cancer survival and metastasis [56–58]. For example, the overexpression of Mst1 suppressed gastric cancer cell viability by inactivating the AMPK–Sirt3 pathway and inducing mitochondrial division [59]. Similarly, overexpressed Mst1 caused mitochondria-dependent breast cancer cell apoptosis via the JNK–Drp1 pathway [60]. Another study reported the tumor-suppressive effects of Mst1 on cancer cell proliferation and metastasis by activating the β -catenin/Drp1 axis [61]. Furthermore, Mst1 overexpression impaired the proliferation and migration of colorectal cancer cells by activating the JNK/ $p53$ /Bnip3 pathway [62]. The overexpression of Mst1 hindered ATP production and redox biology in nonsmall cell lung cancer through the ROCK1/F-actin pathway [63]. Furthermore, Mst2 is a potential target of several anticancer drugs such as

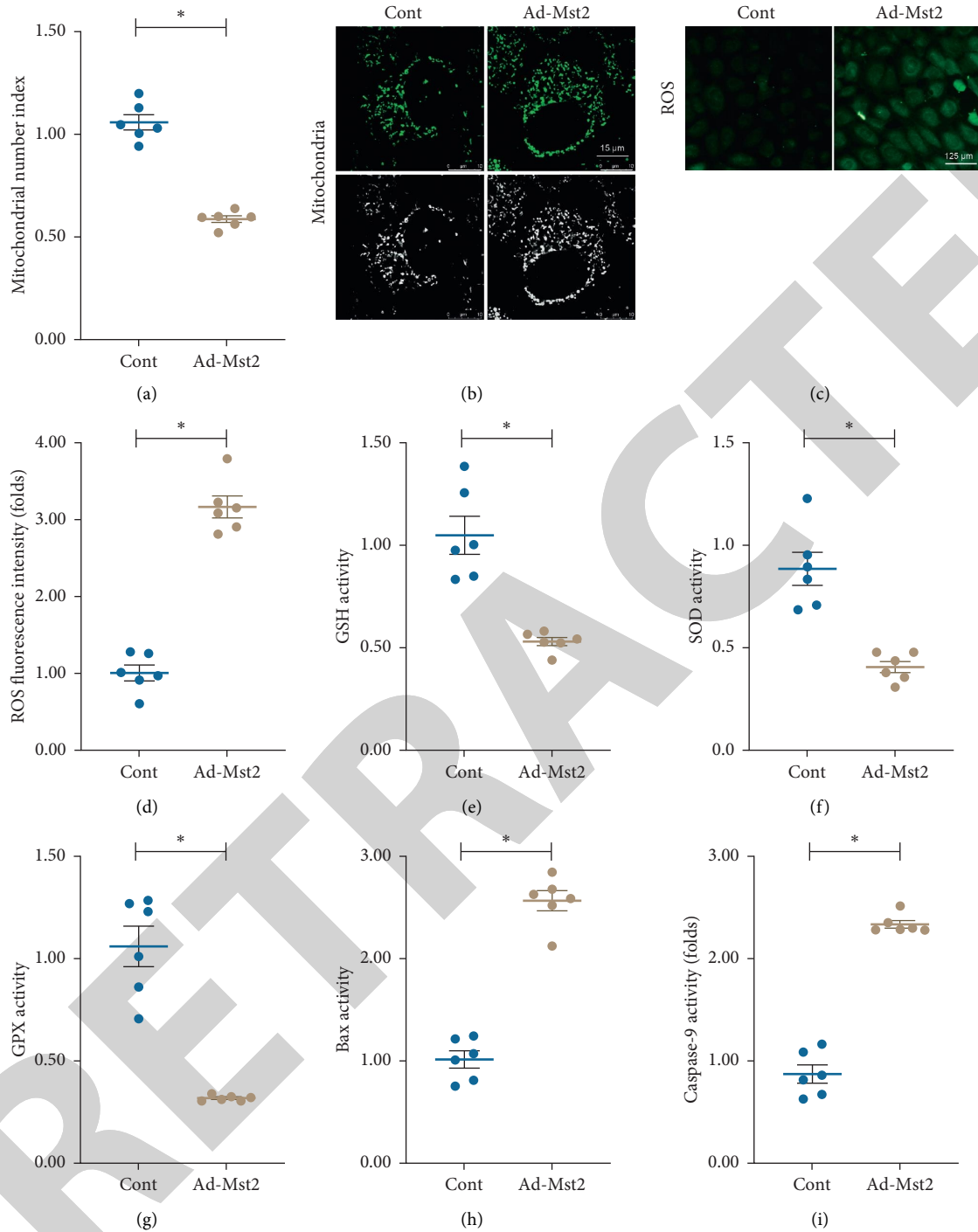


FIGURE 2: Mst2 overexpression promotes mitochondrial damage. (a)–(b) An immunofluorescence assay used to analyze the mitochondrial number. (c)–(d) MitoSOX red staining used to study the mitochondrial ROS production in response to Ad-Mst2 transfection. (e)–(g) ELISA performed to analyze the activity of antioxidative enzymes such as GSH, SOD, and GPX. (h)–(i) ELISA performed to detect the alterations in Bax and caspase-9 activities. * $P < 0.05$.

gemcitabine [64], tanshinone IIA [65], and matrine [66]. In addition to mitochondria, we reported that ER damage, such as ER stress and ER-related apoptosis, was induced by Mst2. Thus, new therapeutic approaches are being explored to simultaneously affect mitochondrial function and ER homeostasis [67].

Our study had certain limitations. First, because Mst2 is an intracellular protein, there is a need to design new drugs to specifically target its expression. Second, animal studies and clinical trials are warranted to study the molecular basis of Mst2 effects on mitochondrial and ER functions in cancer cells. Third, negative effects of Mst2 overexpression on

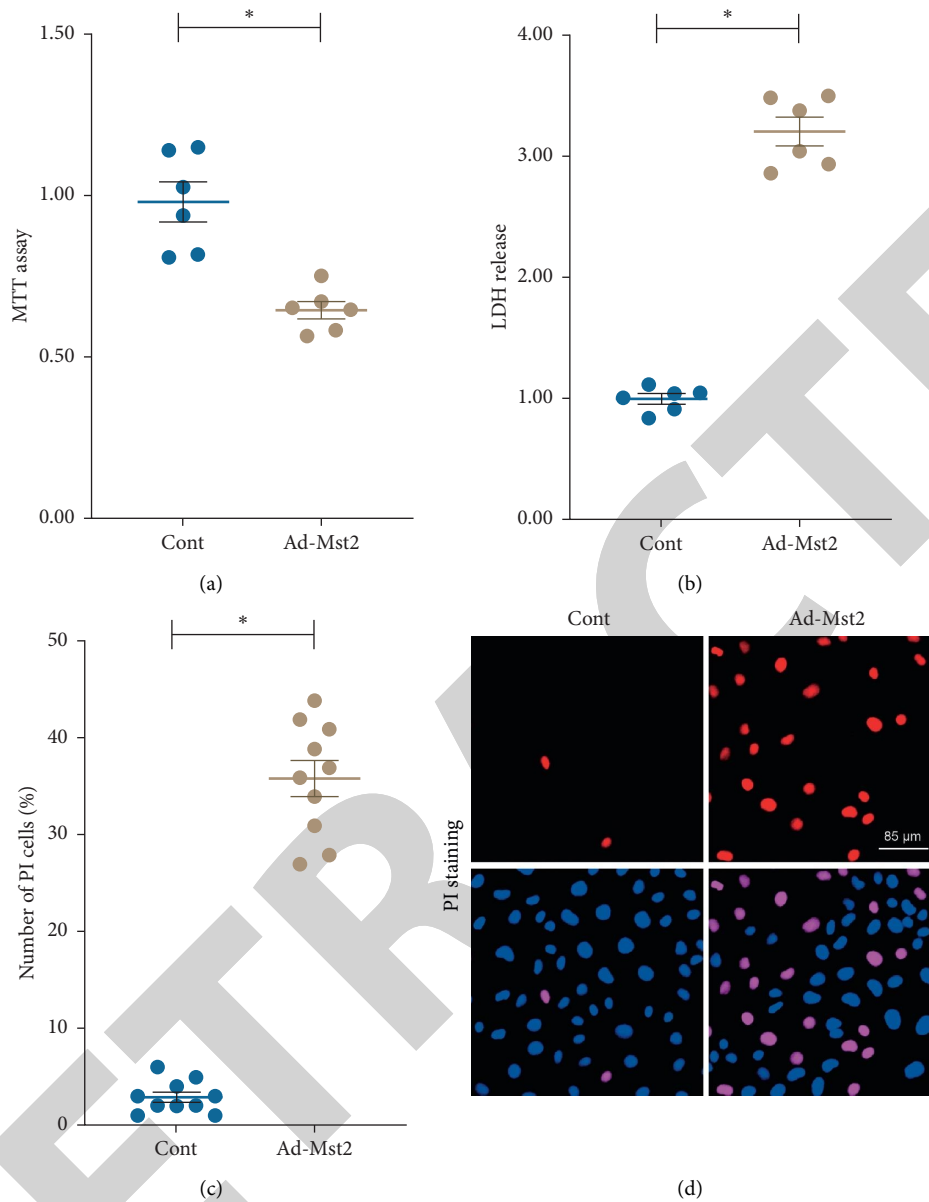


FIGURE 3: Mst2 inhibits the viability of thyroid carcinoma cells. (a) Cell viability measured using the MTT assay. (b) LDH release assay performed to detect cell death. (c)-(d) PI staining used to quantify the number of apoptotic cells. * $P < 0.05$.

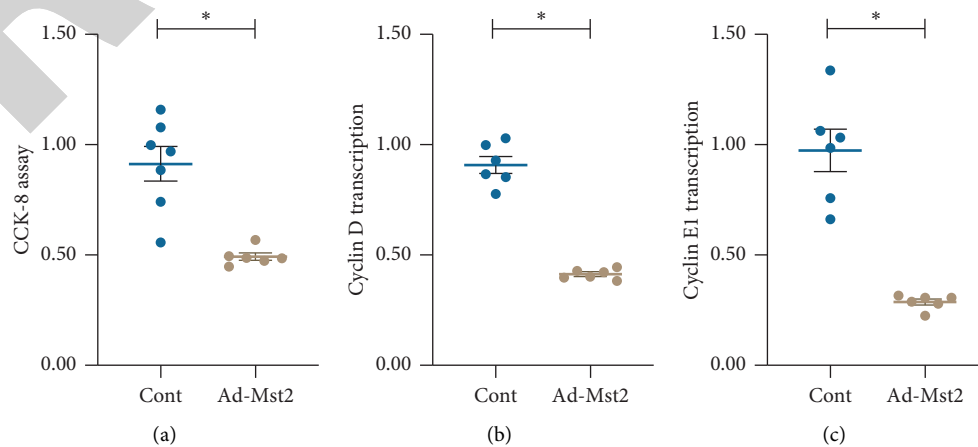


FIGURE 4: Thyroid carcinoma proliferation is impaired by Mst2. (a) Cell proliferation measured using the CCK8 assay. (b)-(c) qPCR assay used to analyze the transcription of cyclin D and cyclin E1. * $P < 0.05$.

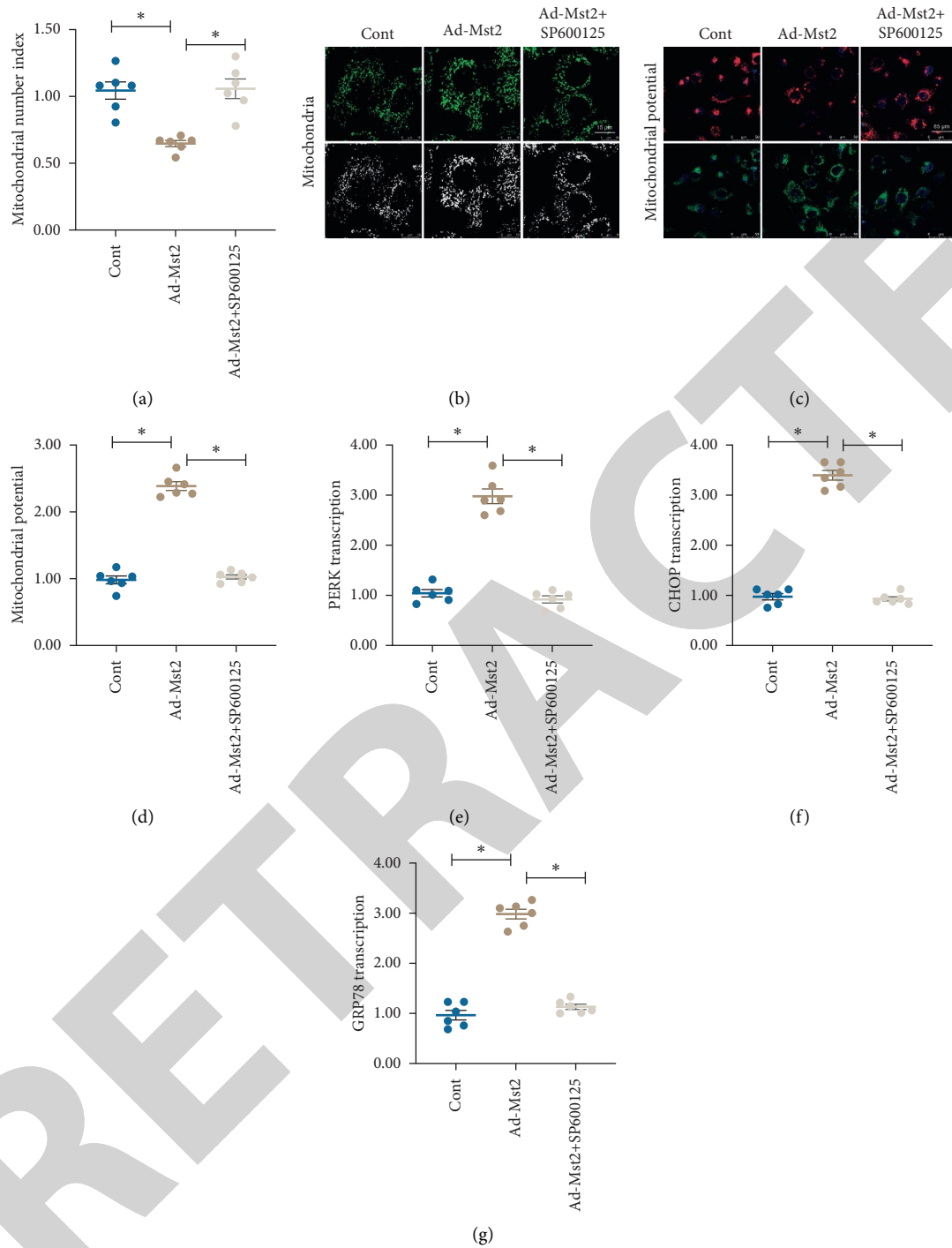


FIGURE 5: Mst2 impairs mitochondrial and ER functions through the JNK pathway. (a)-(b) Mst2-overexpressing MDA-T32 cells treated with SP600525, a JNK inhibitor. An immunofluorescence assay was used to analyze the mitochondrial number. (c)-(d) MitoSOX red staining used to study the mitochondrial ROS production in response to Ad-Mst2 transfection. (e)-(g) qPCR assay performed to analyze the transcription of CHOP, GRP78, and PERK. * $P < 0.05$.

normal tissues should be considered while designing targeted cancer therapies.

Data Availability

The data used to support the findings of this study are available from the corresponding author upon request.

Conflicts of Interest

The authors declare that there are no conflicts of interest.

References

- [1] D. Starenki, S.-K. Hong, P.-K. Wu, and J.-I. Park, "Vandetanib and cabozantinib potentiate mitochondria-targeted agents to suppress medullary thyroid carcinoma cells," *Cancer Biology & Therapy*, vol. 18, no. 7, pp. 473–483, 2017.
- [2] X. Zhang, F. Li, Y. Cui, S. Liu, and H. Sun, "Mst1 overexpression combined with yap knockdown augments thyroid carcinoma apoptosis via promoting MIEF1-related mitochondrial fission and activating the JNK pathway," *Cancer Cell International*, vol. 19, no. 1, p. 143, 2019.
- [3] L. Li, X. Wang, R. Sharvan, J. Gao, and S. Qu, "Berberine could inhibit thyroid carcinoma cells by inducing mitochondrial apoptosis, G0/G1 cell cycle arrest and suppressing migration via PI3K-AKT and MAPK signaling pathways," *Biomedicine & Pharmacotherapy*, vol. 95, pp. 1225–1231, 2017.
- [4] Y. Wang, F. Xie, D. Chen, and L. Wang, "Inhibition of mitochondrial respiration by tigecycline selectively targets thyroid carcinoma and increases chemosensitivity," *Clinical and Experimental Pharmacology and Physiology*, vol. 46, no. 10, pp. 890–897, 2019.
- [5] G. Zhao, J. Kang, G. Xu et al., "Tunicamycin promotes metastasis through upregulating endoplasmic reticulum stress induced GRP78 expression in thyroid carcinoma," *Cell & Bioscience*, vol. 10, no. 1, p. 115, 2020.
- [6] E. M. Mills, V. L. Barlow, L. Y. P. Luk, and Y.-H. Tsai, "Applying switchable Cas9 variants to in vivo gene editing for therapeutic applications," *Cell Biology and Toxicology*, vol. 36, no. 1, pp. 17–29, 2020.
- [7] X.-Y. Wu, R.-T. Fan, X.-H. Yan et al., "Endoplasmic reticulum stress protects human thyroid carcinoma cell lines against ionizing radiation-induced apoptosis," *Molecular Medicine Reports*, vol. 11, no. 3, pp. 2341–2347, 2015.
- [8] N. Abbas, F. Perbellini, and T. Thum, "Non-coding RNAs: emerging players in cardiomyocyte proliferation and cardiac regeneration," *Basic Research in Cardiology*, vol. 115, no. 5, p. 52, 2020.
- [9] L. Zhang, X. Cheng, S. Xu, J. Bao, and H. Yu, "Curcumin induces endoplasmic reticulum stress-associated apoptosis in human papillary thyroid carcinoma BCPAP cells via disruption of intracellular calcium homeostasis," *Medicine*, vol. 97, no. 24, Article ID e11095, 2018.
- [10] M. E. Mossoba, M. S. T. Mapa, M. Araujo et al., "In vitro toxicological assessment of free 3-MCPD and select 3-MCPD esters on human proximal tubule HK-2 cells," *Cell Biology and Toxicology*, vol. 36, no. 3, pp. 209–221, 2020.
- [11] H. Shi, C. Liu, H. Tan et al., "Hippo kinases Mst1 and Mst2 sense and amplify IL-2R-STAT5 signaling in regulatory T cells to establish stable regulatory activity," *Immunity*, vol. 49, no. 5, pp. 899.e6–914.e6, 2018.
- [12] R. K. Adapala, A. K. Kanugula, S. Paruchuri, W. M. Chilian, and C. K. Thodeti, "TRPV4 deletion protects heart from myocardial infarction-induced adverse remodeling via modulation of cardiac fibroblast differentiation," *Basic Research in Cardiology*, vol. 115, no. 2, p. 14, 2020.
- [13] J. Park, G. H. Kim, J. Lee et al., "MST2 silencing induces apoptosis and inhibits tumor growth for estrogen receptor alpha-positive MCF-7 breast cancer," *Toxicology and Applied Pharmacology*, vol. 408, Article ID 115257, 2020.
- [14] N. N. Nazipova and S. A. Shabalina, "Understanding off-target effects through hybridization kinetics and thermodynamics," *Cell Biology and Toxicology*, vol. 36, no. 1, pp. 11–15, 2020.
- [15] C. Meng, G. Tian, C. Xu et al., "Hippo kinases MST1 and MST2 control the differentiation of the epididymal initial segment via the MEK-ERK pathway," *Cell Death & Differentiation*, vol. 27, no. 10, pp. 2797–2809, 2020.
- [16] J. Geng, X. Sun, P. Wang et al., "Kinases Mst1 and Mst2 positively regulate phagocytic induction of reactive oxygen species and bactericidal activity," *Nature Immunology*, vol. 16, no. 11, pp. 1142–1152, 2015.
- [17] M. Liu, S. Liu, W. Tan et al., "Gaseous signalling molecule SO₂ via hippo-MST pathway to improve myocardial fibrosis of diabetic rats," *Molecular Medicine Reports*, vol. 16, no. 6, pp. 8953–8963, 2017.
- [18] A. Daiber and T. Münzel, "Interplay of the red blood cell and vascular endothelial nitric oxide synthase system to combat cardiac complications of anemia," *Basic Research in Cardiology*, vol. 115, no. 4, p. 44, 2020.
- [19] J. Bai, M. Khajavi, L. Sui et al., "Angiogenic responses in a 3D micro-engineered environment of primary endothelial cells and pericytes," *Angiogenesis*, vol. 24, no. 1, pp. 111–127, 2020.
- [20] A. R. Ednie and E. S. Bennett, "Intracellular O-linked glycosylation directly regulates cardiomyocyte L-type Ca²⁺ channel activity and excitation-contraction coupling," *Basic Research in Cardiology*, vol. 115, no. 6, p. 59, 2020.
- [21] D. Bausch, S. Fritz, L. Bolm et al., "Hedgehog signaling promotes angiogenesis directly and indirectly in pancreatic cancer," *Angiogenesis*, vol. 23, no. 3, pp. 479–492, 2020.
- [22] A. C. Fender, S. Kleeschulte, S. Stolte et al., "Thrombin receptor PAR4 drives canonical NLRP3 inflammasome signaling in the heart," *Basic Research in Cardiology*, vol. 115, no. 2, p. 10, 2020.
- [23] A. L. Bayliss, A. Sundaraman, C. Granet, and H. Mellor, "Raftlin is recruited by neuropilin-1 to the activated VEGFR2 complex to control proangiogenic signaling," *Angiogenesis*, vol. 23, no. 3, pp. 371–383, 2020.
- [24] E. Bridges, H. Sheldon, E. Kleibeuker et al., "RHOQ is induced by DLL4 and regulates angiogenesis by determining the intracellular route of the notch intracellular domain," *Angiogenesis*, vol. 23, no. 3, pp. 493–513, 2020.
- [25] A. Grogan, A. Coleman, H. Joca et al., "Deletion of obscurin immunoglobulin domains Ig58/59 leads to age-dependent cardiac remodeling and arrhythmia," *Basic Research in Cardiology*, vol. 115, no. 6, p. 60, 2020.
- [26] D. B. Buglak, E. J. Kushner, A. P. Marvin, K. L. Davis, and V. L. Bautch, "Excess centrosomes disrupt vascular lumenization and endothelial cell adherens junctions," *Angiogenesis*, vol. 23, no. 4, pp. 567–575, 2020.
- [27] S. Hamilton, R. Terentyeva, B. Martin et al., "Increased RyR2 activity is exacerbated by calcium leak-induced mitochondrial ROS," *Basic Research in Cardiology*, vol. 115, no. 4, p. 38, 2020.
- [28] J. Cao, X. Liu, Y. Yang et al., "Decylubiquinone suppresses breast cancer growth and metastasis by inhibiting angiogenesis via the ROS/p53/BAl1 signaling pathway," *Angiogenesis*, vol. 23, no. 3, pp. 325–338, 2020.

- [29] M. Heimerl, I. Sieve, M. Ricke-Hoch et al., "Neuraminidase-1 promotes heart failure after ischemia/reperfusion injury by affecting cardiomyocytes and invading monocytes/macrophages," *Basic Research in Cardiology*, vol. 115, no. 6, p. 62, 2020.
- [30] H. Jiang, D. Jia, B. Zhang et al., "Exercise improves cardiac function and glucose metabolism in mice with experimental myocardial infarction through inhibiting HDAC4 and upregulating GLUT1 expression," *Basic Research in Cardiology*, vol. 115, no. 3, p. 28, 2020.
- [31] T. L. Capasso, B. Li, H. J. Volek et al., "BMP10-mediated ALK1 signaling is continuously required for vascular development and maintenance," *Angiogenesis*, vol. 23, no. 2, pp. 203–220, 2020.
- [32] S. Khadjeh, V. Hindmarsh, F. Weber et al., "CRISPLD1: a novel conserved target in the transition to human heart failure," *Basic Research in Cardiology*, vol. 115, no. 3, p. 27, 2020.
- [33] L. Yan and X. Wu, "Exosomes produced from 3D cultures of umbilical cord mesenchymal stem cells in a hollow-fiber bioreactor show improved osteochondral regeneration activity," *Cell Biology and Toxicology*, vol. 36, no. 2, pp. 165–178, 2020.
- [34] J. Chen, F.-L. Lin, J. Y. K. Leung et al., "A drug-tunable Flt23k gene therapy for controlled intervention in retinal neovascularization," *Angiogenesis*, vol. 24, no. 1, pp. 97–110, 2020.
- [35] P. Kleinbongard, "Cardioprotection by early metoprolol-attenuation of ischemic vs. reperfusion injury?" *Basic Research in Cardiology*, vol. 115, no. 5, p. 54, 2020.
- [36] D. V. C. de Jel, F. J. M. Disch, S. Kroon, J. J. Mager, and F. J. Verdam, "Intranasal Efedine reduces epistaxis in hereditary hemorrhagic telangiectasia," *Angiogenesis*, vol. 23, no. 3, pp. 271–274, 2020.
- [37] C.-H. Tsai, Y. Lee, C.-H. Li, Y.-W. Cheng, and J.-J. Kang, "Down-regulation of aryl hydrocarbon receptor intensifies carcinogen-induced retinal lesion via SOCS3-STAT3 signaling," *Cell Biology and Toxicology*, vol. 36, no. 3, pp. 223–242, 2020.
- [38] S. K. Lahiri, A. P. Quick, B. Samson-Couterie et al., "Nuclear localization of a novel calpain-2 mediated junctophilin-2 C-terminal cleavage peptide promotes cardiomyocyte remodeling," *Basic Research in Cardiology*, vol. 115, no. 4, p. 49, 2020.
- [39] R. A. Deckelbaum, I. B. Lobov, E. Cheung et al., "The potassium channel Kcne3 is a VEGFA-inducible gene selectively expressed by vascular endothelial tip cells," *Angiogenesis*, vol. 23, no. 2, pp. 179–192, 2020.
- [40] K.-Y. So, B.-H. Park, and S.-H. Oh, "Cytoplasmic sirtuin 6 translocation mediated by p62 polyubiquitination plays a critical role in cadmium-induced kidney toxicity," *Cell Biology and Toxicology*, vol. 37, no. 2, pp. 193–207, 2020.
- [41] O. Bakhta, A. Pascaud, X. Dieu et al., "Tryptophane-kynurenine pathway in the remote ischemic conditioning mechanism," *Basic Research in Cardiology*, vol. 115, no. 2, p. 13, 2020.
- [42] L. C. Dieterich, C. Tacconi, F. Menzi et al., "Lymphatic MAFB regulates vascular patterning during developmental and pathological lymphangiogenesis," *Angiogenesis*, vol. 23, no. 3, pp. 411–423, 2020.
- [43] B. Behrouzi, J. J. Weyers, X. Qi et al., "Action of iron chelator on intramyocardial hemorrhage and cardiac remodeling following acute myocardial infarction," *Basic Research in Cardiology*, vol. 115, no. 3, p. 24, 2020.
- [44] M. M. Bekhite, A. González Delgado, F. Menz et al., "Longitudinal metabolic profiling of cardiomyocytes derived from human-induced pluripotent stem cells," *Basic Research in Cardiology*, vol. 115, no. 4, p. 37, 2020.
- [45] S. Díaz del Moral, S. Barrena, R. Muñoz-Chápuli, and R. Carmona, "Embryonic circulating endothelial progenitor cells," *Angiogenesis*, vol. 23, no. 4, pp. 531–541, 2020.
- [46] F. Cao, M. L. Maguire, D. J. McAndrew et al., "Overexpression of mitochondrial creatine kinase preserves cardiac energetics without ameliorating murine chronic heart failure," *Basic Research in Cardiology*, vol. 115, no. 2, p. 12, 2020.
- [47] J. Cui, Z. Zhou, H. Yang et al., "MST1 suppresses pancreatic cancer progression via ROS-induced pyroptosis," *Molecular Cancer Research*, vol. 17, no. 6, pp. 1316–1325, 2019.
- [48] J. L. Chiang, P. Shukla, K. Pagidas et al., "Mitochondria in ovarian aging and reproductive longevity," *Ageing Research Reviews*, vol. 63, Article ID 101168, 2020.
- [49] D. Zhou, C. Conrad, F. Xia et al., "Mst1 and Mst2 maintain hepatocyte quiescence and suppress hepatocellular carcinoma development through inactivation of the Yap1 oncogene," *Cancer Cell*, vol. 16, no. 5, pp. 425–438, 2009.
- [50] M. di Somma, M. Vliora, E. Grillo et al., "Role of VEGFs in metabolic disorders," *Angiogenesis*, vol. 23, no. 2, pp. 119–130, 2020.
- [51] X. F. Liu, Q. Han, M. Yang, X. Y. Lin, and Y. C. Han, "MST1 inhibits cell proliferation and invasion of non-small-cell lung cancer by regulating YAP phosphorylation and hippo pathway," *International Journal of Clinical and Experimental Pathology*, vol. 11, pp. 2613–2620, 2018.
- [52] Y. Li, P. Liang, B. Jiang et al., "CARD9 promotes autophagy in cardiomyocytes in myocardial ischemia/reperfusion injury via interacting with rubicon directly," *Basic Research in Cardiology*, vol. 115, no. 3, p. 29, 2020.
- [53] X. Jin, L. Zhu, S. Xiao et al., "MST1 inhibits the progression of breast cancer by regulating the hippo signaling pathway and may serve as a prognostic biomarker," *Molecular Medicine Reports*, vol. 23, no. 5, 2021.
- [54] D. Zhou, Y. Zhang, H. Wu et al., "Mst1 and Mst2 protein kinases restrain intestinal stem cell proliferation and colonic tumorigenesis by inhibition of yes-associated protein (yap) overabundance," *Proceedings of the National Academy of Sciences*, vol. 108, no. 49, pp. E1312–E1320, 2011.
- [55] S. Shanmughapriya, D. Langford, and K. Natarajaseenivasan, "Inter and intracellular mitochondrial trafficking in health and disease," *Ageing Research Reviews*, vol. 62, Article ID 101128, 2020.
- [56] M. R. Detter, R. Shenkar, C. R. Benavides et al., "Novel murine models of cerebral cavernous malformations," *Angiogenesis*, vol. 23, no. 4, pp. 651–666, 2020.
- [57] I. Cuijpers, S. J. Simmonds, M. van Bilsen et al., "Microvascular and lymphatic dysfunction in HFpEF and its associated comorbidities," *Basic Research in Cardiology*, vol. 115, no. 4, p. 39, 2020.
- [58] Z. D. Zhou and E. K. Tan, "Oxidized nicotinamide adenine dinucleotide-dependent mitochondrial deacetylase sirtuin-3 as a potential therapeutic target of parkinson's disease," *Ageing Research Reviews*, vol. 62, Article ID 101107, 2020.
- [59] S. Yao and W. Yan, "Overexpression of Mst1 reduces gastric cancer cell viability by repressing the AMPK-Sirt3 pathway and activating mitochondrial fission," *OncoTargets and Therapy*, vol. 11, pp. 8465–8479, 2018.
- [60] H. Ouyang, E. Zhou, and H. Wang, "Mst1-hippo pathway triggers breast cancer apoptosis via inducing mitochondrial fragmentation in a manner dependent on JNK-Drp1 axis," *OncoTargets and Therapy*, vol. 12, pp. 1147–1159, 2019.

Retraction

Retracted: Identification of the Novel Methylated Genes' Signature to Predict Prognosis in INRG High-Risk Neuroblastomas

Journal of Osteoporosis

Received 30 November 2022; Accepted 30 November 2022; Published 28 December 2022

Copyright © 2022 Journal of Oncology. This is an open access article distributed under the Creative Commons Attribution License, which permits unrestricted use, distribution, and reproduction in any medium, provided the original work is properly cited.

Journal of Oncology has retracted the article titled “Identification of the Novel Methylated Genes' Signature to Predict Prognosis in INRG High-Risk Neuroblastomas” [1] due to concerns that the peer review process has been compromised.

Following an investigation conducted by the Hindawi Research Integrity team [2], significant concerns were identified with the peer reviewers assigned to this article; the investigation has concluded that the peer review process was compromised. We therefore can no longer trust the peer review process, and the article is being retracted with the agreement of the Chief Editor.

The authors agree to the retraction.

References

- [1] Z. Liu and C. Li, “Identification of the Novel Methylated Genes' Signature to Predict Prognosis in INRG High-Risk Neuroblastomas,” *Journal of Oncology*, vol. 2021, Article ID 1615201, 10 pages, 2021.
- [2] L. Ferguson, “Advancing Research Integrity Collaboratively and with Vigour,” 2022, <https://www.hindawi.com/post/advancing-research-integrity-collaboratively-and-vigour/>.

Research Article

Identification of the Novel Methylated Genes' Signature to Predict Prognosis in INRG High-Risk Neuroblastomas

Zhichao Liu and Changchun Li 

Department of Surgical Oncology, Children's Hospital of Chongqing Medical University, National Clinical Research Center for Child Health and Disorders, Ministry of Education Key Laboratory of Child Development and Disorders; Chongqing Key Laboratory of Pediatrics, Children's Hospital of Chongqing Medical University, 136 Zhongshan 2nd Road, Yuzhong District, Chongqing 400014, China

Correspondence should be addressed to Changchun Li; lichangchun@hospital.cqmu.edu.cn

Received 12 July 2021; Revised 20 August 2021; Accepted 30 August 2021; Published 14 September 2021

Academic Editor: Yun-dai Chen

Copyright © 2021 Zhichao Liu and Changchun Li. This is an open access article distributed under the Creative Commons Attribution License, which permits unrestricted use, distribution, and reproduction in any medium, provided the original work is properly cited.

Background. Neuroblastomas are the most frequent extracranial pediatric solid tumors. The prognosis of children with high-risk neuroblastomas has remained poor in the past decade. A powerful signature is required to identify factors associated with prognosis and improved treatment selection. Here, we identified a strong methylation signature that favored the earlier diagnosis of neuroblastoma in patients. **Methods.** Gene methylation (GM) data of neuroblastoma patients from the Therapeutically Applicable Research to Generate Effective Treatments (TARGET) were analyzed using a multivariate Cox regression analysis (MCRA) and univariate Cox proportional hazards regression analysis (UCPHRA). **Results.** The methylated genes' signature consisting of eight genes (NBEA, DDX28, TMED8, LOC151174, EFNB2, GHRHR, MIMT1, and SLC29A3) was selected. The signature divided patients into low- and high-risk categories, with statistically significant survival rates (median survival time: 25.08 vs. >128.80 months, log-rank test, $P < 0.001$) in the training group, and the validation of the signature's risk stratification ability was carried out in the test group (log-rank test, $P < 0.01$, median survival time: 30.48 vs. >120.36 months). The methylated genes' signature was found to be an independent predictive factor for neuroblastoma by MCRA. Functional enrichment analysis suggested that these methylated genes were related to butanoate metabolism, beta-alanine metabolism, and glutamate metabolism, all playing different significant roles in the process of energy metabolism in neuroblastomas. **Conclusions.** The set of eight methylated genes could be used as a new predictive and prognostic signature for patients with INRG high-risk neuroblastomas, thus assisting in treatment, drug development, and predicting survival.

1. Introduction

Neuroblastomas are peripheral sympathetic nervous system embryonic tumors that arise from embryonic cells that make up the basic neural crest. Extracranial solid tumors are the most common neuroblastomas in children and responsible for up to 15% of cancer-related deaths [1–3]. The clinical course of neuroblastomas constitutes the progression of a complex heterogeneous disease. Localized neuroblastomas (stages L1 and L2), metastatic neuroblastomas (M), and metastatic neuroblastomas with specific characteristics in children younger than 18 months (MS) are the three types of tumors classified by the International Neuroblastoma Risk

Group (INRG) [4, 5]. These risk markers (histology, age, MYCN, INRG stage, ploidy status, and 11q aberration) are used to divide patients into four pretreatment risk groups. There are three levels of difficulty: low, moderate, and high [6]. The low and intermediate groups show greater than 90% five-year survival rates, while the survival of the high-risk group remains poor at approximately 40%. Although advanced treatment consisting of surgery, chemotherapy, radiotherapy, and immunotherapy can be used in the course of treatment, all these have a poor survival rate for high-risk neuroblastomas [7]. This low prognosis needs the development of novel targeted medicines to improve the survival rate of high-risk neuroblastoma patients.

DNA methylation of CpG dinucleotides at gene promoter regions is a major regulatory mechanism involved in cellular processes that does not alter the DNA sequence [8]. DNA methylation reveals the pathogenesis and clinical behavior of neuroblastomas [9]. The most described DNA methylation alterations in neuroblastomas are CASP8 and RASSF1A [10, 11], and both are correlated with risk factors, such as age at diagnosis, MYCN amplification, and tumor stage [12–15]. Additionally, DNA hypomethylation of genes (CCND1, SPRR3, BTC, EGF, and FGF6) affects biological functions and pathogenesis in neuroblastomas [16]. In metastatic neuroblastomas, the hypermethylation status of TDGF1 and RB1 is associated with shorter survival, and genome-wide methylation profiling discovered novel methylated genes (PCDHGA4, TERT, DLX6-AS1, and DLX5) [17, 18]. However, epigenetic biomarkers for neuroblastomas are still very low. In particular, there are fewer methylation biomarkers associated with high-risk neuroblastoma patients.

In the current report, we identified significant and independent methylation prognostic biomarkers in INRG high-risk neuroblastomas from the TARGET database using phrase machine learning methods. The biomarkers could be used to design new therapy regimens for patients with high-risk neuroblastomas, potentially improving existing survival rates.

2. Materials and Methods

2.1. Retrieval of DNA Methylation Data for Analysis. Illumina HumanMethylation450 (Illumina Inc., California, USA) platform was used to evaluate DNA methylation data. There were 482,421 CpG sites on the methylation arrays throughout the genome [19], and each gene's overall beta value was represented by probe-level data. The TARGET data portal provided us with level 3 methylation data. We received 130 samples from the TARGET database, which contained DNA methylation data as well as clinical data such as gender, age, MYCN status, and INSS stage. All neuroblastoma samples are typically divided into two groups: training (86 cases) and testing (44 cases).

2.2. Construction of a Methylated Gene Signature in the Training Dataset. Hu et al. reported the best methods to construct signatures, and we used this approach for our study [20]. To begin, we used a UCPHR analysis to see if there was a link between survival rates and gene methylation in the training dataset [21]. The random survival forest-variable hunting (RSFVH) algorithm was then used to filter methylation genes, with ten being ruled out [22, 23]. For screening of predictive prognostic methylation genes, MCR analysis was utilized for constructing a model that could estimate the prognosis risk in accordance with the following expression:

$$\text{risk score (RS)} = \sum_{i=1}^N \text{Meth}_i * \text{Coef}_i \quad (1)$$

Here, the methylated genes of signature are represented by N , the value of methylation of the signature genes is represented by Meth_i , while single CRO is denoted by Coef_i . The multinode weighted sum of risk scores is known as the risk score (RS).

2.3. Statistical Analysis. A risk model was built using the aforementioned methylation gene signature. As a cutoff number, the median risk score was used for dividing the training and test patients into high-risk and low-risk groups [24]. Next, the ROC analysis and Kaplan–Meier survival (KMS) analysis were used to confirm the methylation gene signature's effective prognostic abilities in the test dataset. MCR analysis was used to determine the signature's independence in survival prediction, and a significant P value was less than 0.05. All analyses used the R program (version 3.5.1). Downloading of the randomForestSRC and pROC survival was carried out from Bioconductor (<https://bioconductor.org>).

2.4. Functional Analysis of the Signature of Methylated Genes. The DAVID bioinformatics tool was employed for predicting the activities of the signature of methylation genes using gene ontology (GO) analysis, which covered molecular functions, cellular components, and biological processes, as well as KEGG pathway enrichment studies (<https://david.ncifcrf.gov/>, version 6.8). The value of $P < 0.05$ is considered significant for GO and KEGG pathways.

3. Results

3.1. Clinical Characteristics' Analysis of TARGET Data. All of the expression data used in this investigation came from patients with neuroblastomas, both clinically and pathologically. We conducted a statistical analysis of the clinical data (gender, age, MYCN status, and INSS stage) in the test group and training group. The results revealed high-risk patients had only occupied no more than 5% <18 months and included 97.7% INSS stage 4 in the test group and training group. The details of clinical/pathological features can be found in Table 1. After that, the 130 patients were randomly separated into two groups (test group, $n = 44$; training group, $n = 86$) to examine if the methylation genes revealed in neuroblastoma patients had any prognostic significance. Figure 1 shows the selection process for the methylated genes' signature.

3.2. Construction of the Survival Methylated Genes' Signature. The training group ($n = 86$) with all clinical data was used to investigate the relationship between overall survival and the presence of methylated genes. We first performed a univariate CPHR analysis of the methylation genes' profiling data with survival status and survival time as dependent factors. We discovered 339 methylation genes that were significantly linked to the patient's overall survival (P value <0.05, Figure 2). The 339 genes were then analyzed using the random forest technique to evaluate the signature of

TABLE 1: Summary of patient characteristics and demographics.

Characteristic	Number of cases (%) in the training set	Number of cases (%) in the testing set
<i>Gender</i>		
Male	47 (54.7%)	29 (82.6%)
Female	39 (45.3%)	15 (17.4%)
<i>Age</i>		
<18 months	2 (2.3%)	2 (2.3%)
≥18 months	86 (97.7%)	42 (97.7%)
<i>MYCN status</i>		
Amplified	31 (36.0%)	17 (38.6%)
Not amplified	54 (62.8%)	27 (61.4%)
NA	1 (1.2%)	
<i>INSS stage</i>		
1	0 (0.0%)	0 (0.0%)
2	0 (0.0%)	0 (0.0%)
3	2 (2.3%)	0 (0.0%)
4	84 (97.7%)	43 (97.7%)
4s	0 (0.0%)	1 (2.3%)
<i>INRG</i>		
Low risk	0 (0.0%)	0 (0.0%)
Intermediate risk	0 (0.0%)	0 (0.0%)
High risk	89 (100%)	44 (100%)
<i>Vital status</i>		
Living	35 (40.7%)	20 (55.5%)
Dead	51 (59.3%)	24 (54.5%)

methylation genes. Based on their permutation importance score (PFI) using the RSFVH method, the analysis found ten genes that were substantially linked with patient overall survival (Figure S1).

We utilized a CMR analysis (Table S1) to develop an eight-methylation gene set model (NBEA, DDX28, TMED8, LOC151174, EFNB2, GHRHR, MIMT1, and SLC29A3) for assessing the risk to survival for screening the most powerful, predictive, prognostic methylated genes. The risk scores (Table S2) of the combination which composed NBEA, DDX28, TMED8, LOC151174, EFNB2, GHRHR, MIMT1, and SLC29A3 were determined as follows:

$$\begin{aligned}
 RS = & (-3.65 \times \text{meth}_{\text{NBEA}}) \\
 & + (-22.66 \times \text{meth}_{\text{DDX28}}) \\
 & + (20.60 \times \text{meth}_{\text{TMED8}}) \\
 & + (-6.13 \times \text{meth}_{\text{LOC151174}}) \\
 & + (8.48 \times \text{meth}_{\text{EFNB2}}) \\
 & + (0.01 \times \text{meth}_{\text{GHRHR}}) \\
 & + (-4.11 \times \text{meth}_{\text{MIMT1}}) \\
 & + (20.43 \times \text{meth}_{\text{SLC29A3}}).
 \end{aligned} \tag{2}$$

Here, risk score is denoted by RS, while the values of methylation are denoted by meth.

3.3. Determining the Survival Power of the Methylated Genes' Signature in the Training and Test Dataset. For each patient, the analysis gave a risk score for the identified methylation genes' signature. Using the median risk score, we divided the training group into two groups: low risk ($n=43$) and high risk ($n=43$). Using the Kaplan–Meier survival (KMS)

analysis, it was observed that the high-risk group had considerably lower survival rates than the low-risk group (median survival time: 25.08 months vs. >128.80 months, log-rank test, $P < 0.001$; Figure 3(a)). The high-risk group had a 5-year survival rate of fewer than 20%, while the low-risk group had a rate of more than 60%. The risk scores based on the methylation genes' signature of the test group patients were calculated using the same prognostic risk score methodology, confirming the predictive value of the signature. Similarly, the two risk groups in the test dataset were displayed using Kaplan–Meier curves (Figure 3(b)). The high-risk group in the study had a significantly lower median survival time than the low-risk group (median survival time: 30.48 months vs. >120.36 months, log-rank test, $P < 0.01$). The high-risk group had a survival rate of less than 30%, whereas the low-risk group had a survival rate of more than 50%.

3.4. The Survival Prediction Power of the Methylated Gene Signature in the Test and Training Groups. ROC analysis was used to assess the methylation gene signature's predictive capacity, with the higher area under the ROC curve indicating a better model for neuroblastoma patients' expected survival. The eight methylated gene signatures had a strong prediction ability in the training group ($\text{AUC}_{\text{Signature}} = 0.87$, Figure 3(c)), indicating that the methylated gene signature in the present study was a highly accurate novel survival biomarker. A similar highly accurate result was also observed in the test group ($\text{AUC}_{\text{Signature}} = 0.71$, Figure 3(d)). The DNA methylation level of each gene in the training dataset has been compared with a t -test (Table S3). The distribution of the DNA methylation level of each of the eight genes in the total group ($N=130$) was analyzed (Figure 4). Most genes except GHRHR showed significant

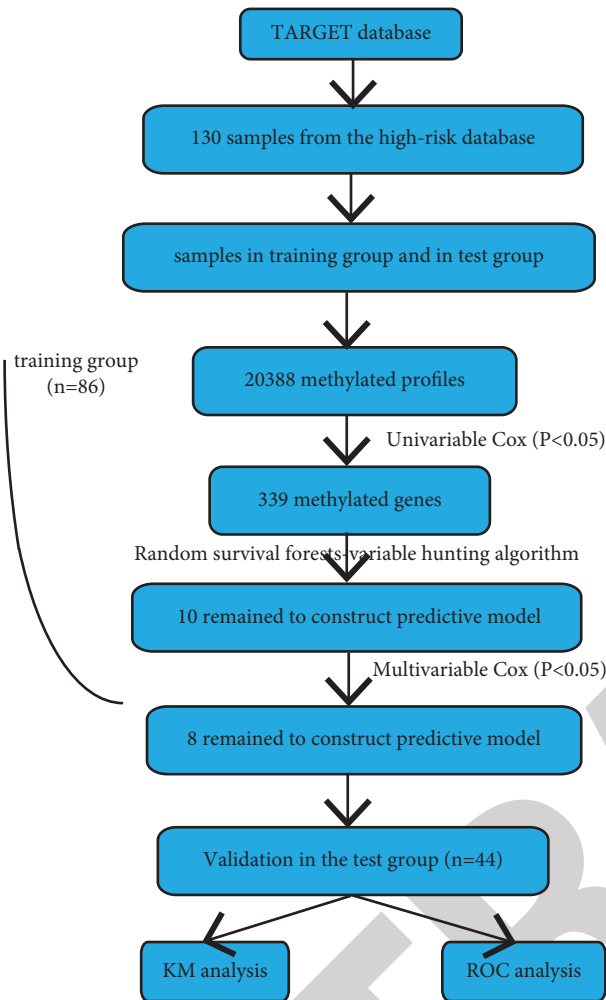


FIGURE 1: The research flowchart. The sequence of analyses for developing the RC model and validating the signature's ability to predict prognostic outcomes.

differences in methylation levels between the low- and high-risk groups.

3.5. The Selected Eight Methylated Genes' Signature Is an Independent Prognostic Factor. We used a MCR analysis, which included the risk scores based on the signature as well as various clinical characteristics (such as gender, age, MYCN status, and INSS stage). This analysis was utilized to show the prognostic efficacy of the methylated genes' signature risk score for overall survival prediction, which was an independent prognostic factor across all datasets (high-risk dataset vs. low-risk dataset, HR = 2.13, 95% CI: 1.70–2.66, $P < 0.001$, $n = 194$, Table 2).

3.6. Functional Analysis of the Methylated Genes' Signature. GO and KEGG analyses were employed for investigating these DNA methylation genes' potential involvement in biological processes associated with neuroblastoma development (Figure 5, Table S4). Results showed that eight methylated genes were involved in butanoate metabolism,

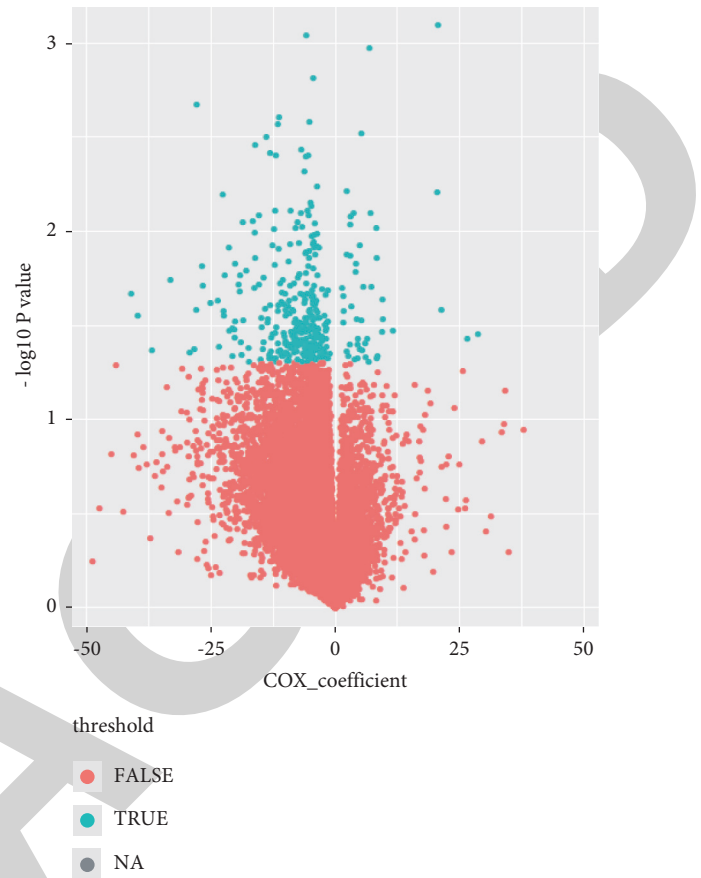


FIGURE 2: Identification of the methylated genes' signature in the training dataset. UCPHRA of the gene methylation profiling data in the training dataset used to predict the methylated genes' signature in the test and training datasets.

beta-alanine metabolism, propanoate metabolism, glutamate metabolism, and tryptophan metabolism, which are all associated with energy metabolism. It was reported that neuroblastoma cells were strictly dependent on glucose metabolism, which has been discovered to be a very frequent feature among tumors that are otherwise biologically diverse. In addition, glycolysis intermediates are key precursors for cell growth in addition to generating ATP [25]. As a result, the modulation of these genes by methylation played various important roles in the process of energy metabolism in neuroblastomas.

4. Discussion

Neuroblastomas are the most prevalent extracranial pediatric solid tumors responsible for a disproportionate amount of pediatric cancer mortality. They arise in the developing sympathetic nervous system [26, 27]. Although there have been advances in therapies for patients, some of which include myeloablative chemotherapy and intensive induction chemotherapy, the overall outcome for high-risk neuroblastoma patients is still unacceptably poor [28]. Three recent studies focused on prognosis in neuroblastoma. An 18-gene signature predicted the clinical outcome in stage 4

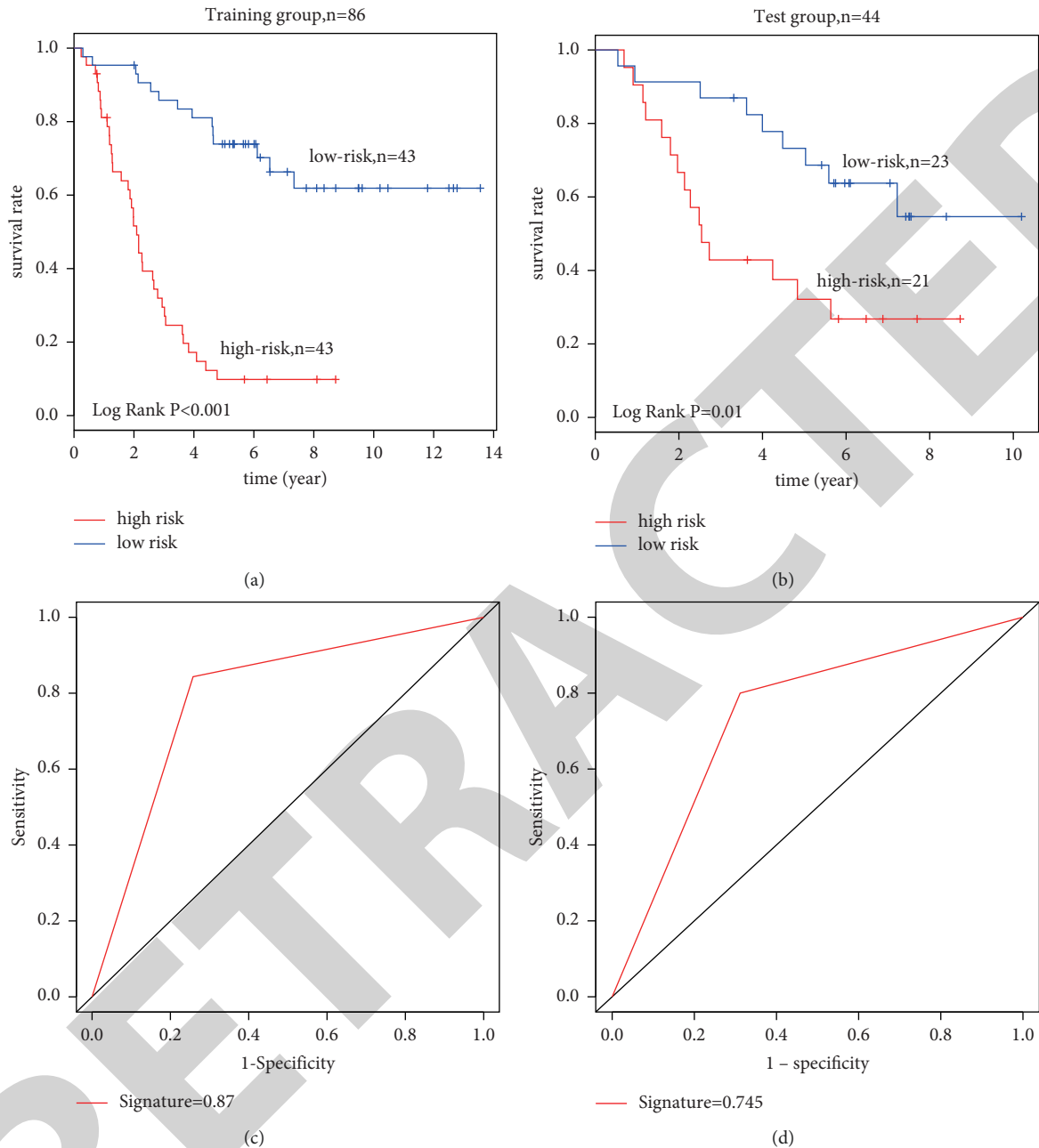


FIGURE 3: Patients with neuroblastoma have a methylated gene signature that predicts overall survival. (a) KMS curves were used for dividing the patients into high- and low-risk groups. Log-rank tests were used to calculate P values. (b) Results of receiver operating characteristic (ROC) analysis.

neuroblastoma [29] and found ERCC6L, AHCY, STK33, and NCAN as a set of genes that could be used to predict prognosis in neuroblastoma patients [30]. MELK was a novel therapeutic target for high-risk neuroblastomas [31]. However, methylation gene signatures and their relationship to neuroblastoma survival have been studied infrequently, particularly in high-risk individuals. We employed a combination of phrase machine learning methods and statistical methodologies to establish a methylation genes' signature composed of ten genes in our investigation. They were found to be relevant to the survival of patients with

neuroblastomas. Using gender, age, MYCN status, and INSS stage as covariables, the independence of the chosen signature in survival prediction of neuroblastoma patients was evaluated using an MCR analysis. The signature-based risk scores of patients were found to be independently associated with overall survival. As a result, we found that the methylated genes' signature predicted independently in patient overall survival. These findings showed that the predictive value of the methylation genes' profile for predicting survival of neuroblastoma patients had no response for other clinical factors.

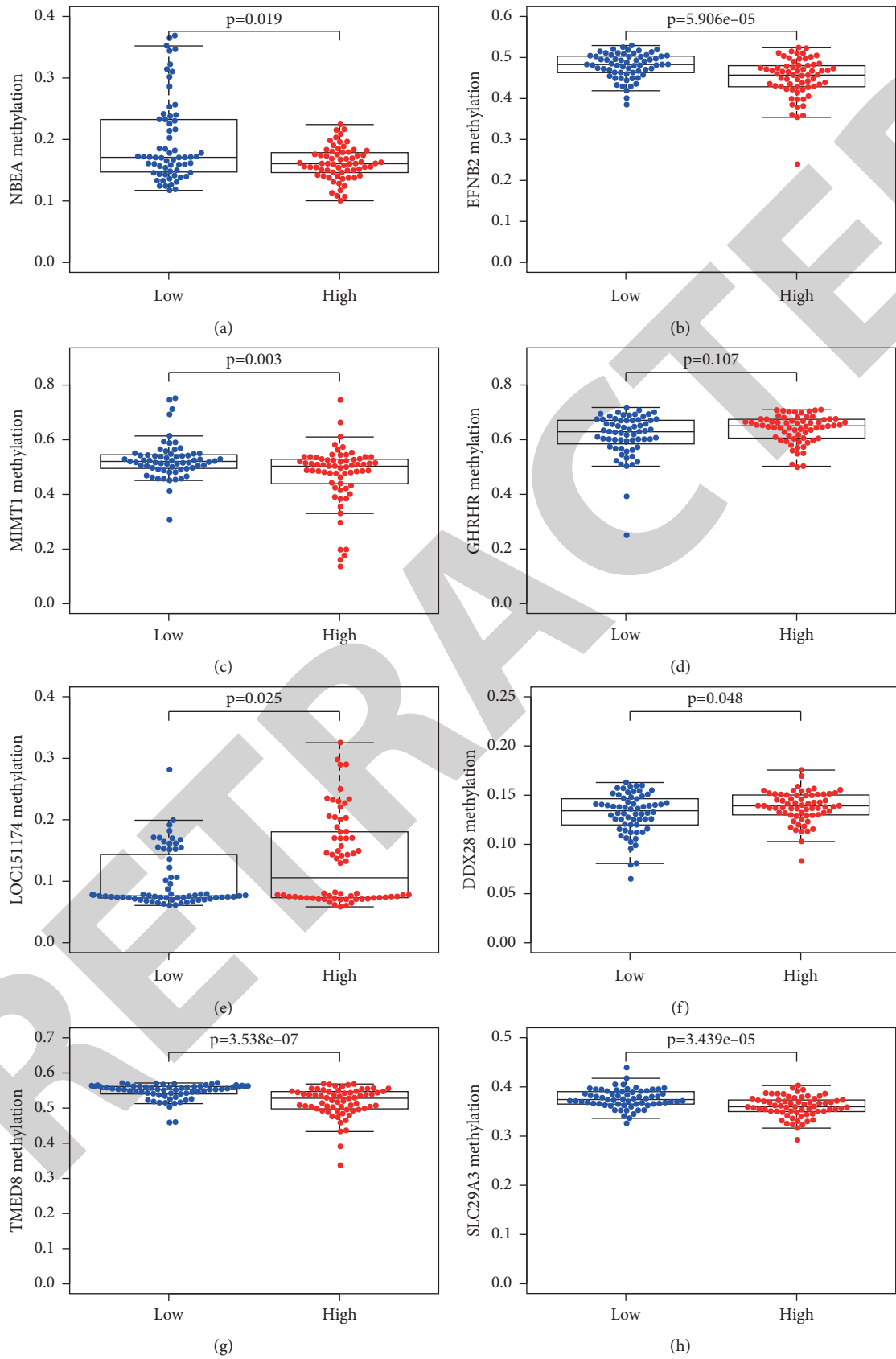


FIGURE 4: The distribution of the DNA methylation level of each of the eight genes between high- and low-risk groups in the total group (N = 130).

TABLE 2: Univariable and multivariable Cox regression analyses of the association between the eight methylated genes' signature and the survival of neuroblastoma patients in the total group ($n = 130$).

Variables	HR	95% CI of HR		P	
		Lower	Upper		
<i>Univariable analysis</i>					
Gender	Male vs. female	1.17	0.73	1.87	0.52
Age	>18 months vs. ≤18	0.97	0.90	1.06	0.51
MYCN status	Amplified vs. non	1.24	0.77	1.98	0.38
Methylated genes' signature	High risk vs. low risk	2.02	1.65	2.47	≤0.001
<i>Multivariable analysis</i>					
Gender	Male vs. female	0.89	0.55	1.44	0.64
Age	>18 months vs. ≤18	1.01	0.93	1.11	0.79
MYCN status	Amplified vs. non	0.77	0.46	1.30	0.33
Methylated genes' signature	High risk vs. low risk	2.13	1.70	2.66	≤0.001

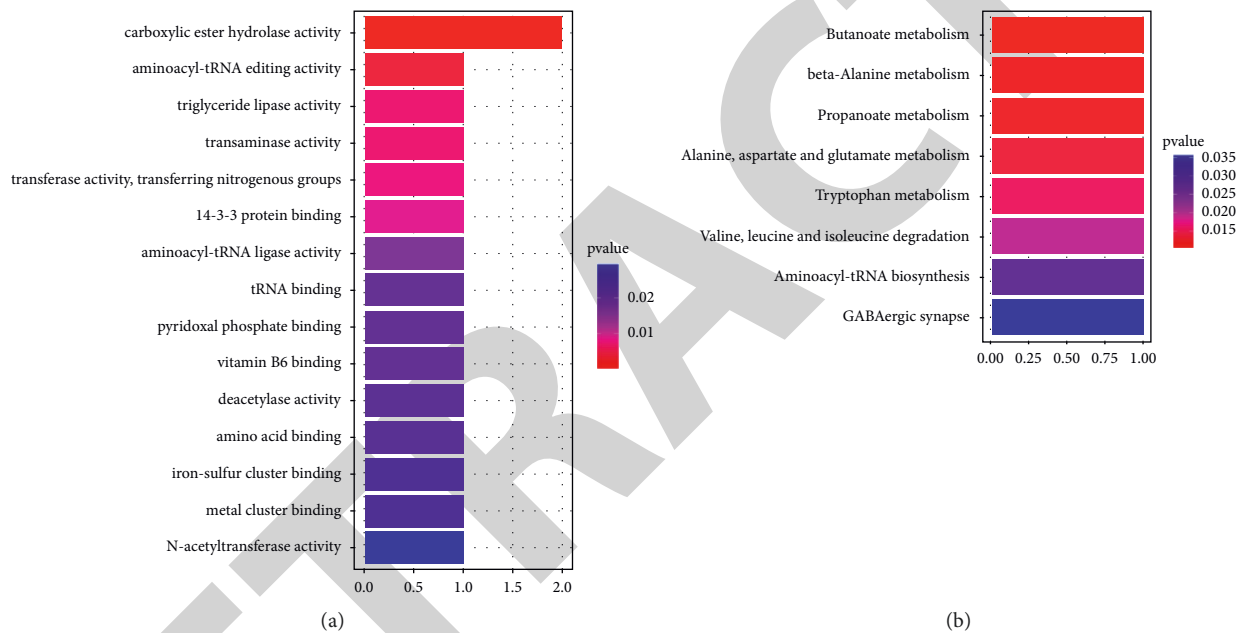


FIGURE 5: Functional enrichment of the eight methylated genes' signature. (a) Gene ontology (GO) plot displaying gene ratios for the eight methylated genes' signature. (b) KEGG analysis of the 8 methylated genes' signature.

After a variety of analyses, eight significant gene methylation events were identified. EFNB is a member of the Eph family receptor tyrosine kinases, and reports have shown that EFNB2 is regulated and can perform prognostic roles in neuroblastomas. For example, high-level expression of transcripts encoding EPHB6 receptors (in association with their ligands EFNB2 and EFNB3) was predictive of neuroblastoma [32], and EFNB2 was induced by WNT signaling. As a result, EFNB is likely to have a role in neuronal development and neuroblastoma cell fate decisions [33]. Previous studies also suggested that there are many potential associations between diseases and EFNB2. One such example was demonstrated when it was found that microRNA-137 inhibited EFNB2 expression affected by a genetic variant in schizophrenia patients [34]. Starting in midgestation, NBEA encoded a member of a broad, diversified set of A-kinase anchor proteins that was substantially expressed in the mouse brain [35, 36], and this

expression affected postsynaptic neurotransmitter receptor trafficking to the cell surface [36, 37]. Studies have demonstrated that NBEA not only was a predicted signature [38–40] but also played an important regulatory role in neurodevelopment [41, 42]. NBEA has been shown to act as a gene signature to predict the prognosis of gastric cancer [43] and as a transcriptional regulator in the nucleus, where it interacts with NOTCH1. This association was found particularly important for pathogenesis as NOTCH signaling is required for brain development [44]. GHRHR is the growth hormone-releasing hormone receptor gene. Over-expression of GHRHR has been shown to have an oncogenic role associated with several types of cancers, including neuroblastoma [45]. SLC29A3 encodes a nucleoside transporter which plays a significant role in the cellular uptake of nucleosides and nucleobases. It was previously reported that many diseases were related to RAD51AP1 expression, including autoimmune diseases [46], H syndrome [47],

insulin-dependent diabetes [48], pigmentary hypertrichosis, autoimmune insulin-dependent diabetes mellitus [49], and sclerosing bone dysplasias [50]. Meanwhile, MIMT1 is an MER1 repeat-containing imprinted transcript, which can undergo hypermethylation in the placenta of intrauterine growth-restricted fetuses in cattle [51], and truncation of exons 3 and 4 of the MIMT1 gene caused intrauterine growth restriction [52]. Furthermore, the transmembrane p24 trafficking protein family member, DDX28, was used to investigate pediatric-onset genetic disorders by digital PCR [53]. However, the biological roles of the two genes (TMED and LOC151174) in cancer are yet unknown, and this has to be researched further in future research. These previous studies demonstrate that the signature outlined in the current work can predict prognostic outcomes and inform clinical treatment.

In terms of neuroblastomas, there are a few drawbacks to this study. Most importantly, more studies into the specific mechanism of gene methylation in neuroblastomas are needed. Furthermore, the methylation genes' signature is yet to be tested in clinical trials. Even after these limitations, the continuous and significant correlation of our methylation genes' signature with overall survival in two separate groups suggested that it could be a useful and powerful predictive signature for neuroblastomas.

The use of phrase machine learning has allowed us to identify a methylated genes' signature which provided more clinically significant prediction accuracy.

Data Availability

All the data used to support the findings of this study are included within the article and are available at The Cancer Genome Atlas (TCGA) database.

Conflicts of Interest

The authors declare no conflicts of interest.

Authors' Contributions

Zhichao Liu and Changchun Li collected the samples' data and obtained the clinical information. Zhichao Liu performed data analysis and designed the study. Changchun Li integrated the results and drafted the manuscript.

Supplementary Materials

Figure S1: random survival forest-variable hunting analysis reveals the error rate for the data as a function of trees. Table S1: methylated genes of univariate Cox regression analysis ($P < 0.05$) in the training set ($n = 86$). Table S2: multivariate Cox regression analysis of the 8 methylated genes and survival of neuroblastomas patients in the training group. Table S3: the signature risk score composed of 8 combinations in the training and test dataset. Table S4: different DNA methylation genes between the high- and low-risk groups. Table S5: functional enrichment of the 8 methylated genes' signature. (*Supplementary Materials*)

References

- [1] S. Barrena Delfa, P. Rubio Aparicio, and L. Martinez Martinez, "[Neuroblastoma]," *Cirugia Pediatrica*, vol. 31, no. 2, pp. 57–65, 2018.
- [2] S. Mahapatra and K. B. Challagundla, *Cancer, Neuroblastoma*, StatPearls, Treasure Island, FL, USA, 2018.
- [3] K. K. Matthay, J. M. Maris, G. Schleiermacher et al., "Neuroblastoma," *Nature Reviews Disease Primers*, vol. 2, no. 1, Article ID 16078, 2016.
- [4] S. L. Cohn, A. D. J. Pearson, W. B. London et al., "The international neuroblastoma risk group (INRG) classification system: an INRG task force report," *Journal of Clinical Oncology*, vol. 27, no. 2, pp. 289–297, 2009.
- [5] T. Monclair, G. M. Brodeur, P. F. Ambros et al., "The international neuroblastoma risk group (INRG) staging system: an INRG task force report," *Journal of Clinical Oncology*, vol. 27, no. 2, pp. 298–303, 2009.
- [6] K. J. van Arendonk and D. H. Chung, "Neuroblastoma: tumor biology and its implications for staging and treatment," *Children (Basel)*, vol. 6, no. 1, 2019.
- [7] J. M. Maris, "Recent advances in neuroblastoma," *New England Journal of Medicine*, vol. 362, no. 23, pp. 2202–2211, 2010.
- [8] Z. D. Smith and A. Meissner, "DNA methylation: roles in mammalian development," *Nature Reviews Genetics*, vol. 14, no. 3, pp. 204–220, 2013.
- [9] S. Gómez, G. Castellano, G. Mayol et al., "DNA methylation fingerprint of neuroblastoma reveals new biological and clinical insights," *Epigenomics*, vol. 7, no. 7, pp. 1137–1153, 2015.
- [10] T. Teitz, T. Wei, M. B. Valentine et al., "Caspase 8 is deleted or silenced preferentially in childhood neuroblastomas with amplification of MYCN," *Nature Medicine*, vol. 6, no. 5, pp. 529–535, 2000.
- [11] D. Astuti, A. Agathangelou, S. Honorio et al., "RASSF1A promoter region CpG island hypermethylation in pheochromocytomas and neuroblastoma tumours," *Oncogene*, vol. 20, no. 51, pp. 7573–7577, 2001.
- [12] M. B. Michalowski, F. de Fraipont, D. Plantaz, S. Michelland, V. Combaret, and M. C. Favrot, "Methylation of tumor-suppressor genes in neuroblastoma: the RASSF1A gene is almost always methylated in primary tumors," *Pediatric Blood & Cancer*, vol. 50, no. 1, pp. 29–32, 2008.
- [13] Q. Yang, S. Liu, Y. Tian et al., "Methylation-associated silencing of the heat shock protein 47 gene in human neuroblastoma," *Cancer Research*, vol. 64, no. 13, pp. 4531–4538, 2004.
- [14] E. Grau, F. Martinez, C. Orellana et al., "Hypermethylation of apoptotic genes as independent prognostic factor in neuroblastoma disease," *Molecular Carcinogenesis*, vol. 50, no. 3, pp. 153–162, 2011.
- [15] A. Misawa, S. Tanaka, S. Yagyu et al., "RASSF1A hypermethylation in pretreatment serum DNA of neuroblastoma patients: a prognostic marker," *British Journal of Cancer*, vol. 100, no. 2, pp. 399–404, 2009.
- [16] G. Mayol, J. I. Martín-Subero, J. Ríos et al., "DNA hypomethylation affects cancer-related biological functions and genes relevant in neuroblastoma pathogenesis," *PLoS One*, vol. 7, no. 11, Article ID e48401, 2012.
- [17] Y. Yáñez, E. Grau, V. C. Rodríguez-Cortez et al., "Two independent epigenetic biomarkers predict survival in neuroblastoma," *Clinical Epigenetics*, vol. 7, no. 1, p. 16, 2015.

- [18] M. Olsson, S. Beck, P. Kogner, T. Martinsson, and H. Carén, “Genome-wide methylation profiling identifies novel methylated genes in neuroblastoma tumors,” *Epigenetics*, vol. 11, no. 1, pp. 74–84, 2016.
- [19] M. Bibikova, B. Barnes, C. Tsan et al., “High density DNA methylation array with single CpG site resolution,” *Genomics*, vol. 98, no. 4, pp. 288–295, 2011.
- [20] S. Hu, X. Yin, G. Zhang, and F. Meng, “Identification of DNA methylation signature to predict prognosis in gastric adenocarcinoma,” *Journal of Cellular Biochemistry*, vol. 120, 2019.
- [21] H. H. Jeong, S. Kim, K. Wee, and K. A. Sohn, “Investigating the utility of clinical outcome-guided mutual information network in network-based Cox regression,” *BMC Systems Biology*, vol. 9, p. S8, 2015.
- [22] C. Strobl, A. L. Boulesteix, A. Zeileis, and T. Hothorn, “Bias in random forest variable importance measures: illustrations, sources and a solution,” *BMC Bioinformatics*, vol. 8, no. 1, p. 25, 2007.
- [23] J. Li, Z. Chen, L. Tian et al., “LncRNA profile study reveals a three-lncRNA signature associated with the survival of patients with oesophageal squamous cell carcinoma,” *Gut*, vol. 63, no. 11, pp. 1700–1710, 2014.
- [24] M. Zhou, M. Guo, D. He et al., “A potential signature of eight long non-coding RNAs predicts survival in patients with non-small cell lung cancer,” *Journal of Translational Medicine*, vol. 13, no. 1, p. 231, 2015.
- [25] S. Aminzadeh, S. Vidali, W. Sperl, B. Kofler, and R. G. Feichtinger, “Energy metabolism in neuroblastoma and wilms tumor,” *Translational Pediatrics*, vol. 4, no. 1, pp. 20–32, 2015.
- [26] J. I. Fletcher, D. S. Ziegler, T. N. Trahair, G. M. Marshall, M. Haber, and M. D. Norris, “Too many targets, not enough patients: rethinking neuroblastoma clinical trials,” *Nature Reviews Cancer*, vol. 18, no. 6, pp. 389–400, 2018.
- [27] E. A. Newman, S. Abdessalam, J. H. Aldrink et al., “Update on neuroblastoma,” *Journal of Pediatric Surgery*, vol. 54, no. 3, pp. 383–389, 2019.
- [28] J. Guan, S. Fransson, J. T. Siaw et al., “Clinical response of the novel activating ALK-I1171T mutation in neuroblastoma to the ALK inhibitor ceritinib,” *Cold Spring Harbor molecular case studies*, vol. 4, no. 4, 2018.
- [29] D. Formicola, G. Petrosino, V. A. Lasorsa et al., “An 18 gene expression-based score classifier predicts the clinical outcome in stage 4 neuroblastoma,” *Journal of Translational Medicine*, vol. 14, no. 1, p. 142, 2016.
- [30] X. Zhong, Y. Liu, H. Liu, Y. Zhang, L. Wang, and H. Zhang, “Identification of potential prognostic genes for neuroblastoma,” *Frontiers in Genetics*, vol. 9, p. 589, 2018.
- [31] S. Guan, J. Lu, Y. Zhao et al., “MELK is a novel therapeutic target in high-risk neuroblastoma,” *Oncotarget*, vol. 9, no. 2, pp. 2591–2602, 2018.
- [32] X. X. Tang, H. Zhao, M. E. Robinson et al., “Prognostic significance of EPHB6, EFNB2, and EFNB3 expressions in neuroblastoma,” *Medical and Pediatric Oncology*, vol. 35, no. 6, pp. 656–658, 2000.
- [33] M. Szemes, A. Greenhough, Z. Melegh et al., “Wnt signalling drives context-dependent differentiation or proliferation in neuroblastoma,” *Neoplasia*, vol. 20, no. 4, pp. 335–350, 2018.
- [34] S. Wu, R. Zhang, F. Nie et al., “MicroRNA-137 Inhibits EFNB2 expression affected by a genetic variant and is expressed aberrantly in peripheral blood of schizophrenia patients,” *EBioMedicine*, vol. 12, pp. 133–142, 2016.
- [35] K. Niesmann, D. Breuer, J. Brockhaus et al., “Dendritic spine formation and synaptic function require neurobeachin,” *Nature Communications*, vol. 2, no. 1, p. 557, 2011.
- [36] R. Nair, J. Lauks, S. Jung et al., “Neurobeachin regulates neurotransmitter receptor trafficking to synapses,” *Journal of Cell Biology*, vol. 200, no. 1, pp. 61–80, 2013.
- [37] D. Castermans, K. Volders, A. Crepel et al., “SCAMP5, NBEA and AMISYN: three candidate genes for autism involved in secretion of large dense-core vesicles,” *Human Molecular Genetics*, vol. 19, no. 7, pp. 1368–1378, 2010.
- [38] G. Gao, J. L. Kasperbauer, N. M. Tombers, M. D. Cornell, and D. I. Smith, “Prognostic significance of decreased expression of six large common fragile site genes in oropharyngeal squamous cell carcinomas,” *Translational Oncology*, vol. 7, no. 6, pp. 726–731, 2014.
- [39] D. Wangsa, R. Braun, C. H. Stuelten et al., “Induced chromosomal aneuploidy results in global and consistent deregulation of the transcriptome of cancer cells,” *Neoplasia*, vol. 21, no. 7, pp. 721–729, 2019.
- [40] N. Lipunova, A. Wesselius, K. K. Cheng et al., “Genome-wide association study for tumour stage, grade, size, and age at diagnosis of non-muscle-invasive bladder cancer,” *European Urology Oncology*, vol. 2, no. 4, pp. 381–389, 2019.
- [41] M. S. Mulhern, C. Stumpel, N. Stong et al., “NBEA: developmental disease gene with early generalized epilepsy phenotypes,” *Annals of Neurology*, vol. 84, no. 5, pp. 788–795, 2018.
- [42] E. A. Afanasyeva, P. Mestdagh, C. Kumps et al., “MicroRNA miR-885-5p targets CDK2 and MCM5, activates p53 and inhibits proliferation and survival,” *Cell Death & Differentiation*, vol. 18, no. 6, pp. 974–984, 2011.
- [43] J. Y. Hou, Y. G. Wang, S. J. Ma, B. Y. Yang, and Q. P. Li, “Identification of a prognostic 5-Gene expression signature for gastric cancer,” *Journal of Cancer Research and Clinical Oncology*, vol. 143, no. 4, pp. 619–629, 2017.
- [44] K. Tuand, P. Stijnen, K. Volders et al., “Nuclear localization of the autism candidate gene neurobeachin and functional interaction with the NOTCH1 intracellular domain indicate a role in regulating transcription,” *PLoS One*, vol. 11, no. 3, Article ID e0151954, 2016.
- [45] M. T. Matsoukas and G. A. Spyroulias, “Dynamic properties of the growth hormone releasing hormone receptor (GHRHR) and molecular determinants of GHRH binding,” *Molecular BioSystems*, vol. 13, no. 7, pp. 1313–1322, 2017.
- [46] I. Karacan, A. Balamir, S. Ugurlu et al., “Diagnostic utility of a targeted next-generation sequencing gene panel in the clinical suspicion of systemic autoimmune diseases: a multi-center study,” *Rheumatology International*, vol. 39, 2019.
- [47] E. Simsek, T. Simsek, M. Eren et al., “Clinical, histochemical, and molecular study of three Turkish siblings diagnosed with H syndrome, and literature review,” *Hormone Research Paediatrics*, vol. 91, pp. 1–10, 2019.
- [48] B. Liu, A. Czajka, A. N. Malik, K. Hussain, P. M. Jones, and S. J. Persaud, “Equilibrative nucleoside transporter 3 depletion in beta-cells impairs mitochondrial function and promotes apoptosis: relationship to pigmented hypertrichotic dermatosis with insulin-dependent diabetes,” *Biochimica et Biophysica Acta*, vol. 1852, pp. 2086–2095, 2015.
- [49] N. K. Rafiq, K. Hussain, and P. A. Brogan, “Tocilizumab for the treatment of SLC29A3 mutation positive PHID syndrome,” *Pediatrics*, vol. 140, no. 5, 2017.
- [50] A. Howaldt, S. Nampoothiri, L. M. Quell et al., “Sclerosing bone dysplasias with hallmarks of dysosteosclerosis in four